AD-A119 784 MASSACHUSETTS INST OF TECH CAMBRIDGE CENTER FOR MATE--ETC F/G 11/6
MOLECULAR-ORBITAL BASIS FOR SUPERCONDUCTIVITY IN HIGH- AND LOW---ETC(U)
SEP 82 K H JOHNSON, R P MESSMER N00014-81-K-0499
UNCLASSIFIED TR-4 NL

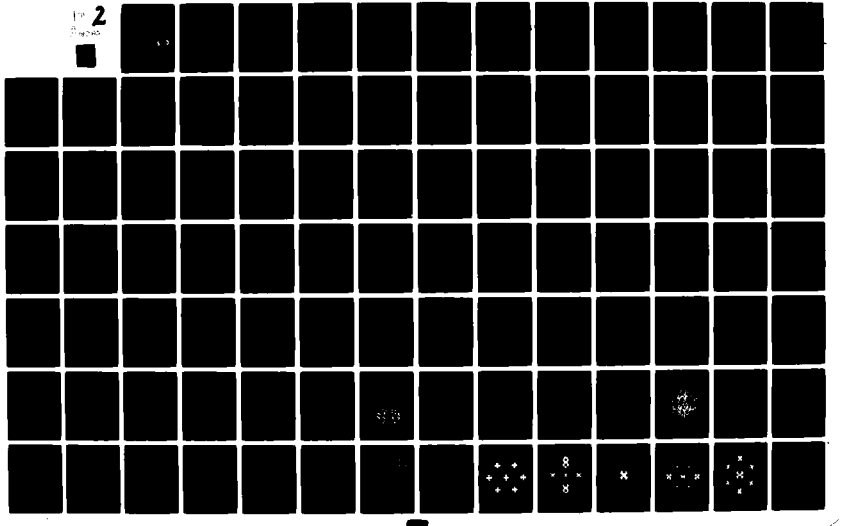

Unclassified

SECURITY CLASSIFICATION OF THIS PAGE (When Data Entered)

(12)

REPORT DOCUMENTATION PAGE		READ INSTRUCTIONS BEFORE COMPLETING FORM
1. REPORT NUMBER 4	2. GOVT ACCESSION NO. AD-A119784	3. RECIPIENT'S CATALOG NUMBER
4. TITLE (and Subtitle) Molecular-Orbital Basis for Superconductivity in High- and Low-Dimensional Metals		5. TYPE OF REPORT & PERIOD COVERED Interim
		6. PERFORMING ORG. REPORT NUMBER
7. AUTHOR(s) K. H. Johnson and R. P. Messmer		8. CONTRACT OR GRANT NUMBER(s) N00014-81-K-0499
9. PERFORMING ORGANIZATION NAME AND ADDRESS Center for Materials Science and Engineering, M.I.T., Cambridge, Massachusetts 02139		10. PROGRAM ELEMENT, PROJECT, TASK AREA & WORK UNIT NUMBERS Task No. Nr 056-757
11. CONTROLLING OFFICE NAME AND ADDRESS Office of Naval Research Department of the Navy Arlington, Virginia 22217		12. REPORT DATE September 24, 1982
		13. NUMBER OF PAGES 98
14. MONITORING AGENCY NAME & ADDRESS(if different from Controlling Office)		15. SECURITY CLASS. (of this report)
		15a. DECLASSIFICATION/DOWNGRADING SCHEDULE

16. DISTRIBUTION STATEMENT (of this Report)

Approval for public release;
distribution unlimited.

17. DISTRIBUTION STATEMENT (of the abstract entered in Block 20, if different from Report)

18. SUPPLEMENTARY NOTES

19. KEY WORDS (Continue on reverse side if necessary and identify by block number)

Molecular Orbital
Superconductivity
High and Low Dimensional Metals

20. ABSTRACT (Continue on reverse side if necessary and identify by block number)

A real-space molecular-orbital description of electronic wave functions which are postulated to be the precursors of the superconducting state in high- and low-dimensional metals is presented, based on self-consistent X-alpha scattered-wave (SCF-Xα-SW) molecular-orbital calculations for clusters representing the local molecular environments in these materials. It is shown that there is a persistent correlation between the occurrence of superconductivity in a material and the existence of spatially

cont

DD FORM 1 JAN 73 1473 EDITION OF 1 NOV 68 IS OBSOLETE S/N 0102-LF-014-6601

Unclassified

SECURITY CLASSIFICATION OF THIS PAGE (When Data Entered)

delocalized molecular orbitals at the Fermi energy which are bonding within and antibonding between "layers" or "tubes" of overlapping atomic orbitals that span many atoms, forming a type of "electron network" at the Fermi energy, as exemplified by $p\pi$ "layered" molecular-orbital topologies in Al and $(TMTSF)_2PF_6$, and by $d\delta$ "tubular" molecular-orbital topologies in Nb and Nb_3Sn. This description of the precursor superconducting state is consistent with the original conjectures of London that the superconducting-state wave function is "molecular" in nature, "rigid" in character, and of wide spatial extent, from which observed physical properties (e.g., diamagnetism and nondissipative electrical currents) of the superconducting state logically follow. The molecular-orbital model is further shown to be consistent with Cooper's concept of electron pairing in the superconducting state through a net attractive electron-electron interaction but differs from the Bardeen-Cooper-Schrieffer (BCS) theory of superconductivity in attributing the pairing to "valence-bond-like" electron occupation of the layered or tubular molecular orbitals at the Fermi energy, coupled with lattice ion displacements through a dynamic Jahn-Teller effect, rather than to the absorption and emission of virtual phonons. However, recent simple physical arguments presented by Weisskopf for the formation of Cooper pairs suggest that the two points of view are not incompatible. Approximate formulae for calculating the electron pair binding energy and superconducting transition temperature, analogous to the BCS formulae but expressed entirely in terms of two simple molecular-orbital parameters, are derived and applied to various superconductors. Moreover, through an elementary phase-space argument, the molecular-orbital description of Cooper pairs is shown to be qualitatively consistent with Schafroth's description of electron pairs as "quasi-molecules" undergoing Bose-Einstein-like condensation to the superconducting state. The above molecular-orbital criteria for superconductivity are diametrical to those for the occurrence of local magnetic moments and ferromagnetism, namely, the existence of spatially localized, exclusively antibonding (e.g., $d\sigma^*$, $d\pi^*$, or $d\delta^*$) molecular orbitals at the Fermi energy. Furthermore, in contrast to the ordering of electron spins on atomic sublattices in conventional antiferromagnetism, the valence-bond-like correlation of Cooper-Schafroth electron pairs at the Fermi energy in composite bonding-antibonding layered or tubular molecular-orbital components, spatially delocalized between the atoms, corresponds to a type of conduction-electron "antiferromagnetism" or spin-density wave, thus offering an explanation for the occurrence of such antiferromagnetism in superconductors such as $(TMTSF)_2PF_6$ and Nb_3Sn. These molecular-orbital criteria therefore provide a conceptual basis for understanding the generally mutually exclusive incidence of superconductivity and magnetism among the elements of the periodic table, although they can also be used to explain the occasional coexistence of superconductivity and ferromagnetism or antiferromagnetism in some materials. The molecular-orbital model for superconductivity complements BCS theory in that it permits the prediction of which materials are likely to be superconductors and which are not entirely on the basis of the molecular-orbital topology at the Fermi energy. It offers an explanation of the vanishing isotope effect in certain superconductors. It contributes to the clarification of the issue of non-phonon mechanisms of superconductivity. It provides insight into the correlations of superconductivity with other physical properties, such as lattice instabilities. It is readily applicable to superconductors lacking long-range crystalline order, such as amorphous alloys and small particles. Finally, the molecular-orbital approach can be used to explain in simple terms why some materials (e.g., Cu, Ag, and Au) are neither superconducting nor magnetic, why certain quasi-one-dimensional organic solids,

such as TTF-TCNQ, are not superconductors while others, such as $(TMTSF)_2PF_6$, are superconductors, and to assess critically the likelihood of superconductivity in certain other types of substances (e.g., other types of organic solids; metallic hydrogen at attainable high pressures), and to suggest ways of systematically improving existing classes or synthesizing novel classes of superconducting materials.

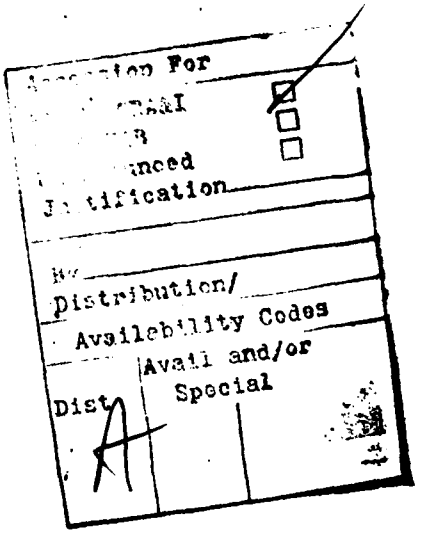

OFFICE OF NAVAL RESEARCH

Contract N00014-81-K-0499

Task No. Nr 056-757

TECHNICAL REPORT NO. 4

MOLECULAR-ORBITAL BASIS FOR SUPERCONDUCTIVITY IN HIGH- AND LOW-DIMENSIONAL METALS

by

K. H. Johnson

Center for Materials Science and Engineering
Massachusetts Institute of Technology
Cambridge, Massachusetts 02139

and

R. P. Messmer

General Electric Corporation Research and Development
Schenectady, New York 02301

September 24, 1982

MOLECULAR-ORBITAL BASIS FOR SUPERCONDUCTIVITY IN HIGH- AND LOW-DIMENSIONAL METALS

K. H. JOHNSON
Department of Materials Science and Engineering
Massachusetts Institute of Technology, Cambridge, Massachusetts 02139

R. P. MESSMER
General Electric Corporate Research and Development
Schenectady, New York 12301

SUMMARY

A real-space molecular-orbital description of electronic wave functions which are postulated to be the precursors of the superconducting state in high- and low-dimensional metals is presented, based on self-consistent X-alpha scattered-wave (SCF-Xα-SW) molecular-orbital calculations for clusters representing the local molecular environments in these materials. It is shown that there is a persistent correlation between the occurrence of superconductivity in a material and the existence of spatially delocalized molecular orbitals at the Fermi energy which are bonding within and antibonding between "layers" or "tubes" of overlapping atomic orbitals that span many atoms, forming a type of "electron network" at the Fermi energy, as exemplified by pπ "layered" molecular-orbital topologies in Al and $(TMTSF)_2PF_6$, and by dδ "tubular" molecular-orbital topologies in Nb and Nb_3Sn. This description of the precursor superconducting state is consistent with the original conjectures of London that the superconducting-state wave function is "molecular" in nature, "rigid" in character, and of wide spatial extent, from which observed physical properties (e.g., diamagnetism and nondissipative electrical currents) of the superconducting state logically follow. The molecular-orbital model is further shown to be consistent with Cooper's concept of electron pairing in the superconducting state through a net attractive electron-electron interaction but differs from the Bardeen-Cooper-Schrieffer (BCS) theory of superconductivity in attributing the pairing to "valence-bond-like" electron occupation of the layered or tubular

molecular orbitals at the Fermi energy, coupled with lattice ion displacements through a dynamic Jahn-Teller effect, rather than to the absorption and emission of virtual phonons. However, recent simple physical arguments presented by Weisskopf for the formation of Cooper pairs suggest that the two points of view are not incompatible. Approximate formulae for calculating the electron pair binding energy and superconducting transition temperature, analogous to the BCS formulae but expressed entirely in terms of two simple molecular-orbital parameters, are derived and applied to various superconductors. Moreover, through an elementary phase-space argument, the molecular-orbital description of Cooper pairs is shown to be qualitatively consistent with Schafroth's description of electron pairs as "quasi-molecules" undergoing Bose-Einstein-like condensation to the superconducting state. The above molecular-orbital criteria for superconductivity are diametrical to those for the occurrence of local magnetic moments and ferromagnetism, namely, the existence of spatially localized, exclusively antibonding (e.g., $d\sigma^*$, $d\pi^*$, or $d\delta^*$) molecular orbitals at the Fermi energy. Furthermore, in contrast to the ordering of electron spins on atomic sublattices in conventional antiferromagnetism, the valence-bond-like correlation of Cooper-Schafroth electron pairs at the Fermi energy in composite bonding-antibonding layered or tubular molecular-orbital components, spatially delocalized between the atoms, corresponds to a type of conduction-electron "antiferromagnetism" or spin-density wave, thus offering an explanation for the occurrence of such antiferromagnetism in superconductors such as $(TMTSF)_2PF_6$ and Nb_3Sn. These molecular-orbital criteria therefore provide a conceptual basis for understanding the generally mutually exclusive incidence of superconductivity and magnetism among the elements of the periodic table, although they can also be used to explain the occasional coexistence of superconductivity and ferromagnetism or antiferromagnetism in some materials. The molecular-orbital model for superconductivity complements BCS theory in that it permits the prediction of which materials are likely

to be superconductors and which are not entirely on the basis of the molecular-orbital topology at the Fermi energy. It offers an explanation of the vanishing isotope effect in certain superconductors. It contributes to the clarification of the issue of non-phonon mechanisms of superconductivity. It provides insight into the correlations of superconductivity with other physical properties, such as lattice instabilities. It is readily applicable to superconductors lacking long-range crystalline order, such as amorphous alloys and small particles. Finally, the molecular-orbital approach can be used to explain in simple terms why some materials (e.g., Cu, Ag, and Au) are neither superconducting nor magnetic, why certain quasi-one-dimensional organic solids, such as TTF-TCNQ, are not superconductors while others, such as $(TMTSF)_2PF_6$, are superconductors, and to assess critically the likelihood of superconductivity in certain other types of substances (e.g., other types of organic solids; metallic hydrogen at attainable high pressures), and to suggest ways of systematically improving existing classes or synthesizing novel classes of superconducting materials.

I. INTRODUCTION

The Bardeen-Cooper-Schrieffer (BCS) theory of superconductivity [1] ascribes the onset of the superconducting state of a crystal at the transition temperature, T_c, to electrons attractively paired via virtual phonons of the lattice. The BCS formula for T_c is

$$T_c \sim \Theta_D \exp [-1/N(0)V], \tag{1}$$

where Θ_D is the lattice Debye temperature, V is the attractive potential between electrons in Cooper pairs [2] induced by the electron-phonon interactions, and N(0) is the electronic density of states for one spin at the Fermi energy. The BCS theory together with its strong-coupling extension has been eminently successful in accounting for the physical properties, e.g., nondissipative current, diamagnetism, and thermodynamics of the superconducting state, and

has correlated many expermental data in terms of a few basic parameters. Nevertheless, it has often been emphasized by Matthias [3] that the BCS theory and formal extensions thereof do not satisfactorily explain the observed dependence of superconductivity on crystal structure and chemistry (especially for transition metals, alloys, and compounds) and are not very useful for predicting which materials should be superconducting and which should not. The existence of superconducting materials possessing only short-range structural order, such as superconducting amorphous alloys [4] and superconducting metal particles down to $\sim 50\text{Å}$ in size, [5,6] would appear to be more conveniently viewed from a local "real-space" chemical approach, than by traditional concepts of long-range cyrstalline order and momentum ($\vec{k}$) space, which lead to coherence lengths of the superconducting state that usually exceed the short-range order and electron mean free path characteristic of amorphous and small-particle superconductors. This emphasizes the desirability of having a local chemical-bonding or real-space molecular description of the superconducting state in order to complement BCS theory. Indeed, London [7,8] in his phenomenological approach to superconductivity discusses the possibility of developing a molecular description of the superconducting state (see Chapter E of Ref. 8), and Slater [9] in an early attempt at describing superconductivity discusses the nature of the spatial character of the superconducting-state wave function. With speculations that mechanisms other than electron-phonon coupling can attractively pair electrons in the superconducting state, [3,10,11] a molecular criterion that accounts for the known chemical trends in the occurrence of superconductivity would be a useful tool in the continuing effort to identify new classes of superconducting materials.

The systematic trends of T_c with valence-electron-per-atom ratio [3] and the difficulty of calculating BCS parameters for transition metals, their alloys, and compounds have prompted the development of rudimentary chemical models, [12-14] based on atomic d orbitals and aimed primarily at the estimation

of T_c. Unfortunately, these models are not easily generalized to non-transition-metal superconductors and do not yield a real-space molecular description of the superconducting state. The most general chemical approach to superconductivity is that of Krebs, [15] who has suggested that superconductivity is possible only if the normal chemical bonding system in the crystal or parts of the crystal permits the construction of a molecular wave function which for at least one space direction is not intersected by plane or conical nodal surfaces, and if the corresponding electron band is not fully occupied. However, Krebs attempts only to account for the incidence of superconductivity through qualitative chemical bonding arguments and not the evaluation of a specific electron-pairing mechanism and T_c. Local reformulations of BCS-type superconductivity theory for crystals in terms of Wannier functions [16-18] should also be mentioned, although these approaches do not establish a direct relationship between superconductivity and the nature of the chemical bond. In the latter regard, one should not fail to cite the paper of Pauling [19] in which a relationship between "resonating valence bonds" in metals and the BCS electron-phonon mechanism for superconductivity is proposed.

In this paper, we present a real-space molecular-orbital description of the wave functions which we believe to be the precursors of the superconducting state, as well as providing simple criteria for determining the occurrence of superconductivity. This theoretical model for superconductivity makes direct use of the results of first-principles self-consistent-field X-alpha scattered-wave (SCF-Xα-SW) molecular-orbital calculations for clusters representing the local molecular environments in these materials. The SCF-Xα-SW method [20] is based on the combined use of the Xα density-functional approximation [21] to electron-electron exchange and correlation and the multiple-scattered-wave technique [22] of solving the Schrödinger self-consistent-field molecular-orbital equations. In conjunction with the "transition-state" procedure [20,21] for calculating electronic transitions between orbitals, this method leads to a

description of both the ground and excited electronic states of a system. The calculation of different molecular orbitals for different spins allows one to consider the effects of magnetic spin polarization. Along with applications to a wide variety of polyatomic molecules, [23,24] including biological macromolecules [25-27] and polymers, [28] this approach has been used successfully to elucidate the local bulk and surface electronic structures and properties of solids [29-31] e.g., crystalline semiconductors and localized defects and impurities therein, [32-35] amorphous semiconductors, [36] crystalline and amorphous metals and alloys [37-42] including magnetic properties [39-41] molecular crystals, [28] and chemisorption on metal surfaces [43,44] along with the calculation of photoelectron emission intensities, [45,46] electron-scattering cross sections, [47] and "shake-up" spectra [48] for chemisorbed species. These theoretical studies collectively suggest that short-range order and local chemical bonding largely determine the measurable electronic structures and properties of many types of materials, whether ordered or disordered.

In view of the apparent complementary natures of superconductivity and magnetism, it should be noted that spin-unrestricted SCF-Xα-SW cluster molecular-orbital studies [39] indicate that the local magnetic moments of Fe and Mn impurities in crystalline copper above the Kondo temperature are associated with the existence of exclusively antibonding Fe(d)-Cu(s,d) molecular orbitals at the Fermi energy (see Figs. 10, 12, and 13 of Ref. 39). Similar spin-polarized cluster models for ferromagnetic bcc crystalline α-iron [41,30] suggest that the onset of collective magnetism below the Curie temperature and the persistence of "spin clusters" above the Curie temperature are associated with the existence of exclusively antibonding Fe(d)-Fe(d) molecular orbitals at the Fermi energy in the non-spin-polarized limit (see Fig. 14 of Ref. 41). Recent spin-polarized SCF-Xα-SW cluster models for amorphous iron-boron and iron-phosphorus alloys [42] are also in good quantitative agreement with measured magnetic properties and clearly show the key role of antibonding molecular orbitals at the Fermi energy

in determining how alloying alters the magnetic properties of iron. For the sake of completeness, it may also be noted that the SCF-Xα-SW method has been applied to iron-containing biological molecules such as ferredoxin [26] and hemoglobin [27] and the results used to explain observed magnetic properties (including the calculation of magnetic hyperfine parameters [27]) as functions of temperature and oxygenation, respectively. Finally, the spin-unrestricted SCF-Xα-SW method, in conjunction with the transition-state procedure, [20,21] has recently been employed with good results to calculate, from first principles, ferromagnetic and antiferromagnetic exchange coupling constants (Heisenberg exchange integrals) for transition-metal cluster coordination complexes. [49] The most general finding of the theoretical studies of magnetic substances summarized above is that for the local and collective forms of magnetism investigated, one finds the occurrence of antibonding molecular orbitals near the Fermi energy in the non-spin-polarized limit (see further discussion in Section VI).

In view of the above work, it was thought that SCF-Xα-SW cluster molecular-orbital studies of superconducting materials might possibly also provide some new insight into the nature of chemical bonding associated with the superconducting state. As will be discussed in Section IV, it appears that the molecular-orbital criteria for the occurrence of superconductivity and certain types of magnetism are diametrical, thereby offering a simple explanation for the mutually exclusive occurrence of these phenomena in a material at the same temperature and pressure. The orbital criteria for superconductivity will further be shown to be consistent with Cooper's [2] concept of electron pairing through a net attractive electron-electron interaction (V in Eq. 1) but differs somewhat from the generally accepted mechanism for superconductivity in attributing this attractive interaction directly to real-space chemical-bond-like formation at the Fermi energy, coupled with the lattice through a dynamic Jahn-Teller effect, rather than to electron-phonon coupling per se.

However, arguments will be presented to show that these two points of view are not necessarily incompatible. The molecular-orbital approach presented herein will also be used to explain simply why some metals (e.g. Cu, Ag, and Au) are neither superconducting nor magnetic. Finally, it is suggested that molecular-orbital criteria might provide a useful theoretical tool for predicting new superconducting materials.

II. CLUSTER MOLECULAR ORBITALS AND BAND STRUCTURE

The relationships of SCF-Xα-SW cluster molecular-orbital energy levels and densities of states to the corresponding crystal band structures and densities of states calculated from Bloch's theorem and measured spectroscopically have been discussed in previous publications and reports for the examples of copper, [37,39] nickel, [37] aluminum, [38,43] and iron. [41] Nevertheless, in order to clarify the use of cluster molecular orbitals as a basis for superconductivity, we point out some specific similarities and differences between cluster electronic structure and crystal band structure.

For simplicity, consider first the example of an isolated benzene molecule, the pπ orbitals of which are shown schematically on the left side of Fig. 1. The π_1 orbital, which is occupied by two spin-paired electrons and has the energy level ε_1, is the most strongly bonding of the pπ molecular orbitals, whereas the degenerate π_2 and π_3 orbitals, which together are occupied by four spin-paired electrons and have the energy level $\varepsilon_{2,3}$, are relatively weakly bonding. The unoccupied π_3^* orbital is strongly antibonding, while the unoccupied π_1^* and π_2^* orbitals are weakly antibonding. Because of the one-dimensional periodicity of the carbon atoms around the benzene ring, the molecular orbitals can be expressed in symmetrized Bloch form, [50] resulting in the discrete one-dimensional "k-space" band profile shown schematically on the right side of Fig. 1. The "Fermi energy" ε_F separates the occupied states from the unoccupied ones. In this particular example,

there is a simple one-to-one correspondence between the "real space" molecular orbitals and "k-space" band structure, as indicated by the connecting lines in Fig. 1. It has often been noted that the diamagnetic "ring currents" induced in benzene and other aromatic molecules through the response of the $p\pi$ electrons to an external magnetic field are nondissipative currents similar in some (but not all) respects to the persistent currents of a superconducting ring. [8,51,52]

On the other hand, the molecular orbitals of a finite cluster representing the local molecular environment in a crystal transform according to the irreducible representations of the cluster point symmetry group and therefore are not generally equivalent on a one-to-one basis to Bloch band eigenstates of the crystal, except at the points in $\vec{k}$-space which have the full cluster point group symmetry. For example, the $\Gamma(\vec{k}=0)$ Bloch state has the full O_h point-group symmetry in a cubic crystal. Nevertheless, it is possible to construct combinations of degenerate Bloch states of different $\vec{k}$ (the so-called "star" of the wave vector) that transform according to the irreducible representations of the cluster point group. [53] From this, one can conclude that there should be a reasonably close correspondence between cluster and crystal densities of states. Examples of such correspondence will be found in Refs. 37,38,41, and 43.

As an illustrative application of the above concepts to a superconducting metal, consider the example of aluminum. In Fig. 2, the SCF-Xα-SW molecular-orbital energy levels of a 43-atom cluster, $AlAl_{12}Al_6Al_{24}$, representing the local environment of fcc crystalline aluminum up to third-nearest neighbors [38] are compared with the energy bands of the crystal [54] shown along high symmetry directions of the Brillouin zone. The principal nearest-neighbor chemical bonding components (σ, π, etc.) of the Al s and p orbitals in the cluster are indicated. The distribution of cluster energy levels is also compared with the X-ray photoelectron spectrum (XPS) of pure crystalline aluminum in Fig. 3. Good agreement between the cluster results and the XPS spectrum is

obtained with respect to both density and total s,p band width of the cluster energy levels, consistent with the comparison of aluminum cluster densities of states and ultraviolet photoemission spectra (UPS) described in Ref. 38. There is a close correspondence between individual cluster molecular orbitals and certain Bloch energy-band eigenstates or combinations thereof. For example, the lowest occupied sσ-bonded cluster energy level, $1a_{1g}$, shown in Fig. 2 is the discrete molecular-orbital analogue of the $\Gamma_1(\vec{k}=0)$ s-band Bloch state. The manifold of s,p σ-bonded cluster levels in the energy range -1.3 Ry to -0.7 Ry corresponds to combinations of Δ_1 and Σ_1 Bloch states in the first band of aluminum, with the high density of s,p σ-bonded cluster levels between -0.85 Ry and -0.65 Ry responsible for a broad maximum in the XPS density of states evident in Fig. 3. The high density of pσ- and pπ-bonded cluster levels between -0.65 Ry and the Fermi energy ε_F is associated with combinations of Δ_1, Σ_3, and Σ_1 Bloch states in the second band of aluminum and is responsible for the peak in the XPS density of states in the vicinity of the Fermi energy. The highest occupied cluster molecular orbital $8t_{1u}(\varepsilon_F)$ indicated in Fig. 2 corresponds to π-bonding combinations of degenerate Σ_3,Σ_1, and Δ_1 p-band Bloch states at the Fermi energy, and the lowest unoccupied orbital $5t_{2g}$ corresponds to σ-nonbonding Σ_1 p-band Bloch states just above the Fermi energy.

As will be shown in the following section of the paper, the cluster $t_{1u}(\varepsilon_F)$ molecular orbital is key to understanding the real-space nature of the superconducting state of aluminum. Wave-function contour maps of this orbital, plotted in the (200) and (110) cyrstallographic planes up to second-nearest neighbors, are shown in Figs. 4 and 5, respectively. The solid and dashed contours represent positive and negative regions, respectively, of the molecular-orbital wave function. Regions of net overlap between contours of the same sign are bonding, whereas regions of positive and negative contours separated by nodes are antibonding. The most striking feature of Figs. 4 and 5

is the π-bonding character of the Al atomic p orbitals along the "horizontal" direction of each figure, much like the $p\pi_1$-bonding character of C atomic p orbitals around the ring of the benzene molecule shown in Fig. 1. Like the planar configuration of pπ atomic orbitals in benzene, the pπ-bonding atomic orbitals in aluminum form two-dimensional "layers" as shown in the perspective contour map of the cluster $t_{1u}(\varepsilon_F)$ molecular-orbital wave function in Fig. 6, which is the three-dimensional counterpart of Figs. 4 and 5. However, in contrast to benzene, where the $p\pi_1$ molecular orbital lies well below the Fermi energy, i.e., it is the "lowest" occupied orbital in Fig. 1, the pπ-bonding molecular orbital of aluminum is located exactly at the Fermi energy, i.e., it is the highest occupied cluster molecular orbital, $8t_{1u}(\varepsilon_F)$, in Fig. 2. Unlike benzene, futhermore, there is also a "one-dimensional" σ*-antibonding component between the p orbitals of second-nearest-neighbor Al atoms along the "vertical" direction in Figs. 4,5, and 6, which effectively isolates the pπ-bonding atomic-orbital components between nearest-neighbor planes of atoms and synergistically promotes covalent bond overlap between neighboring atomic planes to form the layered topology of the molecular orbital shown in Fig. 6. Although Figs. 4 through 6 imply anisotropy in each $t_{1u}(\varepsilon_F)$ molecular-orbital component, the triple degeneracy of this orbital leads to equivalent pπ-bonding and pσ*-antibonding components along complementary orthogonal crystal directions and therefore to an isotropic three-dimensional orbital probability distribution. As the cluster size is systematically increased to include more shells of atoms in the crystal, each pπ-bonding and pσ*-antibonding molecular orbital at the Fermi energy expands spatially and, in the limit of a very large number of atoms, forms a coherent macroscopic molecular-orbital of the type shown schematically in the (200) crystal plane in Fig. 7. This "real-space" character of aluminum molecular orbitals at the Fermi energy cannot be extracted easily from the conventional "$\vec{k}$-space" Bloch description of the crystal band structure, except in hindsight as an appropriate combination of Σ_1, Σ_3, and Δ_1

Bloch eigenstates, and thus has eluded solid-state physics.

III. CLUSTER MOLECULAR ORBITALS AND COOPER PAIRS

In order to understand how cluster molecular orbitals of the layered topology shown in Fig. 6 can be precursors to Cooper electron pairing and the superconducting state, it may be noted first that each layer can be described by a bonding orbital wave-function component, ψ_+ or ψ_-, where the plus and minus signs designate the sign of the wave function. Notice also in Fig. 6 that along the direction perpendicular to each layer, the layer-orbital components of opposite sign, ψ_+ and ψ_-, are mutually <u>antibonding</u> and correspond approximately to a damped standing sine wave having nodes that coincide with parallel planes of atoms and a wavelength $\lambda_F = 2d$, where d is the interlayer atomic spacing. In other words, along the direction perpendicular to the layer orbitals, the wave function is very much like that of a free electron moving back and forth with a de Broglie momentum

$$p_F = h/\lambda_F = h/2d \tag{2}$$

and kinetic energy (the Fermi energy)

$$\epsilon_F = p_F^2/2m = h^2/8md^2. \tag{3}$$

On the other hand, within each layer-orbital component of Fig. 6, the wave function, ψ_+ or ψ_-, corresponds to a nodeless standing wave of wavelength $\lambda_L = 2L$, where L is the layer-orbital diameter, like the lowest-energy eigenstate of a free electron confined to a two-dimensional constant potential well. With increasing cluster size, i.e., increasing cluster diameter L, the two-dimensional component of de Broglie electron momentum parallel to the layers, namely,

$$p_L = h/\lambda_L = h/2L, \tag{4}$$

vanishes

$$\lim_{L \to \infty} p_L = 0, \tag{5}$$

leaving only the sine-wave-like electron motion and momentum component (3) perpendicular to the layers (see Fig. 6). However, as emphasized in Section II, this does not imply a preferred direction for the latter component of electron momentum, since there are three degenerate molecular orbitals of the topology shown in Fig. 6 corresponding to three orthogonal crystal directions which are equally accessible at the Fermi energy, thereby resulting in an effectively isotropic three-dimensional sine-wave-like electron motion.

From one-electron layer orbitals, ψ_+ and ψ_-, of the type shown in Fig. 6, it is possible to construct an electron-pair wave function that has the customary spin-paired singlet symmetry of a Cooper pair. [1,2] This pair wave function can be written as the product of a symmetric two-electron space wave function

$$\psi(1,2) = \psi_+(1)\psi_-(2) + \psi_-(1)\psi_+(2) \tag{6}$$

and an antisymmetric two-electron spin wave function

$$S(1,2) = \alpha(1)\beta(2) - \beta(1)\alpha(2), \tag{7}$$

where α and β are functions representing "spin-up" and "spin-down" electrons, respectively. It is also possible to construct a triplet pair wave function from the ψ_+ and ψ_- orbitals, although we shall not consider this configuration here. Note in the singlet configuration that if the layer molecular-orbital components ψ_+ correspond to a "spin-up" ($\uparrow$) electron, then the layer molecular-components ψ_- correspond to a "spin-down" ($\downarrow$) electron and, vice versa, suggesting a type of "antiferromagnetic" spin polarization of the alternating layer orbitals, i.e., a "spin-density wave" (see Fig. 6). However, the net spin polarization per atom is zero, and therefore this delocalized "conduction-electron antiferromagnetism" should be distinguished from conventional localized antiferromagnetism (see further discussions in Section VI). The above electron pair wave function is similar in form to the ground-state wavefunction of an isolated hydrogen (H_2) molecule in the valence-bond description, [55] namely,

$$\psi_{VB}(1,2) = \psi_a(1)\psi_b(2) + \psi_b(1)\psi_a(2), \tag{8}$$

where ψ_a and ψ_b are the atomic (1s) orbitals of the dissociated H atoms. The difference

$$\Delta = 2\varepsilon_{1s} - E(d) \tag{9}$$

between the dissociated-atom energy $2\varepsilon_{1s}$ and the energy E(d) of the valence-bond state (8) for the equilibrium internuclear distance d defines the chemical binding energy of the H_2 molecule. A stable chemical bond (i.e., positive value of Δ) will not occur for H_2 unless the Coulomb and exchange repulsion energies, respectively,

$$U_{Rep} = e^2 \int\int |\psi_a(1)|^2 |\psi_b(2)|^2 r_{12}^{-1} dv_1 dv_2, \tag{10}$$

$$J_{Rep} = e^2 \int\int \psi_a^*(1)\psi_b^*(2)\psi_a(2)\psi_b(1) r_{12}^{-1} dv_1 dv_2 \tag{11}$$

of the two electrons, together with the electrostatic repulsion of the two nuclei (protons) are more than balanced out at some internuclear distance d by the Coulomb and exchange attractions, respectively,

$$U_{attr} = -e^2 \int |\psi_a(1)|^2 r_{1b}^{-1} dv_1 - e^2 \int |\psi_b(2)|^2 r_{2a}^{-1} dv_2 \tag{12}$$

$$J_{attr} = -e^2 S \int \psi_a^*(1)\psi_b(1) r_{1b}^{-1} dv_1 - e^2 S \int \psi_a^*(2)\psi_b(2) r_{2a}^{-1} dv_2 \tag{13}$$

of the electrons to the opposite nuclei, where

$$S = \int \psi_a^*(1)\psi_b(1) dv_1 = \int \psi_a^*(2)\psi_b(2) dv_2 \tag{14}$$

is the atomic overlap integral.

Analogously, one might expect the energy E(d) for the "valence-bond-like" configuration (6) of a Cooper pair to be lower than the energy $2\varepsilon_F$ of a "dissociated" electron pair at the Fermi energy, leading to "quasimolecular" electron pair binding of the type envisioned in a superconductor by Schafroth et al. [56] with binding energy

$$\Delta = 2\varepsilon_F - E(d), \tag{15}$$

if the Coulomb and exchange repulsion energies of the electrons are more than compensated for by a net attraction of the electrons via the positive ions of the lattice. The Coulomb and exchange repulsions, respectively,

$$U_{Rep}(\varepsilon_F) = e^2 \int\int |\psi_+(1)|^2 |\psi_-(2)|^2 r_{12}^{-1} dv_1 dv_2 \tag{16}$$

$$J_{Rep}(\varepsilon_F) = e^2 \int \psi_+^*(1)\psi_-^*(2)\psi_+(2)\psi_-(1)r_{12}^{-1}dv_1dv_2 \tag{17}$$

of a pair of electrons correlated at the Fermi energy over degenerate, mutually antibonding layer orbitals of the type shown in Fig. 6 are already largely screened out over distances greater than the interlayer spacing d by the positive ions located in the nodal planes between the layer orbitals. Then the quantities (16) and (17) reduce approximately to

$$U_{Rep}(\varepsilon_F) \sim (e^2/d)\int|\psi_+(1)|^2dv_1\int|\psi_-(2)|^2dv_2 = e^2/d \tag{18}$$

$$J_{Rep}(\varepsilon_F) \sim (e^2/d)\int\psi_+^*(1)\psi_-(1)dv_1\int\psi_-^*(2)\psi_+(2)dv_2 = 0 \tag{19}$$

since the layer orbitals are normalized, i.e.,

$$\int|\psi_+(1)|^2dv_1\int|\psi_-(2)|^2dv_2 = 1 \tag{20}$$

and mutually antibonding, i.e., their overlap integral

$$S_{\underline{+}} = S_{\substack{anti-\\bond}}(\varepsilon_F) = \int\psi_+(1)\psi_-(1)dv_1 = \int\psi_+(2)\psi_-(2)dv_2 = 0. \tag{21}$$

Therefore, the screened electrostatic repulsion of two such electrons at a relative distance r can be described approximately by the effective potential

$$V_C(r) \sim U_{Rep}(\varepsilon_F) \sim \begin{cases} e^2/d & \text{for } r \lesssim d \\ 0 & \text{for } r \gtrsim d \end{cases} \tag{22}$$

where $d \sim 2\mathring{A}$ for aluminum. The Coulomb attraction

$$U_{Attr}(\varepsilon_F) = -e^2\int|\psi_+(1)|^2r_1^{-1}dv_1 - e^2\int|\psi_-(2)|^2r_2^{-1}dv_2 \tag{23}$$

of each layer orbital to the intervening positive ions is already accounted for in the potential which determines the molecular-orbital energy $2\varepsilon_F$ of the "dissociated" electron pair, while the exchange attraction

$$J_{Attr}(\varepsilon_F) = -e^2S_{\underline{+}}\int\psi_+(1)\psi_-(1)r_1^{-1}dv_1 - e^2S_{\underline{+}}\int\psi_+(2)\psi_-(2)r_2^{-1}dv_2 \tag{24}$$

vanishes because the overlap integral (21) between the mutually antibonding layer orbitals ψ_+ and ψ_- is zero.

Because of the molecular-orbital degeneracy at the Fermi energy, the electron pair described by the layer orbitals ψ_+ and ψ_- is subject to the Jahn-Teller effect. [57] Therefore, the electron pair can, in principle, lower its energy from the value $2\varepsilon_F$ by the amount (15) by coupling with the lattice

through displacements of the lattice ions. The "driving force" for the Jahn-Teller coupling is the anisotropy of the degenerate ψ_+ and ψ_- layer orbitals, which tends to attract the nearest-neighbor lattice ions along the $p\pi$-bonding directions parallel to the layers and to repel second-nearest-neighbor ions along the $p\sigma^*$-antibonding direction perpendicular to the layers (see Figs. 4 through 7). An instantaneous displacement $\vec{\delta}$ of a lattice ion with respect to the neighboring layer orbitals $\psi_+(1)$ and $\psi_-(2)$ induces an attractive electrostatic dipole potential of the form

$$U_{Attr}^{(2)}(\varepsilon_F) = -e^2 \int |\psi_+(1)|^2 r_1^{-2} \delta dv_1 \; -e^2 \int |\psi_-(2)|^2 r_2^{-2} \delta dv_2. \tag{25}$$

For the range of ion displacements

$$\delta \sim (m/M)^{\beta} d \text{ for } 1/4 \lesssim \beta \lesssim 1/2 \tag{26}$$

between the amplitude $\delta_0 \sim (m/M)^{1/4}\, d$ of the zero-point oscillation of the lattice and the amplitude $\delta_c \sim (m/M)^{1/2}\, d$ of a classical oscillator (where m is the electron mass and M is the ion mass), it is unfavorable for the electron-lattice system to remove the orbital degeneracy at the Fermi energy and lower the electronic energy through a static lattice distortion. [57] Instead, the ψ_+ and ψ_- orbitals and lattice ion displacements δ are coupled <u>dynamically</u>, and the range of β values in (26) corresponds to the so-called <u>dynamic</u> Jahn-Teller effect. [57] From the SCF-Xα-SW cluster molecular-orbital contour map in Fig. 6, which is a direct measure of the average spacing d of the "compressed" layer orbital components ψ_+ and ψ_-, a value of $d \sim 1.8\text{Å}$ appropriate for bulk crystalline aluminum is obtained, giving limiting values of $\delta_0 \sim 0.1\text{Å}$ and $\delta_c \sim 0.01\text{Å}$ for aluminum.

The Jahn-Teller theorem [57] predicts only the occurrence of a coupling between orbitally degenerate electrons at the Fermi energy and lattice-ion displacements and not their actual magnitude. Nevertheless, it is reasonable to expect that the Jahn-Teller-induced lattice-ion displacements δ are proportional to the overlap integral

$$S_{bond}(\varepsilon_F) = \int \psi_+^a(1)\psi_+^b(1)dv_1 = \int \psi_-^a(1)\psi_-^b(1)dv_1 \quad (27)$$

between nearest-neighbor atomic-orbital components a and b of the molecular-orbitals ψ_+ and ψ_- at the Fermi energy along the bonding direction, e.g. the $p\pi$-bond overlap within the π-bonding layers of aluminum shown in Figs. 4 through 7. Then one can write approximately

$$\delta \sim S_{bond}(\varepsilon_F)d, \quad (28)$$

where d is of the order of the interatomic distance. The bond overlap integral, $S_{bond}(\varepsilon_F)$, should be distinguished from the zero overlap integral $S_{anti-bond}(\varepsilon_F)$ defined in (21) between mutually antibonding layer molecular-orbital components in Fig. 6. In the limit of relatively small $S_{bond}(\varepsilon_F)$, it is also reasonable to expect that the lattice-ion displacements δ should approach the classical limit $\delta_c \sim (m/M)^{1/2}$ d mentioned above, whereas in the limit of reasonably large $S_{bond}(\varepsilon_F)$, δ should be bounded by the quantum-mechanical limit $\delta_0 \sim (m/M)^{1/4}d$. In other words, comparing expressions (28) and(26), there is an implied relation

$$(m/M)^{\beta} \sim S_{bond}(\varepsilon_F) \quad (29)$$

between the Jahn-Teller coupling parameter β and the bond overlap at the Fermi energy. For aluminum, where the $p\pi$-bond overlap at the Fermi-energy, as evaluated from the molecular-orbital wave functions mapped in Figs. 4 through 6, is small, expression (29) implies a value of $\beta \sim 1/2$. This value of β defines the limit of "weak" Jahn-Teller coupling, in which Jahn-Teller-induced lattice ion displacements δ defined in (26) are inversely proportional to the square root of the ion mass, and corresponds to the normal "isotope effect" in superconductivity. Indeed, as will be elaborated on in this paper, the dynamic Jahn-Teller coupling of electrons and lattice is the real-space molecular-orbital analogue of the coupling of electrons and virtual phonons responsible for Cooper pair formation in the BCS theory of superconductivity. [1,2] However, in the present model, electron-lattice coupling, Cooper pair formation, and superconductivity will not occur unless there is a prescribed molecular-orbital topology at the

Fermi energy, such as that shown for aluminum in Fig. 6.

In the limit of dynamic Jahn-Teller coupling, all components of the degenerate molecular orbital at the Fermi energy, including the one shown in Fig. 6 and equivalent ones pointing along orthogonal crystal directions, are dynamically accessible, resulting in an effectively isotropic attractive potential (25) of two electrons. From (25) and (26), this interaction can be written as a simple pair potential

$$V_A(r) \sim U^{(2)}_{Attr}(\varepsilon_F) \sim \begin{cases} -e^2\beta/d^2 \sim -e^2(m/M)^{\beta}/d \sim -e^2/\ell & \text{for } r < \ell \\ \sim 0 & \text{for } r > \ell \end{cases} \qquad (30)$$

where r is the relative distance of the two electrons and

$$\ell \sim (M/m)^{\beta} d \qquad (31)$$

is the effective distance and ultimate cluster radius over which the dynamic Jahn-Teller effect and attractive pair potential (30) are operative. In aluminum, where $\beta \sim \frac{1}{2}$, $\ell \sim 400\text{Å}$. Combining (22) and (30), one finds the total effective potential between the valence-bond-like pair of electrons at the Fermi energy to be

$$V(r) = V_C(r) + V_A(r) \sim \begin{cases} e^2/d - e^2/\ell & \text{for } r < d \\ -e^2/\ell & \text{for } d < r < \ell \\ 0 & \text{for } r > \ell \end{cases} \qquad (32)$$

Thus, over a distance $d < r < \ell$ spanning many atoms ($2\text{Å} < r < 400\text{Å}$ in aluminum), the effective potential of two electrons at the Fermi energy, induced by the dynamic Jahn-Teller effect, is weakly attractive relative to the average equilibrium lattice potential. As will be argued below, this attractive potential leads to Cooper-Schafroth [2,56] "quasimolecular" electron-pair binding of the type prerequisite for superconductivity.

While a value of $\beta \sim 1/2$ in (26), (29), (30), and (31) is appropriate for aluminum and other "weakly" Jahn-Teller coupled $p\pi$-electron superconductors exhibiting the normal isotope effect, values of $\beta < 1/2$ are more appropriate for transition-metal superconductors. As will be discussed in Section IV, transition-metal superconductors are characterized by degenerate molecular orbitals at the Fermi energy of "tubular" topology (see Figs. 11 through 14) arising

from dδ-bond overlap and of "layered" topology (see Fig. 16) arising from d_{z^2} planar overlap. These orbitals are argued to be responsible for Jahn-Teller coupling and Cooper-Schafroth pairing in transition-metal superconductors, just as pπ orbitals are responsible for these effects in aluminum. In general, however, dδ-bond overlap in transition metals is greater than pπ-bond overlap in non-transition metals such as aluminum, implying from (26), (28), and (29) stronger Jahn-Teller coupling and values of $\beta < 1/2$ for transition metal superconductors consistent with deviations from the ideal isotope effect (see Section IV).

If bond overlap at the Fermi energy is large enough to yield a value of $\beta \lesssim 1/4$, the Jahn-Teller coupling can result in lattice ion displacements δ greater than the zero-point amplitude $\delta_0 \sim (m/M)^{1/4} d$, i.e.,

$$\delta \sim (m/M)^{\beta} d \text{ for } \beta \lesssim 1/4. \tag{33}$$

Then the electrons at the Fermi energy can lower their energy through a periodic three-dimensional static Jahn-Teller lattice distortion [57] (or alternatively a "one-dimensional" Peierls distortion [58]) which removes or lowers the orbital degeneracy and opens up an energy gap around the Fermi energy. This process can compete with the electronic energy reduction effected by the dynamic Jahn-Teller effect, Cooper-Schafroth pairing, and the opening up of the superconducting state energy gap Δ defined in Eq. (15). Indeed structural phase transitions corresponding to static Jahn-Teller distortions of the crystal lattice from cubic to lower (e.g., tetragonal) symmetry are well known to occur in certain high-temperature transition-metal-compound superconductors (e.g., A15 compounds), [58] and such "lattice instabilities" are suspected to reduce the superconducting-state transition temperature T_c otherwise attainable. [58,3] In any case, the conjecture that the interactions responsible for these structural transformations and high-temperature superconductivity are similar [58] is supported by the present theoretical model.

Finally, when the degeneracy of the spatially extended bonding molecular orbitals at the Fermi energy is removed or lowered by a static Jahn-Teller

distortion, Peierls distortion, or intrinsically low (non-cubic) crystal symmetry, it is still possible, within the framework of this model, for Cooper-Schafroth electron pairing and superconductivity to occur via dynamic "pseudo-Jahn-Teller" electron-lattice coupling [57] triggered by dynamical fluctuations in electron occupancy or "mixing" of the nearly degenerate molecular orbitals. Because of the different spatial orientations of these orbitals, this process can involve fluctuations in orbital charge distribution around the Fermi energy and therefore fluctuations δ in the relative instantaneous locations of bond charge and lattice-ion positions at the Fermi energy approaching the interorbital spacing d. Such large relative displacements of electrons and nuclei imply, according to (33), a value of β approaching zero. Since fluctuations in electron occupancy or electronic "excitations" between nearly degenerate molecular orbitals around the Fermi energy are associated with the dynamic "quasi-Jahn-Teller" effect, [57] this process can be viewed as having a purely electronic (i.e., "non-phonon") component. However, this "excitational" mechanism is dependent on the same molecular-orbital topologies prerequisite to the above-described conventional dynamic Jahn-Teller (electron-phonon) coupling mechanism and thus should not be confused with "excitonic" mechanisms for superconductivity proposed by other workers. [10,11] Like the ordinary dynamic Jahn-Teller effect, the dynamic "quasi-Jahn-Teller" effect can produce an attractive electron pair potential of the form (30), although since $\delta \sim d$ and $\beta \sim 0$, the potential is of short-range character and is largely cancelled out by the screened repulsive Coulomb potential (22). It is possible that the latter mechanism is primarily responsible for Cooper-Schafroth pairing and superconductivity in certain non-cubic transition models (e.g., Zr and Ru), transition-metal compounds (e.g., A15 and "layered" compounds), and amorphous transition-metal alloys (e.g., CuZr), which exhibit vanishing ($\beta \sim 0$) or anomalous isotope effects and where the molecular orbitals at the Fermi energy responsible for superconductivity are dd-bonding "tubular"

orbitals of the types shown in Figs. 11 through 14 (see Section IV).

In order to make a more formal connection between this model and the BCS theory of superconductivity, [1] one can make use of simple physical arguments recently proposed by Weisskopf [59] for the formation of Cooper pairs in the BCS theory. In Weisskopf's model for a superconductor, an electron moving at the Fermi energy with momentum (2) and speed

$$v_e = p_F/m \approx h/2md \tag{34}$$

transfers some of its momentum to neighboring ions of the lattice, causing ion displacements δ toward the electron path of magnitude (26) in the limit $\beta \sim \frac{1}{2}$. However, the ions do not remain in their displaced positions indefinitely but return to their equilibrium lattice positions in a time of order ω_D^{-1}, where

$$\omega_D \sim h/2(mM)^{1/2}d^2 \tag{35}$$

is the approximate expression for the lattice Debye frequency derived by Weisskopf. [59] Thus, an ion displacement toward the electron path can be viewed as extending over a distance

$$\ell \sim v_e/\omega_D \tag{36}$$

behind the electron and producing over this distance an attractive potential for a second electron moving "head-on" in the opposite direction. This is Weisskopf's simple physical picture of the emission of a virtual phonon by one electron and the absorption of the phonon by a second electron responsible for electron-electron attraction and Cooper pair formation in the BCS theory. [1,2] Substitution of (34) and (35) into (36) yields the expression (31) for ℓ derived above in the limit $\beta \sim \frac{1}{2}$ from the dynamic Jahn-Teller effect, so that the effective attractive electron-pair potential can be written in the form (30), which Weisskopf views as being contained in a "long thin tube" of length ℓ and diameter d while acting only on electrons of opposite linear momentum, opposite spin, and in a relative "S-state" (relative angular momentum L = 0).

Thus, Weisskopf's model and the present molecular-orbital model are in

basic agreement as to the general form of the attractive potential responsible for Cooper pairing in a superconductor in the limit $\beta \sim \frac{1}{2}$, and both models lead to simple "real-space" pictures of the electron-lattice coupling which are analogous to the electron-phonon coupling mechanism in the BCS theory. However, Weisskopf's intuitive picture of the electron-lattice coupling in a superconductor, like the original BCS theory, does not address the question of which materials are superconductors and which are not, and it does not account for superconductors with vanishing isotope effect ($\beta \sim 0$). On the other hand, the molecular-orbital model suggests that superconductivity will not occur unless there are certain types of spatially extended orbital topology (e.g., like that in Fig. 6) at the Fermi energy, which promote Cooper-Schafroth electron pairing via the dynamic Jahn-Teller effect for $\beta \sim \frac{1}{2}$ and via the dynamic "quasi-Jahn-Teller" effect for $\beta \sim 0$.

To determine the quasimolecular binding energy (15) of a Cooper-Schafroth electron pair and the superconducting transition temperature T_c from the present theoretical model, one can follow Weisskopf's [59] procedure and solve Schrödinger's equation

$$[p^2/2\mu + V(r)]\psi(r) = E\psi(r) \tag{37}$$

for two electrons of relative distance r, relative linear momentum p, total linear momentum P = 0, relative angular momentum L = 0, and reduced mass $\mu = m/2$, subject to the potential (32). Because this potential is attractive over a distance $d < r < \ell$ ($2\text{Å} < r < 400\text{Å}$ in Al) spanning many atoms and vanishes for $r > \ell$, the repulsive component for $0 < r < d$ ($0 < r < 2\text{Å}$ in Al) should not strongly influence the binding energy and large spatial extent of the pair wave function. Thus one can solve Eq. (37) to good approximation only for the attractive component (30) of the potential, subject to the boundary condition $\psi(d) = 0$.

The Schrödinger equation (37) is effectively a one-dimensional wave equation whose solution $\psi(r)$ is actually r times the three-dimensional valence-

bond-like wave function (6). Since the latter wave function is expressed in terms of the cluster layer orbitals ψ_+ and ψ_- shown in Fig. 6, which have damped standing-sine-wave-like character along r, it is appropriate to expand the solution of (37), namely

$$\psi(r) = \sum_{p' > p_F} a(p')\psi(p';r), \tag{38}$$

in the set of sinusoidal basis functions

$$\psi(p;r) = (2/R)^{1/2}\sin(pr/\hbar) \tag{39}$$

normalized to a large sphere of radius $R \gtrsim \ell$, as given by (31). This sphere radius defines the ultimate cluster size necessary to describe the full spatial extent of the quasimolecular electron-pair wave function (e.g., $R \gtrsim 400\text{Å}$ in Al). The summation in (38) excludes the momenta $p < p_F$ corresponding to other electrons below the Fermi energy, and for a pair wave function of large spatial extent the coefficients a(p) will be large only for $p \sim p_F \sim h/2d$ [see Eq. (2)]. Note that for such values of momentum the basis functions (39) satisfy the boundary condition $\psi(p;d) = 0$. It should be emphasized that, while the basis functions (39) are identical to the free-electron basis set adopted by Weisskopf [59] and are equivalent ot the plane-wave basis of the BCS theory, [1] their simple sinusoidal form is actually a by-product of the layered topology of the composite bonding-antibonding molecular orbitals at the Fermi energy shown in Fig. 6. Thus the following derivation of the Cooper pair binding energy and transition temperature for superconductivity using this basis set is strictly valid only for substances that have the prerequisite molecular-orbital topology at the Fermi energy.

Substitution of (38) into (37), multiplication of both sides of the resulting equation by (39), and integration over the sphere of radius R yields

$$a(p)(p^2/m - E) = -\sum_{p' > p_F} a(p')\int_0^R \psi(p;r)V(r)\psi(p';r)dr. \tag{40}$$

Using the identity

$$\psi(p;r)\psi(p';r) = (1/R)\{\cos[(p-p')r/\hbar] - \cos[(p + p')r/\hbar]\}, \tag{41}$$

and the fact that the largest terms in the summation of (40) occur for momenta $p' \sim p \sim p_F \sim h/2d$, for the potential given in (30), the integral in (40) reduces approximately to

$$\int_0^R \psi(p;r)V(r)\psi(p';r)dr \sim \begin{cases} -(e^2/R)(1 - d/\ell) & \text{for } p - p' < \hbar/\ell \\ 0 & \text{for } p - p' > \hbar/\ell \end{cases} \tag{42}$$

or substituting (31) in the right side of (42), to

$$\int_0^R \psi(p;r)V(r)\psi(p';r)dr \sim \begin{cases} -(e^2/R)[1 - (m/M)^{\beta}] & \text{for } p - p' < \hbar/(M/m)^{\beta}d \\ 0 & \text{for } p - p' > \hbar/(M/m)^{\beta}d, \end{cases} \tag{43}$$

which is an attractive pair pseudopotential for $\ell > d$ or $\beta > 0$. Since the electron pair binding energy is to be determined with respect ot the Fermi energy of otherwise independent electrons, it is convenient to introduce the new energy variable

$$\varepsilon \equiv (p^2/m) - 2\varepsilon_F = (p^2 - p_F^2)/m \tag{44}$$

and to rewrite Eq. (40) in terms of ε and the quasimolecular pair binding energy Δ defined in Eq. (15). Thus, in place of (40), one can write

$$a(\varepsilon)(\varepsilon + \Delta) = -\sum_{\varepsilon' > 0} a(\varepsilon')\int_0^R \psi(\varepsilon;r)V(r)\psi(\varepsilon';r)dr, \tag{45}$$

where the summation excludes the energies corresponding to electron states below the Fermi energy, since such states do not contribute to Cooper pairing. The energy interval $\varepsilon - \varepsilon'$ that corresponds to the maximum momentum difference $p - p' \sim \hbar/\ell$ in (42) is, using expressions (2) and (31),

$$\begin{aligned} \Delta\varepsilon = (\varepsilon - \varepsilon')_{max} &\sim (2p_F/m)(p - p')_{max} \\ &\sim (h/md)(\hbar/\ell) \\ &\sim h^2/2\pi m(M/m)^{\beta}d^2. \end{aligned} \tag{46}$$

Thus the integral in (45) reduces to a pseudopotential expression analogous to (43), namely,

$$\int_0^R \psi(\varepsilon;r)V(r)\psi(\varepsilon';r)dr \sim \begin{cases} -(e^2/R)[1 - (m/M)^\beta] & \text{for } \varepsilon - \varepsilon' < \Delta\varepsilon \\ 0 & \text{for } \varepsilon - \varepsilon' > \Delta\varepsilon. \end{cases} \tag{47}$$

Substitution of (47) in (45) and conversion of the summation in the latter equation to an integration yields

$$a(\varepsilon)(\varepsilon + \Delta) \sim N(0)(e^2/R)[1 - (m/M)^\beta]\int_0^{\Delta\varepsilon + \varepsilon} a(\varepsilon')d\varepsilon', \tag{48}$$

where

$$N(0) \sim (R/2\pi)(m/\hbar p_F) \sim 2mRd/h^2 \tag{49}$$

is the number of sinusoidal basis functions (39) of de Broglie wavelength $\lambda_F = 2d$ [see Eq. (2)] per molecular orbital (e.g.,per layered molecular orbital in Fig. 6) per unit energy $d\varepsilon$ around the Fermi energy ε_F, normalized to the sphere of radius R. Expression (49) defines the molecular-orbital "density of states" at the Fermi energy. Substitution of (49) into (48) yields

$$\begin{aligned} a(\varepsilon)(\varepsilon + \Delta) &\sim (2me^2d/h^2)[1 - (m/M)^\beta]\int_0^{\Delta\varepsilon + \varepsilon} a(\varepsilon')d\varepsilon' \\ &\sim (2me^2d/h^2)[1 - (m/M)^\beta]\int_0^{\Delta\varepsilon} a(\varepsilon')d\varepsilon' \end{aligned} \tag{50}$$

in which the R-dependence of the orbital density of states (49) and the R-dependence of the pseudopotential $(e^2/R)[1 - (m/M)^\beta]$ are cancelled out through their product in (48). Furthermore, because the coefficients a(p') in (40) are significantly different from zero only for p' close to p_F, the coefficients $a(\varepsilon')$ in (50) are significant only for $\varepsilon' << \Delta\varepsilon$, thus allowing one to use $\Delta\varepsilon$ as the upper limit of integration in (50). Since the resulting integral in (50) is independent of ε, it can be set equal to the constant

$$C \equiv \int_0^{\Delta\varepsilon} a(\varepsilon')d\varepsilon', \tag{51}$$

and Eq. (50) can be solved for $a(\varepsilon)$, giving

$$a(\varepsilon) \sim (2me^2d/h^2)[1 - (m/M)^\beta]C(\varepsilon + \Delta)^{-1}. \tag{52}$$

Substituting (52) for $\varepsilon = \varepsilon'$ in (51) and cancelling out the constant C, one finds

$$1 \sim (2me^2d/h^2)[1 - (m/M)^{\beta}]\int_0^{\Delta\varepsilon}(\varepsilon' + \Delta)^{-1}d\varepsilon'$$
$$\sim (2me^2d/h^2)[1 - (m/M)^{\beta}]\ell n[(\Delta\varepsilon + \Delta)/\Delta] \qquad (53)$$
$$\sim (2me^2d/h^2)[1 - (m/M)^{\beta}]\ell n(\Delta\varepsilon/\Delta),$$

where the final expression (53) results from the fact that the quasimolecular electron-pair binding energy Δ should be significantly less than the maximum energy interval $\Delta\varepsilon$ defined in (46). Substituting (46) in (53) and solving for Δ, one obtains

$$\Delta \sim [h^2(m/M)^{\beta}/2\pi md^2]\exp\{-h^2/2me^2d[1 - (m/M)^{\beta}]\}. \qquad (54)$$

Using the established relation between the superconducting energy gap and transition temperature, namely, [1,60,61]

$$\Delta \sim 2k_BT \text{ (or, more precisely, } k_BT = 0.57\ \Delta), \qquad (55)$$

where k_B is Boltzmann's constant, expression (54) can be reformulated in terms of T_c, giving

$$k_BT_c \sim [h^2(m/M)^{\beta}/4\pi md^2]\exp[-h^2/\{2me^2d[1 - (m/M)^{\beta}]\}] \qquad (56)$$

In turn, expression (56) can be put into the form

$$k_BT_c \sim \hbar\omega_c \exp[-1/(\lambda - \mu^*)] \qquad (57)$$

where

$$\hbar\omega_c \equiv h^2(m/M)^{\beta}/4\pi md^2 \qquad (58)$$

$$\lambda \equiv 2me^2d/h^2 = N(0)(e^2/R) \equiv N(0)V \qquad (59)$$

and

$$\mu^* \equiv (2me^2d/h^2)(m/M)^{\beta} = N(0)(e^2/R)(m/M)^{\beta} \equiv N(0)U. \qquad (60)$$

The molecular-orbital "density of states" at the Fermi energy, N(0) defined in Eq. (49), has been incorporated into expressions (59) and (60).

Expression (56) reformulated as (57) is the product of a preexponential function of the "cut-off frequency" ω_c defined in (58) and an exponential function of the attractive electron pair interaction parameter λ (or attractive electron pair pseudopotential V) defined in (59) and the repulsive screened

Coulomb interaction parameter μ^* (or Coulomb pseudopotential U) defined in (60). Thus (56) and (57), derived directly from molecular-orbital theory, are in the form of a generalized BCS-like expression for the superconducting transition temperature which allows for values of the Jahn-Teller coupling parameter $\beta \lesssim \frac{1}{2}$ [see (26) and (33)] and consequently is applicable to all superconducting materials, including transition metals (see Section V) where the simple $M^{-1/2}$ dependence of T_c predicted by the original BCS theory [1] is not confirmed by experiment [60].

To relate the present molecular-orbital formulation to the original BCS theory, [1] we consider the reduction of expressions (56) and (57) for the value $\beta \sim \frac{1}{2}$. In this limit, the factor $(m/M)^{\beta}$ in (56) is negligible compared with unity and $\mu^* << \lambda$ in (57). Furthermore, for $\beta \sim \frac{1}{2}$, the cut-off frequency ω_c, defined in (58), reduces to the lattice Debye frequency ω_D defined in (35). Therefore, in place of (56) and (57), one can write

$$\lim_{\beta \to 1/2} k_B T_c \sim [h^2/4\pi(mM)^{1/2}d^2]\exp(-h^2/2me^2d), \tag{61}$$

and, using (35) and (59),

$$\begin{aligned} \lim_{\beta \to 1/2} k_B T_c &\sim \hbar\omega_D \exp(-1/\lambda) \\ &\sim \hbar\omega_D \exp[-1/N(0)V]. \end{aligned} \tag{62}$$

Finally, since the Debye frequency ω_D is related to the Debye temperature Θ_D through the formula

$$k_B\Theta_D = \hbar\omega_D, \tag{63}$$

the last expression in (62) reduces to

$$\lim_{\beta \to 1/2} T_c \sim \Theta_D \exp[-1/N(0)V],$$

which is identical in form to the original BCS expression (1) for T_c.

The original BCS formula (1) for the superconducting transition temperature has been difficult to apply from first principles to real materials because it presumes a knowledge of the band-structure density of states at the Fermi energy, N(0), and the attractive electron-phonon coupling potential V. These two quantities are often not known to high accuracy, especially V, and therefore

must be estimated semiempirically to correlate with experimentally determined values of T_c. Furthermore, for certain transition metals, their alloys and compounds, the simple dependence of T_c on $M^{-1/2}$ predicted by the BCS formula (1) [see also expression (61)] is not confirmed experimentally by the "isotope effect."[60] In attempts to explain the variation in isotope effect among superconductors, without invoking alternative mechanisms for Cooper pairing, the original BCS theory has been generalized by various workers [60,64] to include a more accurate treatment of the combined effects of Coulomb electron-electron repulsion and phonon-induced electron-electron attraction in determining the net potential V in expression (1). The formulae for T_c in these generalized versions of BCS theory are in the form of expression (57), although the specific definitions of the parameters $\bar{h}\omega_c$, λ, and μ^* differ from expressions (58) through (60) and vary somewhat with the investigator. [60,64] Exciton models [10,11] and other "non-phonon" mechansism [65-67] for superconductivity also assume a generalized BCS-like formula (57) for T_c, in which $\bar{h}\omega_c$ is the maximum energy of the electronic excitation, λ is the electron-exciton coupling constant, and μ^* is the screened Coulomb repulsion. Thus far, there is no definitive experimental evidence for the existence of superconductors based on excitonic or other non-phonon mechanisms of the types described in Refs. 10, 11, 65, 66, and 67.

The present molecular-orbital model for Cooper-Schafroth pairing and superconductivity complements BCS theory and clarifies the issue of non-phonon mechanisms for superconductivity in the following respects:

1. It permits one to assess which materials are likely to be superconductors and which are not on the basis of simple criteria for extended molecular-orbital topology at the Fermi energy, as deduced from SCF-Xα-SW cluster molecular-orbital calculations.
2. It permits the approximate calculation of the superconducting transition temperature via Eq. (56) directly in terms of two simple parameters derived

from first principles SCF-Xα-SW cluster molecular-orbital studies, namely, a local distance parameter d of the order of magnitude of the interatomic distance and a Jahn-Teller coupling parameter β, instead of in terms of the electronic density of states N(0), electron-phonon pseudopotential V, and Coulomb pseudopotential U.

3. While the present molecular-orbital model reduces to a BCS-like theory for weakly Jahn-Teller-coupled pπ-bonded superconductors such as aluminum, where $\beta \sim \frac{1}{2}$, it is also readily applicable to more strongly Jahn-Teller-coupled dδ-bonded transition-metal superconductors, including compounds and alloys, that exhibit an anomalous "isotope effect," i.e., where $\beta < \frac{1}{2}$ (see Section IV). In this respect, Eq. (56) written in the form (57) already includes, without further generalizations of the types described in Refs. 60-64, the effects of screened Coulomb repulsion through the dependence of both the quantity μ^* [defined in (60)] and pre-exponential energy $\bar{\hbar}\omega_c$ [defined in (58)] on the factor $(m/M)^3$, which increases rapidly with decreasing β.

4. For $1/4 < \beta \lesssim 1/2$, where the relative displacement (26) of the electron pair and lattice ions is less than the zero-point vibrational amplitude $\delta_0 \sim (m/M)^{1/4} d$ of the lattice, <u>dynamic</u> Jahn-Teller coupling of the electrons and lattice ions, driven by the degeneracy of the spatially extended (e.g., pπ, dδ-bonding) molecular orbitals at the Fermi energy, is responsible for Cooper-Schafroth pairing and superconductivity. This range of β implies very small values of $(m/M)^\beta$ and μ^* [see Eq. (60)] and values of $\bar{\hbar}\omega_c$ approaching the Debye energy $\bar{\hbar}\omega_D$ [see Eqs. (35) and (58)]. In the limit $\beta \sim \frac{1}{2}$, corresponding to $(m/M)^{1/2}$ (the "isotope effect"), the present model is fully equivalent ot the original BCS theory [see Eq. (62)].

5. For $\beta \lesssim 1/4$, where the relative displacement (33)of the electron pair and lattice ions is greater than or equal to the zero-point vibrational amplitude $\delta_0 \sim (m/M)^{1/4} d$ of the lattice, a static Jahn-Teller (or Peierls) distortion of the lattice can remove the molecular-orbital degeneracy at the Fermi energy, producing a lattice instability and structural transformation (e.g., from cubic to tetragonal symmetry). An intrinsically low crystal symmetry or amorphous structure can also remove the molecular-orbital degeneracy at the Fermi energy. If the energy gaps between the resulting non-degenerate orbitals are not too large, then Cooper-Schafroth pairing and superconductivity can still occur via dynamic pseudo-Jahn-Teller coupling of the electrons and lattice ions induced by the mixing of the nearly degenerate molecular orbitals around the Fermi energy or through fluctuations in orbital occupancy. The above values of β imply relatively large values of $(m/M)^{\beta}$ and μ^* [see Eq. (60)] and values of $\bar{h}\omega_c$ approaching the Fermi energy [see Eq. (58)]. In the limit $\beta \sim 0$, the present model yields an explanation of the vanishing isotope effect in certain (e.g., transition-metal) superconductors, thereby precluding the necessity for ad hoc generalizations of BCS theory [60-64] or esoteric non-phonon mechanisms of superconductivity [10,11,65-67] in such materials. Finally, this model, based on molecular-orbital topology at the Fermi energy and Jahn-Teller effects, supports the conjecture that the interactions responsible for lattice instabilities and structural phase transformations are similar to those responsible for superconductivity in the same materials (e.g, A15 compounds). [58]
6. the present theoretical model permits a simple description, analogous to that originally suggested by Schafroth, [56] of Cooper pairs as "quasimolecules" undergoing Bose-Einstein-like condensation to the many-electron superconducting state. The spatially delocalized "valence-bond-like" correlation of an electron pair over many "layered" or "tubular"

molecular-orbital components ψ_+ and ψ_- [see Figs. 6 and 11 and Eq. (6)] uses up only a very small fraction of the available phase space defined by the layered or tubular "cells." Thus there is ample phase space left to put more electron pairs into the same valence-bond-like pair function (6).

As an illustration of the quantitative application of the above formulae, we continue with the example of the "weakly Jahn-Teller coupled" ($\beta \sim \frac{1}{2}$) superconductor , aluminum, where expression (61) for the superconducting transition temperature is valid. From the SCF-Xα-SW cluster molecular-orbital contour map in Fig. 6, which is a direct measure of the layer orbital parameter d, a value of $d \sim 1.8\mathring{A}$ appropriate to bulk crystalline aluminum is obtained. Substitution of the latter in Eq. (61) yields the transition temperature $T_c \sim 1.2°K$. The latter agrees very well with the experimental value $(T_c)_{expt} \sim 1.18°K$ for bulk aluminum. [68] The Debye temperature of aluminum, calculated on the basis of expressions (35) and (63), is 385°K, which also compares well with the experimental value $(\Theta_D)_{expt} \sim 375°K$. [68] Expression (61) is further consistent with the observed increase of transition temperature with decreasing aluminum particle size, namely, $(T_c)_{expt} \sim 1.5°K$ to 2.5°K for particle diameters between $150\mathring{A}$ and $50\mathring{A}$, respectively. [5,6] Similar increases of T_c with decreasing grain size have been measured for evaporated aluminum thin films. [69,70] Close scrutiny of Figs. 4 through 6 reveals a significant increase of the layer-orbital parameter d to a value of $\sim 2.1\mathring{A}$ around the coordinatively unsaturated atoms at the cluster periphery, due to decreased net bonding-antibonding interactions there, as compared with the value $d \sim 1.8\mathring{A}$ appropriate to the fully coordinated central atom of the cluster representing the local environment of the bulk crystal. For particle diameters from $150\mathring{A}$ to $50\mathring{A}$, the percentage of surface atoms with respect to the total number of atoms in the particle varies from ~ 15% to 40%, respectively. [71] Thus, according to expression (61), such increases of d at small-particle surfaces and grain boundaries should increase T_c to a measurable degree. Substitution of

the value $d \sim 2.1\text{Å}$ into (61) yields $T_c \sim 1.9°K$, which is within the range $(T_c)_{expt} \sim 1.5°K$ to $2.5°K$ observed for particles between $\sim 150\text{Å}$ and 50Å. [5,6] Using weighted averages of the value $d \sim 2.1\text{Å}$ appropriate to atoms at the cluster boundary or "surface" and the value $d \sim 1.8\text{Å}$ appropriate to bulk atoms in Eq. (61) with the weighting determined by the relative percentages of surface and bulk atoms, accounts for the measured variation of T_c with particle size. Note that, according to Eq. (35), such increases of d imply a reduction or "softening" of the phonon cut-off frequency (the Debye frequency) ω_D, explaining the larger T_c within the framework of BCS theory. [72] Finally, comparative decreases of the orbital parameter d under compression of the atoms seem to account through Eq. (61) for substantial decreases of T_c for aluminum under pressure.

The above theoretical model for superconducting aluminum is also consistent with the observation that certain types of magnetic impurities in aluminum destroy or degrade its superconductivity. A good example is Mn, whose effects in aluminum can be modeled in a fashion analogous to the treatment of Mn in copper (see Ref. 39) by substituting a Mn atom for the central Al atom in the 43-atom cluster model of crystalline aluminum. This yields a $MnAl_{12}Al_6Al_{24}$ cluster representing the local crystal environment of the impurity up to third-nearest neighbors. The SCF-Xα-SW molecular-orbital energy levels for this cluster are shown in Fig. 8, where they are compared with the X-ray photoelectron spectrum (XPS) [73] of crystalline aluminum containing a small percentage of substitutional Mn impurities. Comparing Fig. 8 with the SCF-Xα-SW cluster moelcular-orbital energies for pure aluminum shown in Figs. 2 and 3, we see that the main effects of alloying Mn impurities in an aluminum host, neglecting impurity-impurity interactions, are: (1) to empty out locally the otherwise spatially extended $t_{1u}(p\pi)$ "layered" molecular orbital (mapped in Figs. 4 through 7) shown above to be responsible for the superconductivity of pure aluminum; and (2) for the Mn 3d orbitals to

overlap and hybridize with the surrounding Al 3p orbitals to produce a narrow manifold of occupied spatially localized bonding and antibonding t_{2g} and e_g molecular orbitals , which are responsible for the peak in XPS intensity just below the Fermi energy (the dashed line) in Fig. 8. The highest occupied molecular orbitals of the $MnAl_{12}Al_6Al_{24}$ cluster are nearly degenerate t_{2g} and e_g dpσ*-dpπ* antibonding orbitals sharing five electrons, immediately above which lies the emptied aluminum $t_{1u}(p\pi)$ orbital, as indicated in the inset of Fig. 8. The dpσ*-dpπ* antibonding topology of the former orbitals is clearly evident in the wave function contour maps of Figs. 9 and 10. These orbitals are analogous to the t_{2g} and e_g dsdσ*-ddsπ* antibonding orbitals previously shown in Ref. 39 to be associated with the local spin magnetic moments of Mn and Fe impurities in a copper host above the Kondo temperature. However, for Mn impurities in aluminum, the fluctuations in occupancy of the nearly degenerate individual t_{2g} and e_g antibonding orbitals by five electrons, coupled with relatively small exchange splitting of the orbital energies, prevent stable magnetic moment formation and are responsible for "spin fluctuations" in this system. [74] The SCF-Xα-SW cluster molecular-orbital model thus provides a real-space chemical picture of how Mn impurities in aluminum host degrade the superconductivity of aluminum by locally emptying the otherwise spatially extended layered pπ orbital responsible for Cooper-Schafroth electron pairing and producing as the highest occupied orbitals spatially localized dpσ*-dpπ* antibonding orbitals with flucuating spin magnetic moment. These findings are relevant to the general issue of superconductivity vs. magnetism which will be discussed in Section VI of this paper.

IV. TRANSITION-METAL SUPERCONDUCTORS

As illustrations of the ways d orbitals of transition metals, their alloys and compounds can combine to form around the Fermi energy coherent, spatially extended bonding molecular-orbital precursors to Cooper-Schafroth

pairing and superconductivity, consider Figs. 11 and 12. These diagrams show schematically how d_{xy} and $d_{x^2-y^2}$ atomic orbitals, for the chosen coordinate system, can overlap along a line of atoms extending along the z-axis to form "dδ-type" molecular orbitals. It is well known in inorganic chemistry [75] that dδ molecular orbitals contribute to multiple (e.g. quadruple) metal-metal bond formation in certain transition-metal coordination complexes (e.g., $Mo_2Cl_8^{4-}$). [76] In such complexes, the dδ-bonding orbitals are the highest occupied molecular orbitals, while the fully occupied dπ- and dσ-bonding orbitals have significantly larger binding energies. [77] Likewise, dδ orbitals are known to be the principal components of the d-band density of states around the Fermi energy in superconducting A15 compounds (e.g., Nb_3Sn), [78,79] where they may be viewed simplistically as forming a three-dimensional network of intersecting chains of dδ-bonding orbitals like those shown schematically in Figs. 11 and 12. What has not been widely recognized by many solid state physicists is that dδ-bonding molecular orbitals of the types shown schematically in Figs. 13 and 14 are mainly responsible for the peak in the d-band density of states around the Fermi energy for bcc transition-metal superconductors such as V, Nb, and Ta, as indicated in the composite density-of-states diagram of Fig. 15 based on SCF-Xα-SW cluster molecular-orbital calculations.

In Figs. 11 through 14, it can be seen that the dδ-bond overlap is such as to form "tubes" parallel to the z-axis. From these "tubular orbitals," labeled ψ_+ and ψ_- according to the sign of the wave function d-lobe, in analogy to the pπ "layer orbitals" in Fig. 6, one can construct a Cooper-Schafroth electron-pair singlet wave function as a "valence-bond-like" product of space and spin components of the form (6) and (7). Note in Figs. 11 through 14 that, if the tubular molecular-orbital components ψ_+ correspond to a "spin-up" (↑) electron, then the tubular components ψ_- correspond to a "spin-down" (↓) electron, and, vice versa, suggesting an "antiferromagnetic" ordering of the alternating dδ tubular orbitals analogous to the "antiferromagnetic" ordering

of $p\pi$ layered orbitals (fig. 6) in superconducting aluminum described in Section III. However, the net spin polarization per atom is zero, and therefore this delocalized "conduction-electron antiferromagnetism" should be distinguished from conventional antiferromagnetism localized on paramagnetic atoms (see further discussion in Section VI). Indeed, there is recent experimental evidence for the "antiferromagnetic" ordering of conduction electrons in A15 superconductors. [80]

All of the mathematical steps in going from the pair wave-function components (6) and (7) to the final expression (56) for the superconducting transition temperature, derived on the basis of $p\pi$ layer-orbital components ψ_+ and ψ_-, are also applicable to the $d\delta$ tubular orbitals ψ_+ and ψ_-. In the latter case, the interorbital distance d for the screened Coulomb repulsion (22) is the perpendicular distance between parallel nearest-neighbor tubular orbitals ψ_+ and ψ_- at maximum $d\delta$ bond overlap. The Jahn-Teller coupling parameter λ is determined by the $d\delta$ covalent overlap in much the same fashion as the $p\sigma$ covalent overlap determines the value of $\beta \sim \frac{1}{2}$ for aluminum. As already mentioned in Section III, values of β spanning the range $0 < \beta < 1/2$ are appropriate for various transition-metal systems, depending on $d\delta$-bond overlap and molecular-orbital degeneracy at the Fermi energy.

While the d_{xy} (or degenerate d_{yz}, d_{xz}) and $d_{x^2-y^2}$ orbitals in transition metals can produce $d\delta$ tubular molecular orbitals of the topology shown in Figs. 11 through 14, which are precursors to the superconducting state, d_{z^2} orbitals can weakly bond through annular overlap of the type shown schematically in Fig. 16. This overlap results in "layered" molecular-orbital components ψ_+ and ψ_- which, like the layered $p\pi$ orbitals shown in Fig. 6, can be used to construct valence-bond-like Cooper-Schafroth electron-pair wave functions of the form (6). SCF-$X\alpha$-SW cluster molecular-orbital calculations indicate that overlapping d_{z^2} orbitals of the type shown in Fig. 16 are principal components of the d band at the Fermi energy in superconducting transition-

metal dichalcogenides (e.g., NbS_2) [81] having a layered crystal structure. As will be shown below, somewhat similar layered d_z2 orbitals also occur in the vicinity of the Fermi energy in certain elemental transition metals (e.g., Nb) and contribute along with dδ-type orbitals to superconductivity.

A. Elemental Transition-Metal Superconductors with bcc Structure

With the above general characteristics of dδ and d_z2 molecular-orbital topologies in superconducting transition-metal systems in mind, specific examples using the formalism developed in Section III will now be discussed. Consider first the group of elemental transition-metal superconductors having bcc crystal structure, namely, V, Nb, Ta, Mo, and W. SCF-Xα-SW cluster molecular-orbital models for these systems, along with similar studies of antiferromagnetic bcc Cr and ferromagnetic Fe, can be summarized in the form of an approximate composite non-spin-polarized "density-of-states" profile (shown in Fig. 15), in which the locations of the Fermi energies of the various metals are indicated and the principal component bonding and antibonding molecular orbitals associated with peaks in the density of states are shown. Note in particular that the Fermi energies of V, Nb, and Ta are located near the density-of-states peak associated with dδ-bonding orbitals of the types shown in Figs. 13 and 14. These Group-VB elements are among those having the highest superconducting transition temperatures in the periodic table, namely, V(T_c = 5.4°K), Nb(T_c = 9.2°K), and Ta(T_c = 4.5°K). [82] Most certainly, the high T_c values correlate roughly with the BCS formula (1) through the nigh density of states N(0) at the Fermi energy. However, the variations of T_c and significant deviations from the isotope effect among these elements are not consistent with the original BCS theory, [1] although formal extensions of this theory have been made to account for these discrepancies. [61-64] As will be shown below, details of the molecular-orbital topology at the Fermi energy, in conjuntion with expression (56) for T_c, can rationalize the

differences among the superconducting properties of V, Nb, and Ta.

SCF-Xα-SW cluster model calculations for vanadium reveal that the Fermi level coincides with a triply-degenerate $t_{2g}(d_{xy}, d_{yz}, d_{xz})$ molecular orbital of the dδ "tubular" topology shown schematically in Fig. 13. The actual SCF-Xα-SW numerical wave function contour map of this orbital is displayed in Fig. 17. From this wave function, the intertubular-orbital distance parameter is approximately determined to be $d \sim 1.5\text{Å}$, and the Jahn-Teller coupling parameter appropriate to the dδ bond overlap is, using expression (29), $\beta \sim 0.25$. Note that this value of β is on the borderline between the ranges of values appropriate to the dynamic and static Jahn-Teller effects [cf. Eqs. (26) and (33)]. Indeed, there is some experimental evidence [83] for a cubic-to-tetragonal structural phase transformation (static Jahn-Teller distortion) above the superconducting transition to the superconducting state. Substitution of the above values of d and β in expression (56) yields a value of $T_c \sim 5.2°K$, which is in good agreement with the experimental value $(T_c)_{expt} \sim 5.4°K$.

For the example of niobium, SCF-Xα-SW cluster calculations indicate that, in contrast to vanadium, the Fermi level coincides with a molecular orbital of $e_g(d_{x^2-y^2}, d_{z^2})$ symmetry. In V the latter orbital is just below the Fermi level, $t_{2g}(d_{xy}, d_{yz}, d_{xz})$, whereas in Nb this ordering is reversed. Contour maps of the $e_g(d_{x^2-y^2})$ orbital wave function at the Fermi energy of Nb are shown for two different planes in Figs. 18(a) and 18(b), revealing the "tubular" dδ bonding along a chain of Nb atoms. On the other hand, the degenerate $e_g(d_{z^2})$ partner of this representation produces a "layered" orbital configuration of the type shown in Fig. 19, where the "pd hybridization" between nearest-neighbor Nb atoms is responsible for the complex topology of the wave function. Clearly, the anisotropy between the degenerate $e_g(d_{x^2-y^2})$ "tubular" dδ orbital and $e_g(d_{z^2})$ "planar" dp-hybrid orbital at the Fermi energy of Nb, as compared with the topologically equivalent degenerate $t_{2g}(d_{xy}, d_{yz}, d_{xz})$ orbitals of V, suggests that the superconducting properties

of these two transition metals are likely to be intrinsically different, in spite of the fact that they are located in the same column of the periodic table and have qualitatively similar densities of states (Fig. 15). Indeed, it has been found by some workers [84] that it is difficult to explain certain tunneling experiments on Nb without violating the conventions of strong-coupling superconducting theory, whereas V seems to conform to the latter theory. The present theoretical model straightforwardly yields through expression (56), for parameters $d \sim 2.3\text{Å}$ and $\beta \sim 0.35$ derived from the calculated SCF-Xα-SW molecular orbitals of Nb and relation (29), a transition temperature of $T_c \sim 8.6°K$, which is in reasonable agreement with the experimental value $(T_c)_{expt} = 9.2°K$. The higher calculated and measured transition temperatures (and perhaps other superconducting properties) of Nb, as compared with V, are thus explained within the framework of the present theoretical model as resulting form a reversal in the ordering of two nearly degenerate topologically different molecular orbitals, $e_g(d_{x^2-y^2}, d_{z^2})$ and $t_{2g}(d_{xy}, d_{yz}, d_{xz})$, at the Fermi energy, a detail of the electronic structure which heretofore has not been suspected on the basis of conventional band-structure density-of-states analyses. [85] Although SCF-Xα-SW molecular-orbital calculations have not yet been carried out for Ta, and therefore the exact ordering of e_g and t_{2g} orbitals at the Fermi energy undetermined for this metal (relativistic effects, e.g., spin-orbit splittings may furtner complicate this issue), it is reasonable to expect on the basis of crystal chemistry that the orbital parameters β and d for Ta are more similar to those for Nb than to those for V. Assuming that the Nb parameters given above are valid for Ta, one calculates from formula (56) a value of $T_c \sim 2.2°K$ if the $e_g(d_{x^2-y^2}, d_{z^2})$ orbital of Ta is coincident with the Fermienergy and a value of $T_c \sim 6.8°K$ if the $t_{2g}(d_{xy}, d_{yz}, d_{xz})$ orbital of Ta is coincident with the Fermi energy. These calculated values bracket the measured value $(T_c)_{expt} = 4.5°K$ for Ta.

It will be noticed in Fig. 15 that the Fermi energies of the Group-VIB transition metals Cr, Mo, and W coincide with a region of low density of states (between the bonding and antibonding manifolds) which would normally be considered to be nonbonding. However, as revealed by the contour map in Fig. 20 for the $e_g(d_z2)$ cluster molecular orbital wave function of Cr at the Fermi energy, this low-density-of-states region actually corresponds to molecular orbitals that are antibonding between nearest-neighbor atoms and bonding between second-nearest neighbors. Since there are eight nearest neighbors and six second-nearest neighbor in the bcc structure, the net result of this composite antibonding-bonding orbital topology at the Fermi energy is indeed mainly nonbonding. Similar molecular-orbital topologies are also found at the Fermi energies of Mo and W. We suggest that this type of composite antibonding-bonding molecular-orbital topology at the Fermi energy is responsible for the low-transition-temperature superconductivity of bcc Mo (T_c = 0.92°K) and W (T_c = 0.01°K), as compared with bcc Nb, through the formation of spatially extended dδ "tubular" orbitals (cf. Figs. 12 and 14), along the direction perpendicular to the plane of Fig. 20, of smaller "intertubular" distance d than is the case for Nb. These smaller values of d imply proportionally lower orbital densities of states at the Fermi energy, as defined by Eq. (49), and correspond to the density-of-states minimum in Fig. 15. For Mo, the molecular-orbital parameters derived from the SCF-Xα-SW cluster studies are $d \sim 1.3\text{Å}$ and $\beta \sim 0.35$ (cf. $d \sim 2.3\text{Å}$ and $\beta \sim 0.35$ for Nb), which yield from formula (56) a transition temperature of $T_c \sim 0.8$°K in good agreement with the experimental value given above. For W, preliminary relativistic SCF-Xα-SW cluster molecular-orbital analysis suggests that the interorbital parameter d is further reduced by the combined effects of relativity and greater d-orbital covalency along the bonding direction between second-nearest-neighbor atoms, which accounts for the even lower transition temperature of this superconductor.

As indicated above, Cr, Mo, and W are all characterized by largely

nonbonding molecular orbitals at the Fermi energy which nevertheless are antibonding between nearest neighbors and bonding between second-nearest neighbors (Fig. 20), yet Cr is an antiferromagnet while Mo and W are superconductors. It will be discussed in Section VI of this paper that for this type of composite molecular-orbital topology at the Fermi energy, the relative amounts of spatial delocalization of orbital charge between the atoms and spatial localization of charge on the atoms could largely determine whether the metal is a superconductor or a true antiferromagnet. Indeed, it has already been argued above that the spatially delocalized correlation of Cooper-Schafroth electron pairs in the tubular dδ molecular orbitals of the species shown in Figs. 11 through 14 corresponds to a type of "conduction-electron antiferromagnetism" or "spin-density wave" delocalized between the atoms (no net spin per atom), whereas conventional antiferromagnetism is associated with spin orbitals localized primarily on the atoms (nonzero net spin per atom). Somewhat similar arguments can be used to explain the occasional coexistence of superconductivity and antiferromagnetism in the same material (e.g., $REMo_6S_8$ Chevrel-phase compounds to be discussed in Section IVE).

B. Elemental Transition-Metal Superconductors with hcp Structure

Elemental transition-metal superconductors having the hcp structure and an even number of valence d orbitals per atom (e.g., Ti, Zr, Ru, and Os) are generally characterized by relatively low transition temperatures (as compared, for example, with bcc V and Nb) and vanishing (or nearly vanishing) isotope effects. [60] SCF-Xα-SW cluster molecular-orbital studies of these materials indicate that the orbital degeneracy at the Fermi energy characteristic of cubic transition metals [e.g., the $t_{2g}(d_{xy}, d_{yz}, d_{xz})$ and $e_g(d_z2, d_x2-y2)$ orbitals of V and Nb, respectively, considered in the preceding section] is removed by the lower local symmetry of the hcp structure, leaving fully occupied and empty molecular orbitals, respectively, separated by a small energy

gap around the Fermi energy. In other words, from a real-space molecular-orbital point of view, a transition metal such as Zr can be considered to have undergone a static Jahn-Teller distortion from the cubic to hcp structure, removing the orbital degeneracy at the Fermi energy, opening a small energy gap there, and consequently lowering the energy of the system. The resulting fully occupied molecular orbital just below the Fermi energy is dδ-bonding along the c-axis between the hexagonal basal plane and triangular atomic planes above and below the basal plane (as shown for Zr in Fig. 21), whereas the resulting empty molecular orbital just above the Fermi energy is of composite dσ, dπ-bonding character within the basal and triangular planes (as shown for Zr in Fig. 22) and is dδ-bonding perpendicular to these planes (i.e., perpendicular to the plane of Fig. 22). Configurational mixing of these two orbitals will produce "tubular" dδ bonds around the Fermi energy like those shown in Figs. 11 and 12 spatially extended along the c-axis and passing continuously through the basal and triangular planes of each unit cell. These are the conditions described in Section III for Jahn-Teller coupling in the limit $\beta < 1/4$ and for Cooper-Schafroth pairing via dynamic exchange of electrons between the Jahn-Teller-split molecular orbitals immediately above and below the Fermi energy. For Zr, these fluctuations in orbital occupancy around the Fermi energy correspond to dynamic displacements δ of the electronic charge distribution at the Fermi energy along the c-axis equal to $\delta \sim c/4 \sim 1.3\text{Å}$ in Zr relative to the average lattice ion positions. The intertubular-orbital distance parameter for Zr derived from the calculated SCF-Xα-SW cluster molecular-orbital wave functions (Fig. 22) is $d \sim 2.3\text{Å}$. These two quantities, δ and d, are consistent with Eq. (33) only if $\beta \sim 0.045$, which corresponds to essentially vanishing isotope effect. Substitution of these values of β and d into formula (56) yields the transition temperature $T_c \sim 0.56°K$, which is in excellent agreement with the value $(T_c)_{expt} \sim 0.55°K$ measured for pure Zr. It should be noted that for this very small value of β, and thus for the

correspondingly large value of the quantity $(m/M)^{\beta}$, the repulsive Coulomb interaction parameter μ^* (or pseudopotential U) defined in Eq. (60) is approximately 60% of the attractive interaction parameter λ (or pseudopotential V) defined in (59). The comparative magnitudes of μ^* and λ in Zr are qualitatively consistent with strong-coupling extensions [61-64] of BCS theory which ascribe the vanishing isotope effect and low T_c for Zr (and similar transition metals) to the effects of Coulomb interactions. It may be noted further that for the value of $\beta \sim 0.045$ appropriate to Zr, the pre-exponential "cut-off" energy (58) is much larger than the Debye energy $\hbar\omega_D$ [see Eq. (35)] which corresponds to a value of $\beta \sim 1/2$. A similar molecular-orbital analysis of hcp Ti can be made, yielding the parameters $\delta \sim c/4 \sim 1.2\text{Å}$, $d \sim 2.1\text{Å}$, and $\beta \sim 0.050$, again consistent with the vanishing isotope effect. Substitution of the last two quantities into (56) gives $T_c \sim 0.39°K$, in (clearly fortuitously) exact agreement with the measured value $(T_c)_{expt} = 0.39°K$.

The same theoretical approach can also be applied to the hcp transition-metal superconductors Ru and Os, although because of their positions further toward the right of the periodic table and hence their greater number of valence d orbitals per atom, the dδ-bonding molecular orbitals around the Fermi energy responsible for superconductivity have a somewhat different orientation from those described above for Zr and Ti. Nevertheless, the molecular-orbital parameters, $d \sim 2.0\text{Å}$ and $\beta \sim 0.05$, calculated for both Ru and Os are of the same order of magnitude as those given above for Zr and Ti. Substitution of these parameters in Eq. (56) yields the transition temperatures, Ru($T_c \sim 0.43°K$) and Os($T_c \sim 0.64"K$), consistent with the respective measured values Ru[$(T_c)_{expt} = 0.49°K$] and Os[$(T_c)_{expt} = 0.66°K$]. The only major descrepancy between theory and experiment here is that, while both indicate effectively vanishing isotope effect for Ru, the measured dependence of T_c on atomic mass corresponds to a value of $(\beta)_{expt} = 0.20$, whereas the calculated value is $(\beta)_{theor} \sim 0.05$. However, since all four

hcp transition metals, Ti, Zr, Ru, and Os, have similar bonding configurations, transition temperatures, and Jahn-Teller coupling parameters β, it is possible that the observed larger isotope effect in Os is an artifact of materials preparation. In any case, the all-over agreement between the present theoretical model and experiment for these superconductors is somewhat better than that obtained from "strong-coupling" BCS-type theories. [61-64]

The hcp transition-metal superconductors, Tc and Re, deserve separate discussion from Ti, Zr, Ru, and Os, because they have comparatively high transition temperatures, Tc(T_c = 7.8°K) and Re(T_c = 1.7°K), and in the case of Re where isotope measurements have been carried out, a comparatively large isotope effect corresponding to $(\beta)_{expt}$ = 0.39. [64] These differences are explained, first of all, by the fact that Tc and Re have an odd, rather than even, number of valence d electrons per atom, so that the $d\delta$ molecular-orbital degeneracy at the Fermi energy is not completely removed, despite the non-cubic structure. Consequently, these materials are subject to ordinary dynamic Jahn-Teller coupling in the range of $1/4 \lesssim \beta \lesssim 1/2$[see Eq. (26)]. On the basis of SCF-Xα-SW cluster molecular-orbital analysis, one obtains for Tc values of $\beta \sim 0.30$ and $d \sim 1.9\mathring{A}$, yielding from formula (56) a transition temperature of $T_c \sim 8.1°K$. For Re, the calculated molecular-orbital parameters are $\beta \sim 0.40$ and $d \sim 1.9\mathring{A}$, giving $T_c \sim 2.1°K$. Both theoretical values of the transition temperature are in good agreement with the measured values for Tc and Re given above, and the calculated values of β are consistent with the measured isotope effect.

In conclusion to this and the preceding section on elemental transition-metal superconductors, it should be pointed out that the well-known correlation of T_c with electron-to-atom ratio , originally emphasized by Matthias [3] and discussed by many other workers [12-15,60-64] can be understood in terms of the molecular-orbital character, occupancy, and degeneracy at the Fermi energy, as described above.

C. A15 Transition-Metal Compound Superconductors

Transition-metal compounds such as Nb_3Sn and Nb_3Ge crystallize in the A15 structure, where the Nb atoms form a three-dimensional network of orthogonal linear chains extending along the faces of the cubic unit cells and the Sn or Ge atoms are located at the corners and center of each unit cell. These compounds are among the highest temperature superconductors known, e.g. Nb_3Sn(T_c = 18.0°K) and Nb_3Ge(T_c = 23.2°K).[86] SCF-Xα-SW cluster molecular-orbital studies of Nb_3Sn reveal the presence of spatially delocalized "tubular" dδ-bonding molecular orbitals in the vicinity of the Fermi energy of the types shown schematically in Figures 11 and 12 and quantitatively in Figure 23 along four atoms of each chain. While these tubular dδ orbitals at the Fermi energy will be shown below to be solely responsible for the superconductivity of Nb_3Sn (and other A15 compounds), they are not the sole contributors to metal-metal bonding in these materials, which also depends on dσ and dπ-bonding molecular orbitals that are spatially localized between pairs of Nb atoms in each chain and lie well below the Fermi energy as they do in elemental bcc crystalline Nb (see Fig. 15). Indeed, the effective electron configuration of a pair of nearest-neighbor Nb atoms along each chain in Nb_3Sn is close to that, $(d\sigma)^2(d\pi)^4(d\delta)^2$, for "quadruply-bonded" coordination complexes (e.g. $Mo_2Cl_8^{4-}$) of inorganic chemistry. [75-77] Although the Sn atoms and neighboring Nb chains are not explicitly shown in Figures 11, 12, and 23, the dδ bonding (as well as the dσ and dπ bonding) along each chain is due not only to the direct covalent overlap between nearest-neighbor Nb 4d orbitals but is also promoted by the interaction and hybridization between Nb 4d orbitals and neighboring Sn 5p orbitals and between the 4d orbitals of Nb atoms on neighboring chains. The net effect of these interactions is to produce a Nb-Nb nearest-neighbor bond distance (2.64Å) along each chain in Nb_3Sn which is significantly less than the nearest-neighbor distance (2.86Å) characteristic of elemental bcc crystalline

Nb. The influence of the Sn atoms on Nb-Nb bonding is analogous to that of the Cl ligands on Mo-Mo bonding in the molecular coordination complex $Mo_2Cl_8^{4-}$, where the Mo-Mo bond distance (2.14Å) is even shorter than the nearest-neighbor distance (2.73Å) characteristic of elemental bcc crystalline Mo. As will be shown below, this type of ligand-metal interaction is a key contributing factor in understanding the variation of the transition temperature, which is related to the dδ bonding at the Fermi energy through parameters d and 3 in (56), among the A15 superconductors.[86] Thus it should be emphasized that Figs. 11, 12, and 23 do not imply uncoupled one-dimensional dδ-bonded Nb chains as in the simple qualitative Labbe-Friedel [87] band-structure model for A15 compounds, but instead a three-dimensional network of coupled dδ-bonded Nb chains including the effects of Nb(4d)-Sn(5p) metal-ligand interactions, consistent with the results of more recent quantitative band-structure calculations. [78,79,88] The predicted spatial delocalization of metal-metal bond charge along the Nb chains in Nb_3Sn is qualitatively consistent with x-ray data [89] showing an excess of charge along the metal chains in the A15 compound V_3Si, although in the latter compound somewhat less dδ-bond overlap is predicted by the present theoretical model because of the greater spatial localization of V 3d orbitals in comparison to Nb 4d orbitals.

As in the preceding examples of elemental transition-metal superconductors, the three-dimensional networks of tubular dδ molecular orbitals at the Fermi energy of the types shown in Figs. 11 and 12 can be used to construct a Cooper-Schafroth singlet pair function as a "valence-bond-like" product of space and spin components of the form (6) and (7). Note in Figs. 11 and 12 the spatially delocalized "antiferromagnetic" ordering of electron-pair spins along the "tubular" dδ bonds, with a net spin per atom equal to zero, as discussed in preceding sections. Indeed, there is recent experimental evidence, in the form of conduction-electron-spin-resonance (CESR) measurements, for "antiferromagnetic" ordering of conduction electrons in the A15 compound, Nb_3Ge. [80] This type

of "antiferromagnetic" ordering of conduction electrons at the Fermi energy should not be confused with the conventional antiferromagnetism of spatially localized, paramagnetic d electrons, nor should it be confused with the "coexistence" of antiferromagnetism and superconductivity observed in certain other transition-metal compounds (see Section IVE). The antiferromagnetic ordering in A15 superconductors can, in fact, be viewed as a conduction-electron spin-density wave of the type predicted by Overhauser. [90]

It has been customary to calculate T_c values for A15 compounds using the BCS formula (1) and the total electronic density of states at the Fermi energy, N(0) derived from band-structure calculations. [91,78,79] The occupied d-band densities of states of these compounds can be partitioned into dσ-, dπ-, and dδ-bonding molecular-orbital components, as for the example of bcc transition metals in Fig. 15, with the dδ*-, dπ*, and dσ*-antibonding components lying above the Fermi energy. [78] The Fermi energies themselves generally coincide with a density-of-states peak corresponding primarily to a three-dimensional array of intersection chains of "tubular" dδ($d_{x^2-y^2}$, $d_{y^2-z^2}$, $d_{x^2-z^2}$) orbitals or the type shown in Fig. 12. For Nb_3Sn, the dδ-bond overlap at the Fermi energy, as revealed by SCF-Xα-SW studies, is substantial, implying from expression (29) a value of $\beta \sim 0.15$. For the derived interorbital distance $d \sim 1.9\text{Å}$ [the maximum distance between neighboring tubular functions ψ_+ and ψ_- in Fig. 12] in Nb_3Sn, formula (56) yields $T_c \sim 18.4°K$. The relatively small value of the Jahn-Teller coupling parameter β is consistent with the nearby vanishing isotope effect in Nb_3Sn and further suggests that the static Jahn-Teller effect can compete with Cooper-Schafroth electron pairing, resulting in a structural phase transformation of the type mentioned in Section III. Indeed, a distortion of the lattice from cubic to tetragonal structure is known to occur in Nb_3Sn and other high-T_c A15 superconductors and is suspected to lower the superconducting transition temperature from that otherwise attainable for the cubic structure. [58] A reduction of

the intertubular orbital distance d in Eq. (56) with such a lattice distortion would be consistent with a reduction in the value of T_c.

D. "Layered-Structure" Transtion-Metal Compounds

Another interesting class of superconducting transition-metal compounds are the layered transition-metal dichalcogenides, such as NbS_2, TaS_2, $NbSe_2$, and $TaSe_2$. [81] SCF-Xα-SW cluster molecular-orbital calculations for these compounds indicate that the Fermi energy is coincident with molecular orbitals of d_z2 symmetry, shown schematically in Fig. 16 for three neighboring metal atoms in a single layer. This orbital is moderately antibonding between the transition-metal d orbitals and chalcogen "ligand" p orbitals (not shown in Fig. 16) but weakly bonding between the "doughnut-like annular regions of the metal d_z2 orbitals in each layer (the dashed profiles shown in Fig. 16). The bonding between annular regions forms a diffuse but spatially coherent wave function throughout each layer, thereby satisfying the orbital criterion for the existence of superconductivity. In this respect, the superconducting state of the layered transition-metal dichalcogenides is "two-dimensional." However, the total superconducting state of the crystal is a composite result of the three-dimensional array of layered d_z2 orbitals, just as the superconducting states of aluminum and A15 compounds discussed above are the composite results of three-dimensional networks of layered σ and tubular dδ orbital configurations. The relatively low transition temperatures of these layered superconductors, e.g., NbS_2(T_c = 6°K) and $TaSe_2$ (T_c = 0.2°K), as compared with those of the dδ-bonded A15 compounds, e.g., Nb_3Sn (T_c = 18°K) and V_3Sn (T_c = 3.8°K). are consistent with the fact that the bond overlap between the annular parts of the d_z2 orbitals in the former compounds (see Fig. 16) is significantly less than that between the dδ orbitals in the latter compounds (cf. Fig. 11). The exact amounts of bond overlap and concomitant T_c values for the layered superconductors are dependent on the antibonding contributions of the chalcogen

ligand p orbitals to the d_z2 molecular orbitals, in much the same fashion as the $p\pi$ bonding orbital components in aluminum are promoted by the $p\sigma^*$ antibonding components (see Figs. 4 through 6), and in much the same way as the net $d\delta$ bonding along the chains of metal atoms in the A15 compounds, Nb_3Sn and V_3Sn, is dependent on the interaction of the metal atoms with the neighboring Sn ligands. The intercalation of organic molecules, such as pyridine, between the layers of superconducting transition-metal dichalcogenides does not appreciably alter their T_c values. [81] This is explained by the fact that the bonding between the layers and intercalate molecules occurs via the d_z2 lobes perpendicular to each layer (the solid orbital contours in Fig. 16), which leaves largely unaffected the bonding between annular regions within each plane (the dashed orbital contours in Fig. 16) responsible for the superconducting state. The weak annular type of bonding between d_z2 orbitals is not strictly limited to layered transition-metal compounds but can also contribute, along with the more dominant $d\delta$ bonding, to the superconducting state in transition metals and their alloys.(see Section IVA).

E. "Chevrel-Phase" Molybdenum Sulfide Compounds

Superconducting molybdenum sulfides having the composition $RE_xMo_6S_8$ (Chevrel compounds) containing a high concentration ($x \sim 1$) of magnetic (RE) ions [92] are of considerable interest because of the apparent coexistence of superconductivity and magnetism. [93] A preliminary molecular-orbital analysis of the Mo_6S_8 octahedral cluster which is the key structural unit in the superconducting Chevrel phases has been carried out, using the results of recent SCF-Xα-SW studies of similar Mo-atom cluster compounds by Cotton and Stanley. [94] This analysis suggests that the superconducting state of these Chevrel phases and the more common ones not containing Re ions [95] arises exclusively from coherent spatially delocalized d-orbital bonding between the Mo atoms, promoted in part by the direct covalent overlap between Mo d

orbitals in the Mo_6S_8 clusters and in part by the antibonding contribution of the interaction between Mo d orbitals and S ligand p orbitals. The latter contribution may be compared with the above-described effect of the $p\sigma^*$-antibonding component of aluminum in promoting coherent spatially extended $p\pi$ bonding (see Figs. 4 through 6). On the other hand, the magnetic properties of the $Re_xMo_6S_8$ compounds are associated exclusively with localized f orbitals on the RE ions which are formally but weakly antibonding with respect ot the Mo_6S_8 clusters. Thus the interaction between the magnetic RE ions and the superconducting electrons is weak, explaining why the presence of such ions does not generally destroy the superconductivity of the Chevrel phases.

F. Palladium Hydride (PdH_x)

Pure palladium is strongly exchange enhanced but not superconducting. [64] On the other hand, the addition of large amounts of interstitial hydrogen to palladium to form the alloy, palladium hydride (PdH_x), eliminates the spin fluctuations and produces a good superconductor (e.g. $2.1°K \lesssim T_c \lesssim 9.1°K$ for $0.85 \lesssim x \lesssim 1$). [96] SCF-Xα-SW molecular-orbital studies of a 19-atom palladium cluster representing the local molecular environment of pure crystalline palladium up to second-nearest neighbors indicate the presence of degenerate spin-polarized $dd\pi^*$ and $dp\sigma^*$ antibonding orbitals at the Fermi energy. [97] Fluctuations of electron occupancy between these two types of degenerate orbitals are discrete cluster analogs of the observed magnetic spin fluctuations. Similar SCF-Xα-SW cluster molecular-orbital studies of PdH_x [9 indicate that the interstitial hydrogen in palladium raises the Fermi energy above the Pd-Pd $dd\pi^*$ and $dp\sigma^*$ antibonding orbitals and makes it coincident with orbitals having spatially delocalized components which are $s\sigma$-bonding within and $s\sigma^*$-antibonding between parallel planes of weakly interacting H atoms (see Fig. 24), thereby quenching the spin fluctuations. The present theoretical model further suggests that these $s\sigma$-bonded planes of H atoms form layer

orbitals ψ_+ and ψ_- at the Fermi energy (Fig. 24) which are somewhat similar to those for aluminum (cf. Fig. 6), and that the valence-bond-like correlation of electrons in these layer orbitals [see Eq. (6)], in conjunction with with the dynamic Jahn-Teller effect is responsible for Cooper-Schafroth electron pairing and superconductivity in PdH_x.

V. OTHER SUPERCONDUCTORS

A. Polymeric and Organic Superconductors

Prime examples of superconducting polymeric and organic solids are polysulfur nitride $(SN)_x$ and tetramethyltetraselenafulvalene-hexafluorophosphate $(TMTSF)_2PF_6$. Crystalline $(SN)_x$ is not only a good ordinary electrical conductor along the direction of "fiber bundles" formed by large aggregates of individual polymer molecules, but is also an anisotropic superconductor, albeit a low-T_c($\sim$ 0.25°K) one.[99] Previous SCF-Xα-SW studies [100] reveal that the Fermi energy is coincident with coherent pπ-bonding molecular orbitals spatially delocalized along the $(SN)_x$ chains. Despite the one-dimensional nature of the individual chains, they result in an effective three-dimensional array of pπ-bonding orbitals due to the pπ interchain coupling in the (100) plane and pσ interchain coupling in the ($\bar{1}$02) plane. [100] These orbitals are somewhat analogous to the composite pπ-pσ* molecular orbitals (Figs. 4 and 5) shown in Section III to be precusors to superconductivity in aluminum. However, in $(SN)_x$ the pπ-bonding components are exclusively along the direction of the fibers and thus lead to anisotropic superconductivity, whereas in aluminum there are three principal cubic crystallographic directions which result in isotropic superconductivity. The anisotropic pπ bonding and relatively weak pπ bond overlap associated with the "zig-zag" structure of the $(SN)_x$ polymers are likely responsible for the low T_c value of this material.

The organic charge-transfer salt, $(TMTSF)_2PF_6$, the crystal structure of which consists of stacks of TMTSF molecules ordered in sheets separated by PF_6

sheets (see Fig. 25), is observed to be superconducting at $T_c \sim 0.9°K$ for an applied presure of 12k bar. [101] A structurally similar compound, $(TMTSF)_2ClO_4$, has more recently been found to be superconducting at $T_c \sim 1.2°K$ without any applied pressure[102] A preliminary molecular-orbital analysis, based on previous SCF-Xα-SW calculations [103] for TTF dimers and trimers in the somewnat similar (but nonsuperconducting) compound, TTF-TCNQ, suggests that Cooper-Schafroth pairing and superconductivity in $(TMTSF)_2PF_6$ and $(TMTSF)_2ClO_4$ arise from the "valence-bond-like" pairing [see Eq. (6)] of pπ-bonding "layer-orbital" components ψ_+ and ψ_- at the Fermi energy analogous to those shown in Figs. 4 through 7 for aluminum. In $(TMTSF)_2PF_6$ and $(TMTSF)_2ClO_4$, the layer orbitals ψ_+ and ψ_- originate from the <u>combined</u> effects of interacting pπ-bonded TMTSF molecules in each stack <u>and</u> "phase-locked" coupling between TMTSF stacks via weak overlap with the otherwise "nonbonding" pπ orbitals localized on the F and O ligands, respectively, of the intervening PF_6^- and ClO_4^- anions. The layer-orbital components ψ_+ and ψ_- are shown schematically for $(TMTSF)_2PF_6$ in Fig. 25, including the "antiferromagnetic" correlation of conduction-electron spins between the molecules, in analogy to the spin correlations of the layer orbitals of aluminum shown in Fig. 6. Indeed, there is some experimental evidence for such antiferromagnetic ordering in $(TMTSF)_2PF_6$, corresponding to spin-density waves. [104] It is further suggested that in the crystal, $(TMTSF)_2PF_6$, the TMTSF-PF_6-TMTSF pπ-bond overlap necessary for phase-locked interchain coupling and hence for Cooper-Schafroth pairing of spatially extended layer orbitals ψ_+ and ψ_- cannot be attained unless external pressure reducing the TMTSF-PF_6 intermolecular distance is applied, whereas in $(TMTSF)_2ClO_4$ these conditions are present without applied pressure. Under these conditions, the interlayer $(\psi_+ - \psi_-)$ orbital distance in these components is $d \sim 1.8\text{Å}$, i.e. approximately half the TMTSF intermolecular distance in a stack (see Fig. 25). The pπ-bond overlap is small, so that according to expression (29) the Jahn-Teller coupling

parameter is $\beta \sim \frac{1}{2}$, i.e. the limit of weak dynamic Jahn-Teller (electron-phonon) coupling. Substitution of these parameters into formula (56), using for M weighted averages of the masses of the atoms, [Se, C, and F in $(TMTSF)_2PF_6$] and [Se, C, and O in $(TMTSF)_2ClO_4$], participating in layered $p\pi$ bonding yields $0.8°K \lesssim T_c \lesssim 1.2°K$, which is in excellent agreement with the range of measured values $(T_c)_{expt} \sim 0.9°K$ and 1.2°K for $(TMTSF)_2PF_6$ and $(TMTSF)_2ClO_4$, respectively. The absence of superconductivity and presence of charge-density (instead of spin-density) waves in TTF-TCNQ [104] is most likely due to the "herringbone" structure (Fig.26) of the TTF and TCNQ chains, which prevents the two-dimensional interchain coupling and pahse locking of the $p\pi$ electrons and thus does not meet the conditions [present in $(TMTSF)_2PF_6$] for spatially extended layer orbital formation.

B. Lanthanides and Actinides

Of the lanthanides, only La is superconducting, while there are three actinides, Th, Pa, and V which are superconducting. [64] Of these, the superconductivity of α-uranium is most anomalous because of the sensitivity of T_c to pressure and because of the large, positive isotope effect. [105] The latter effect has been presented as evidence for a "nonphonon" mechanism of superconductivity in α-U involving virtual excetations of electrons to low-lying f states. [105] On the other hand, theoretical arguments have been presented to show that the large, positive isotope effect in α-U can be explained within the framework of BCS theory. [106] Preliminary SCF-Xα-SW cluster molecular-orbital models for α-U indicate that the superconductivity of this material is mainly associated with dδ-bonding orbitals and dynamic Jahn-Teller instability at the Fermi energy, but with important effects due to "mixing" with or excitations (of the type described in Section III) to nearly degenerate f orbitals. Thus these preliminary results support the original conjecture [105] of virtual excitations to low-lying f orbitals in α-U, although it is the dδ-orbital topology at the Fermi energy and associated

dynamic Jahn-Teller electron-lattice ("phonon") coupling that is the mechanism for superconductivity in α-U, consistent with the conclusions of Ref. 106.

C. Amorphous Alloys

Since the first superconducting amorphous alloy obtained by rapid liquid quenching was reported in 1975, a systematic search for new superconducting amorphous alloy compositions has been made. Approximately fifteen amorphous alloys are now known to be superconductors with transition temperatures ranging from 1.5 to 9.0°K. [107] Among these are zirconium-based metallic glasses such as $Zr_{65}Cu_{35}$(T_c = 2.0°K), $Zr_{70}Ni_{30}$(T_c = 2.9"K), and $Zr_{70}Co_{30}$(T_c = 3.3°K). [108] Of course, there are many amorphous alloys, such as the Si-Pd system, which are not superconducting.

Recently, SCF-Xα-SW cluster molecular-orbital models for the local electronic structures of Zr-Cu and Si-Pd metallic glasses have been constructed. [109] Both alloys are characterized by a fully occupied d band associated primarily with the Cu or Pd components and a partially occupied Zr d band or Si p band lying at higher energies, although there is significant Cu-Zr or Pd-Si bonding and Zr-Cu or Si-Pd antibonding character within these respective bands and some electron transfer from Zr to Cu or from Si to Pd. The calculated electronic structures are in good quantitative agreement with and provide an interpretation of published photoelectron spectra for these alloys.

Perhaps the most striking feature of the calculated electronic structures is the nature of the electronic states coincident with or just below the Fermi energy, i.e. the highest occupied molecular orbitals. These states can be described as forming highly delocalized and spatially directed Zr-Zr d-orbital or Si-Si p-orbital chemical bonds which are promoted, in part, by the composite bonding-antibonding interaction with the d orbitals localized on neighboring Cu or Pd components. These bonds are clearly visible in the

molecular-orbital wave-function contour maps shown in Fig. 27 for the Zr-Cu and Si-Pd systems, respectively.

The existence of directed Zr-Zr and Si-Si bonds in amorphous Zr-Cu and Si-Pd alloys, respectively, may, at first right, seem surprising since the Zr and Si atoms are not nearest neighbors in these alloys and the Zr-Zr and Si-Si bond distances are significantly larger than those in elemental crystalline Zr and Si. Nevertheless, the effects of the nearest-neighbor Cu and Pd d orbitals in acting as "bridges" for the formation of Zr-Zr and Si-Si bonds are clearly evident in Fig. 27.

On a scale spanning many atoms, the Zr-Zr and Si-Si bonds at the Fermi energy form a topologically disordered "network" which is believed to be related to the glass-forming capabilities of these and similar alloys. [110] In the case of amorphous Zr-Cu alloys, the Zr-Zr bonds at the Fermi energy, despite the lack of long-range crystalline order, are of the $d\delta$ type shown in Section IV to be precursors to superconductivity in transition metals and their compounds. On the other hand, the Si-Si bonds at the Fermi energy of amorphous Si-Pd alloys are of the more localized $p\sigma$ type which is not favorable for Cooper-Schafroth pairing and superconductivity. Indeed, amorphous Zr-Cu alloys are superconductors, [108] whereas amorphous Si-Pd alloys are not.

VI. MAGNETISM VS. SUPERCONDUCTIVITY

Although magnetism and superconductivity can occasionally coexist in some complex materials (see Section IV E), it is more generally true that superconductivity and magnetism are mutually exclusive in a material at the same temperature and pressure. For example, among the Group-VIIB elements of the periodic table, the first-row transition metal, iron, in its bcc crystalline form (α-Fe) is exclusively ferromagnetic, whereas the second-and third-row metals; ruthenuim and osmium, which have the hcp structure, are exclusively superconducting. This can be understood directly and simply in terms of the

diametrical cluster molecular-orbital criteria for these two phenomeon. As already discussed in Section III, for superconductivity to occur, there must be degenerate or nearly degenerate molecular orbitals at the Fermi energy with spatially extended bonding components, e.g. the "layered" $p\pi$-bonding components of Al and $(TMTSF)_2PF_6$ shown in Figs. 6 and 25, respectively, and the "tubular" $d\delta$-bonding components shown in Figs. 11 through 14. In contrast, for ferromagnetism or local magnetic moment formation, as already pointed out in Section I, there must be spatially localized, exclusively antibonding molecular orbitals at the Fermi energy in the non-spin-polarized limit, as exemplified for iron in Fig. 14 of Ref. 41 and for Mn impurities in aluminum in Figs. 9 and 10. Indeed, it was shown in Section III how one can understand the destructive effect of such magnetic impurities on the superconductivity of pure aluminum simply in terms of the emptying of the aluminum $p\pi$-bonding molecular orbitals at the Fermi energy (Figs. 4 through 6) and the occupation of purely antibonding Mn-Al $dp\sigma^*$ and $dp\pi^*$ orbitals [Figs. 9 and 10], which are responsible for magnetic spin fluctuations. Recent SCF-$X\alpha$-SW molecular-orbital studies of the electronic structures and magnetism of iron clusters [41] indicate that a high density of localized antibonding molecular orbitals at the Fermi energy in the non-spin-polarized limit is consistent with the Stoner criteria for the occurence of ferromagnetism, namely, that a paramagnetic metal such as iron will be unstable with respect to ferromagnetic ordering if

$$I(\varepsilon_F)N(\varepsilon_F) > 1, \tag{65}$$

where $N(\varepsilon_F)$ is the electronic density of states at the Fermi energy of the paramagnetic metal and $I(\varepsilon_F)$ is the Stoner exchange parameter. In Fig. 15, it is clear that the Fermi energy of paramagnetic iron is coincident with a region of high density of states corresponding to antibonding cluster molecular orbitals. In Ref. 41, it is shown that these antibonding orbitals also lead to large values of $I(\varepsilon_F)$ because of the spatial localization of the wave

functions in regions between the antibonding nodes and atomic nuclei (see Fig. 14 of Ref. 41).

The case for antiferromagnetism vs. superconductivity deserves separate discussion. It has been shown in Section III [see Eqs. (6) and (7)] that the "valence-bond-like" singlet configuration of "layered" $p\pi$-bonding or "tubular" $d\delta$-bonding molecular-orbital components ψ_+ and ψ_- at the Fermi energy in a superconductor, which are $d\sigma^*$ or $d\pi^*$ antibonding between second-nearest-neighbor atoms along directions perpendicular to the layers or tubes, corresponds to an "antiferromagnetic" ordering of spatially delocalized spins on the alternating layers or tubes. This spin configuration is somewhat similar to the conduction-band collective antiferromagnetism or spin-density wave predicted by Overhauser[90] to occur in certain metals and to be lower in energy than the paramagnetic state. Indeed, there is recent experimental evidence for an "antiferromagnetic" ordering of conduction electrons in A15 superconductors [80] (see also Section IVC). On the other hand, recent SCF-$X\alpha$-SW cluster models for the electronic structure of chromium, [111] including the effects of magnetic spin polarization, suggest that conventional antiferromagnetism in this material is associated with molecular orbitals at the Fermi energy which have spatially localized $d\pi^*$-antibonding character between nearest-neighbor atoms and spatially delocalized $d\sigma$-bonding character between second-nearest neighbors (see Fig. 20). Thus while both Cooper-Schafroth pair formation and conventional antiferromagnetism are associated with composite bonding-antibonding molecular-orbital topology at the Fermi energy, the two phenomena are distinguished, at least for the systems investigated thus far, by different spatial distributions of this composite character between the atoms.

Thus the SCF-$X\alpha$-SW cluster molecular-orbital approach can be considered to provide a simple unifying chemical picture for understanding the incidence of superconductivity, ferromagnetism, and antiferromagnetism entirely on the basis of the molecular-orbital topology at the Fermi energy.

VII. METALS THAT ARE NEITHER SUPERCONDUCTING NOR MAGNETIC

The molecular-orbital criteria for superconductivity and magnetism described in the preceding sections can also be employed to explain some metals are neither superconducting nor magnetic. Among these, the noble metals Cu, Ag, and Au have been the subject of much discussion concerning the possibility of observing superconductivity at extremely low temperatures. [112] SCF-Xα-SW studies of a 19-atom copper cluster representing bulk crystalline copper [39] suggest that superconductivity is unlikely to occur at any temperature (or reasonable pressure). The Fermi energy coincides with a molecular orbital of a_{1g} "spherical" symmetry which is primarily of the sσ*-antibonding type and which therefore lacks the coherent extended spatial character necessary for superconductivity (see Fig. 4 of Ref. 39 for a picture of this orbital). While there is some antibonding d-orbital contribution to this orbital due to the hybridization effect of the filled d band below the Fermi energy, it is too small and diffuse to give rise to localized or collective magnetic moments in pure copper. The only orbital that is capable, in principle, of forming a superconducting state in copper is an unoccupied t_{1u} pπ-pσ* orbital of the type shown above (Figs. 4-7) to be occupied at the Fermi energy in aluminum and responsible for its superconducting state. Thus the question of superconductivity in copper depends on whether this type of orbital, which lies well above the Fermi energy, can be brought into coincidence with the Fermi energy by any practically attainable pressure. Similar arguments are applicable to silver and gold.

Another interesting example where there has been much speculation about the possibility of superconductivity is metallic hydrogen at very high pressure. [113-115] SCF-Xα-SW molecular-orbital studies [98] suggest that, while the electronic structure of solid atomic hydrogen at high-pressure interatomic distances and crystal structure is consistent with metallic behavior, this substance is unlikely to be superconductor. The Fermi energy

coincides with an $s\sigma^*$ antibonding molecular orbital of the type shown above to be associated with the nonsuperconducting, nonmagnetic state of copper. Thus, as in the example of copper, the occurrence of superconductivity in metallic hydrogen depends on whether an unoccupied spatially extended $p\pi$-bonding orbital, which lies well above the Fermi energy, can be brought into coincidence with the Fermi energy at any attainable pressure.

ACKNOWLEDGMENTS

Sponsorship of this research at M.I.T. by the Office of Naval Research is gratefully acknowledged. KHJ is also grateful to Professor W.A. Little of Stanford University for his critical and helpful remarks concerning an early version of this manuscript, and to Professor V.F. Weisskopf of M.I.T. for communicating his ideas about the nature of superconductivity and for encouraging this research. The authors further wish to thank Dr. J.M. Bray and Dr. F.S. Ham of the General Electric Corporate Research and Development Center for valuable discussions relevant to this research.

REFERENCES

1. J. Bardeen, L. N. Cooper, and J. R. Schrieffer, Phys. Rev. 108, 1175 (1957).
2. L. N. Cooper, Phys. Rev. 104, 1189 (1956).
3. B. T. Matthias, Phys. Rev. 97, 74 (1955); in Progress in Low Temperature Physics, Vol. II, edited by C. J. Gorter (North-Holland, Amsterdam, 1957), p. 138; in The Science and Technology of Superconductivity, Vol. 1, edited by W. D. Gregory, W. N. Matthews, Jr., and E. A. Edelsack (Plenum, New York, 1973), p. 263; Physica 55, 69 (1971).
4. W. L. Johnson, S. J. Poon, and P. Duwez, Phys. Rev. B11, 150 (1975).
5. S. Matsuo, H. Sugiura, and S. Noguchi, J. Low Temp. Phys. 15, 481 (1974).
6. K. Ohshima, T. Kuroshi, and T. Fujita, J. Phys. Soc. Japan 41, 1234 (1976).
7. F. London, and H. London, Proc. Roy. Soc. A149, 71 (1935); Physica 2, 341 (1935); F. London, Proc. Roy. Soc. A152, 24 (1935).
8. F. London, Superfluids, Vol. 1 (Wiley, New York, 1950).
9. J. C. Slater, Phys. Rev. 51, 195 (1937); 52, 214 (1937).
10. W. A. Little, Phys. Rev. 134, A1416 (1964); H. Gutfreund and W. A. Little, in Highly Conducting One-Dimensional Solids, edited by J. T. Devreese, R. P. Evrard, and V. E. Van Doren (Plenum, New York, 1979), p. 305.
11. D. W. Allender, J. M. Bray, and J. Bardeen, Phys. Rev. B7, 1020 (1973); Phys. Rev. B8, 4433 (1973).
12. J. J. Hopfield, Phys. Rev. 186, 443 (1969).
13. D. M. Gualtieri, J. Appl. Phys. 45, 1880 (1974).
14. C. M. Varma and R. C. Dynes, in Superconductivity in d- and f-Band Metals, edited by D. H. Douglas (Plenum. New York, 1976), p. 507.

15. H. Krebs, Prog. in Solid State Chem. 9, 269 (1975).

16. J. Appel and W. Kohn, Phys. Rev. B4, 2162 (1971).

17. A. Birnbeim and H. Gutfreund, Phys. Rev. B9, 139 (1974).

18. E. Krüger, Phys. Stat. Sol. (b) 85, 261 (1978); 85, 493 (1978); 90, 719 (1978).

19. L. Pauling, Proc. Natl. Acad. Sci. (USA) 60, 59 (1968).

20. J. C. Slater and K. H. Johnson, Phys. Rev. B5, 831 (1972); J. C. Slater and K. H. Johnson, Physics Today 27, 34 (1974).

21. J. C. Slater, in Advances in Quantum Chemistry, Vol. 6, edited by P.-O. Löwdin (Academic, New York, 1972); The Self-Consistent Field for Molecules and Solids, Vol. 4 of Quantum Theory of Molecules and Solids (McGraw-Hill, New York, 1974).

22. K. H. Johnson, J. Chem. Phys. 45, 3085 (1966); in Advances in Quantum Chemistry, Vol. 7, edited by P.-O. Löwdin (Academic, New York, 1973), p. 143.

23. K. H. Johnson, J. G. Norman, Jr., and J. W. D. Connolly, in Computational Methods for Large Molecules and Localized States in Solids, edited by F. Herman, A. D. McLean, and R. K. Nesbet (Plenum, New York, 1973), p. 161.

24. K. H. Johnson, in Annual Review of Physical Chemistry, Vol. 26, edited by H. Eyring, C. J. Christensen, and H. S. Johnston (Annual Reviews, Palo Alto, California, 1975), p. 39.

25. F. A. Cotton, E. E. Hazen, Jr., V. W. Day, S. Larsen, J. G. Norman, Jr., S. T. K. Wong, and K. H. Johnson, J. Am. Chem. Soc. 95, 2367 (1973).

26. C. Y. Yang, K. H. Johnson, R. H. Holm, and J. G. Norman, Jr., J. Am. Chem. Soc. 97, 6596 (1975).

27. B. H. Huynh, D. A. Case, and M. Karplus, J. Am. Chem. Soc. 99, 6103 (1977); D. A. Case and M. Karplus, J. Am. Chem. Soc. 99, 6182 (1977); D. A. Case, B. H. Huynh, and M. Karplus, J. Am. Chem. Soc. 101, 4433 (1979).

28. K. H. Johnson, F. Herman, and R. Kjellander, in Electronic Structure of Polymers and Molecular Crystals, edited by J.-M. Andre, J. Ladik, and J. Delhalle (Plenum, New York, 1975), p. 601.

29. R. P. Messmer, in Theoretical Chemistry, Vol. 1, edited by A. D. Buckingham and C. A. Coulson (Butterworths, London, 1975), p. 217.

30. K. H. Johnson, Crit. Rev. Solid State and Mat. Sci. 7, 101 (1978).

31. R. P. Messmer, in The Nature of the Surface Chemical Bond, edited by T.-N. Rhodin and G. Ertl (North Holland, Amsterdam, 1979), p. 51.

32. G. D. Watkins and R. P. Messmer, Phys. Rev. Lett. 32, 1244 (1974).

33. B. G. Cartling, J. Phys. C. 8, 3171; 3183 (1975).

34. L. A. Hemstreet, Phys. Rev. B15, 834 (1977).

35. A. Fazzio, J. R. Leite, and M. L. DeSiqueira, J. Phys. C. 11, L175 (1978); 12, 513 (1979).

36. K. H. Johnson, H. J. Kolari, J. P. deNeufville, and D. L. Morel, Phys. Rev. B21, 643 (1980).

37. R. P. Messmer, S. K. Knudson, K. H. Johnson, J. B. Diamond, and C. Y. Yang, Phys. Rev. B13, 1396 (1976).

38. D. R. Salahub and R. P. Messmer, Phys. Rev. B16, 2526 (1977).

39. K. H. Johnson, D. D. Vvedensky, and R. P. Messmer, Phys. Rev. B19, 1519 (1979).

40. T. E. Fischer, S. R. Kelemen, K. P. Wang, and K. H. Johnson, Phys. Rev. 20, 3124 (1979).

41. C. Y. Yang, Ph.D. Thesis, Department of Materials Science and Engineering (Massachusetts Institute of Technology, June, 1977) (unpublished);

C. Y. Yang, K. H. Johnson, D. R. Salahub, J. Kasper, and R. P. Messmer, Phys. Rev., B24, 5673 (1981).

42. R. P. Messmer, Phys. Rev. B23, 1616 (1981).

43. R. P. Messmer and D. R. Salahub, Phys. Rev. B16, 2526 (1977).

44. H. L. Yu, Phys. Rev. B15, 3609 (1977); J. Chem. Phys. 69, 1755 (1978).

45. J. W. Davenport, Phys. Rev. Lett. 36, 945 (1976).

46. R. P. Messmer, D. R. Salahub, and J. W. Davenport, Chem. Phys. Lett. 57, 29 (1978).

47. J. W. Davenport, W. Ho, and J. R. Schrieffer, Phys. Rev. B17, 3115 (1978).

48. R. P. Messmer and S. H. Lamson, Chem. Phys. Lett. 65, 465 (1979).

49. A. P. Ginsberg, J. Am. Chem. Soc. 102, 111 (1980).

50. J. C. Slater, Quantum Theory of Matter, Second Edition (McGraw-Hill, New York, 1968), p. 578.

51. F. London, J. Phys. Radium 8, 397 (1937).

52. R. C. Haddon, J. Am. Chem. Soc. 101, 1722 (1979).

53. J. C. Slater, The Self-Consistent Field for Molecules and Solids, Vol. 4 of Quantum Theory of Molecules and Solids (McGraw-Hill, New York, 1974), p. 117.

54. B. Segall, Phys. Rev. 124, 1797 (1961).

55. C. A. Coulson, Valence, 2nd Edition (Oxford University Press, New York, 1961), p. 113.

56. M. R. Schafroth, J. M. Blatt, and S. T. Butler, Helv. Phys. Acta 30, 93 (1957); M. R. Schafroth, Phys. Rev. 130, 1244 (1958); see also J. M. Blatt, Theory of Superconductivity (Academic, New York, 1964), p. 83.

57. L. Salem, The Molecular Orbital Theory of Conjugated Systems (Benjamin, New York, 1966), p. 466.

58. L. R. Testardi, in Electron-Phonon Interactions and Phase Transitions, edited by T. Riste (Plenum, New York, 1977), p. 181.

59. V. F. Weisskopf, private communication and to be published.

60. For example, see the review article by B. Meservey and B. B. Schwartz, in Superconductivity, Vol. 1, edited by R. D. Parks (Dekker, New York, 1969), p. 124.

61. P. Morel and P. W. Anderson, Phys. Rev. 125, 1263 (1962).

62. J. W. Garland, Jr., Phys. Rev. Lett. 11, 111; 114 (1963); Phys. Rev. 153, 460 (1967).

63. W. L. McMillan, Phys. Rev. 167, 331 (1968).

64. For example, see review article by G. Gladstone, M. A. Jensen, and J. R. Schrieffer, in Superconductivity, Vol. 2, edited by R. D. Parks (Dekker, New York, 1969), p. 665.

65. A. A. Abrikosov, JETP Lett. 87, 219 (1978).

66. J. Ruvalds and L. M. Kahn, Phys. Lett. 70A, 477 (1979).

67. J. Ihm, M. L. Cohen, and S. F. Tuan, Phys. Rev. B23, 3258 (1981).

68. C. Kittel, Introduction to Solid State Physics, 5th Edition (Wiley, New York, 1976), Chapter 12.

69. R. B. Petit and J. Silcox, Phys. Rev. B13, 2865 (1976).

70. B. Abeles, in Applied Solid State Science, Vol. 6 (Academic, New York, 1976), p. 1.

71. J. H. Sinfelt, in Annual Review of Materials Science, edited by R. A. Huggins, R. H. Bube, and R. W. Roberts, Vol. 2 (Annual Reviews, Palo Alto, 1972), p. 641.

72. D. U. Gubser and A. W. Webb, Phys. Rev. Lett. 35, 104 (1975).

73. P. Steiner, H. Höchst, W. Steffen, and S. Hüfner. Z. Phys. B38, 191 (1980).

74. G. Gruner, Adv. Phys. 23, 941 (1974).

75. F. A. Cotton and G. Wilkinson, Advanced Inorganic Chemistry, 4th Edition (Wiley, New York, 1980), p. 1080.

76. J. G. Norman, Jr., and H. J. Kolari, J. Am. Chem. Soc. 97, 33 (1975).

77. L. Noodleman and J. G. Norman, Jr., J. Chem. Phys. 70, 4903 (1979).

78. L. F. Mattheiss, Phys. Rev. B12, 2161 (1975).

79. B. M. Klein, L. L. Boyer, D. A. Papaconstantopoulos, and L. F. Mattheiss, Phys. Rev. B18, 6411 (1978).

80. S. N. Ekbote and A. V. Narlikar, Mat. Res. Bull. 15, 827 (1980).

81. F. R. Gamble, F. J. DiSalvo, R. A. Klemm, and T. H. Geballe, Science 168, 568 (1970).

82. B. W. Roberts, NBS Technical Note 983 (U.S. Department of Commerce, 1978).

83. R. M. Rose, private communication.

84. J. Bostock, V. Diadiuk, W. N. Cheung, K. H. Lo, R. M. Rose, and M. L. A. MacVicar, Phys. Rev. Lett. 36, 603 (1976); J. Bostock and M. L. A. MacVicar, Phys. Rev. Lett. 71A, 373 (1979).

85. L. F. Mattheiss, Phys. Rev. B1, 373 (1970).

86. R. A. Hein, in The Science and Technology of Superconductivity, Vol. 1, edited by W. D. Gregory, W. N. Matthews, Jr., and E.A. Edelsack (Plenum, New York, 1973), p.333.

87. J. Labbé and J. Friedel, J. Phys. Radium 27, 153, 303, 708 (1966).

88. W. E. Pickett, in Superconductivity in d- and f- Band Metals, edited by H. Suhl and M. B. Maple (Academic, 1980), p. 77.

89. J. L. Staudenmann, Solid State Commun. 26, 461 (1978); J. L. Staudenmann, P. Coppens, and J. Muller, Solid State Commun. 19, 29 (1976).

90. A. W. Overhauser, Phys. Rev. 128, 1437 (1962).

91. B. M. Klein, L. L. Boyer, and D. A. Papaconstantopoulos, Phys. Rev. Lett. 42, 530 (1979).

92. Ø. Fischer, A. Treyvaud, R. Chevral, and M. Sergent, Solid State Comm. 17, 721 (1975).

93. D. E. Moncton, G. Shirane, W. Thomlinson, M. Ishikawa, and Ø. Fischer, Phys. Rev. Lett. 41, 1133 (1978).

94. F. A. Cotton and G. G. Stanley, Chem. Phys. Lett. 58, 450 (1978).

95. B. T. Matthias, M. Murenzio, E. Corenzwit, A. S. Cooper, and H. E. Barz, Science 175, 1465 (1972).

96. R. J. Miller and C. B. Satterthwaite, Phys. Rev. Lett. 34, 144 (1975).

97. D. D. Vvedensky, Ph.D. Thesis, Department of Materials Science and Engineering (Massachusetts Institute of Technology,1979) (unpublished).

98. D. D. Vvedensky and K. H. Johnson, manuscript in preparation.

99. R. L. Greene, and G. B. Street, in Chemistry and Physics of One-Dimensional Metals, edited by H. J. Keller (Plenum, New York, 1977).

100. R. P. Messmer and D. R. Salahub, Chem. Phys. Lett. 41. 73 (1976); D. R. Salahub and R. P. Messmer, Phys. Rev. 14, 2592 (1976).

101. D. Jerome, A. Hazaud, M. Ribault, and K. Bechgaard, J. Phys. Lett. 41, 95 (1980); M. Ribauet, G. Benedek, D. Jerome, and K. Bechgaard, J. Phys. Lett. 41,397 (1980).

102. K. Bechgaard, K. Carneiro, M. Olsen, F. B. Rasmussen, and C. S. Jacobsen, Phys. Rev. Lett. 46, 852 (1981).

103. F. Herman, D. R. Salahub, and R. P. Messmer, Phys. Rev. B15, 2453 (1977); D. R. Salahub, R. P. Messmer, and F. Herman, Phys. Rev. B13, 4252 (1976).

104. See, for example, News---Search and Discovery Section of Physics Today 34, February, p. 17 (1981).

105. R. D. Fowler, J. D. G. Lindsay, R. W. White, H. H. Hill, and B. T. Matthias, Phys. Rev. Lett. 19, 892 (1967).

106. H. Capellman and J. R. Schrieffer, Phys. Rev. Lett. 21, 1060 (1968).

107. P. Duwez and W. L. Johnson, J. Less-Common Metals 62, 215 (1978).

108. O. Rapp, B. Lindberg, H.S. Chen, and K. V. Rao, J. Less-Common Metals 62, 221 (1978).

109. F. A. Leone and K. H. Johnson, in Rapidly Solidified Amorphous and Crystalline Alloys, edited by B. H. Kear and B. C. Giessen (Elsevier, in press).

110. M. E. Eberhart, K. H. Johnson, and R. C. O'Handley, in Rapid Solidified Amorphous and Crystalline Alloys, edited by B. H. Kear and B. C. Giessen (Elsevier, in press).

111. D. R. Salahub and R. P. Messmer, Surface Sci. 106, 415 (1981).

112. B. T. Matthias, Intern. J. Quantum Chem. 105, 435 (1976).

113. N. W. Ashcroft, Phys. Rev. Lett. 21, 1748 (1968).

114. T. Schneider, Helv. Phys. Acta 42, 957 (1969).

115. V. L. Ginsberg, Physica 55, 207 (1971).

FIGURE CAPTIONS

Fig. 1. Schematic representation of the "real space" molecular orbitals and corresponding "$\vec{k}$-space" band structure of a benzene molecule.

Fig. 2. Comparison of the SCF-Xα-SW molecular-orbital energy levels of a 43-atom aluminum cluster, representing the local environment of fcc crystsalline aluminum up to third-nearest neighbors, with the bulk energy bands.

Fig. 3. Comparison of the SCF-Xα-SW molecular-orbital energy levels of a 43-atom aluminum cluster, representing the local environment of crystalline aluminum up to third-nearest neighbors, with the measured X-ray photoelectron spectrum (XPS) of an aluminum crystal.

Fig. 4. Contour map of the wave function for the highest occupied molecular orbital, $t_{1u}(\varepsilon_F)$, of a 43-atom aluminum cluster, plotted in the (200) crystallographic plane up to second-nearest neighbors. The solid and dashed contours represent positive and negative values, respectively, of the wave function.

Fig. 5. Contour map of the wave function for the highest occupied molecular orbital, $t_{1u}(\varepsilon_F)$, of a 43-atom aluminum cluster, plotted in the (110) crystallographic plane up to second-nearest neighbors.

Fig. 6. Three-dimensional contour map of the wave function for the highest occupied molecular orbital, $t_{1u}(\varepsilon_F)$, of a 43-atom aluminum cluster, i.e. the three-dimensional version of the contour maps of Figs. 4 and 5.

Fig. 7. Schematic representation of the spatially extended wave function of the highest occupied molecular orbital, $t_{1u}(\varepsilon_F)$, of an aluminum cluster, plotted in the (200) crystallographic plane, when the cluster size is increased to include many atoms in the crystal.

Fig. 8. SCF-Xα-SW molecular-orbital energy levels of a 43-atom cluster representing the local environment of a Mn impurity in an aluminum crystal up to third-nearest neighbors. The calculated levels are

compared with the measured X-ray photoelectron spectrum (XPS) of bulk aluminum containing a dilute concentration of substitutional Mn impurities.

Fig. 9. Contour map of the highest occupied t_{2g} cluster molecular-orbital wave-function for a Mn impurity in an aluminum crystal.

Fig.10. Contour map of the highest occupied e_g cluster molecular-orbital wave function for a Mn impurity in an aluminum crystal.

Fig.11. Schematic perspective drawing of "tubular" dδ-bonding molecular-orbital components along a line of atoms arising from the overlap of d_{xy} atomic orbitals along the z-axis.

Fig.12. Schematic perspective drawing of "tubular" dδ-bonding molecular-orbital components along a line of atoms arising from the overlap of $d_{x^2-y^2}$ atomic orbitals along the z-axis.

Fig.13. Schematic perspective drawing of "tubular" dδ-bonding cluster molecular-orbital components in a bcc crystal arising from the overlap of d_{xy} atomic orbitals.

Fig.14. Schematic perspective drawing of "tubular" dδ-bonding cluster molecular-orbital components in a bcc crystal arising from the overlap of $d_{x^2-y^2}$ atomic orbitals.

Fig.15. Composite molecular-orbital density-of-states profile for bcc transition metals.

Fig.16. Schematic perspective drawing in a plane of three atoms of "layered" bonding molecular-orbital components arising from the overlap of d_{z^2} atomic orbital annular regions (the dashed contours).

Fig.17. Contour map of the wave function for the highest occupied t_{2g} (d_{xy}, d_{yz}, d_{xz}) cluster molecular orbital of vanadium

Fig.18. Contour maps in two different planes of the wave function for the highest occupied $e_g(d_{x^2-y^2})$ cluster molecular orbital of niobium.

Fig.19. Contour map of the wave function for highest occupied $e_g(d_{z^2})$ cluster molecular orbital of niobium.

Fig.20. Contour map of wave function for the highest occupied $e_g(d_{z^2})$ cluster molecular orbital of chromium.

Fig.21. Contour map of the wave function for the highest occupied cluster molecular orbital of zirconium.

Fig.22. Contour map of the wave function for the lowest unoccupied cluster molecular orbital of zirconium.

Fig.23. Contour map of the wave function for the dδ-bonding molecular orbital at the Fermi energy of Nb_3Sn, shown along four atoms of a Nb chain.

Fig.24. Schematic representation of the wave function for the molecular orbital at the Fermi energy of PdH_x ($x \sim 1$).

Fig.25. Schematic representation of the wave function for the molecular orbital at the Fermi energy of $(TMTSF)_2PF_6$ in relation to the crystal structure.

Fig.26 Crystal structure of TTF-TCNQ.

Fig.27(a) Contour map of the wave function for the cluster molecular orbital at the Fermi energy of amorphous Cu-Zr.

Fig.27(b) Contour map of the wave function for the cluster molecular orbital at the Fermi energy of amorphous Pd-Si.

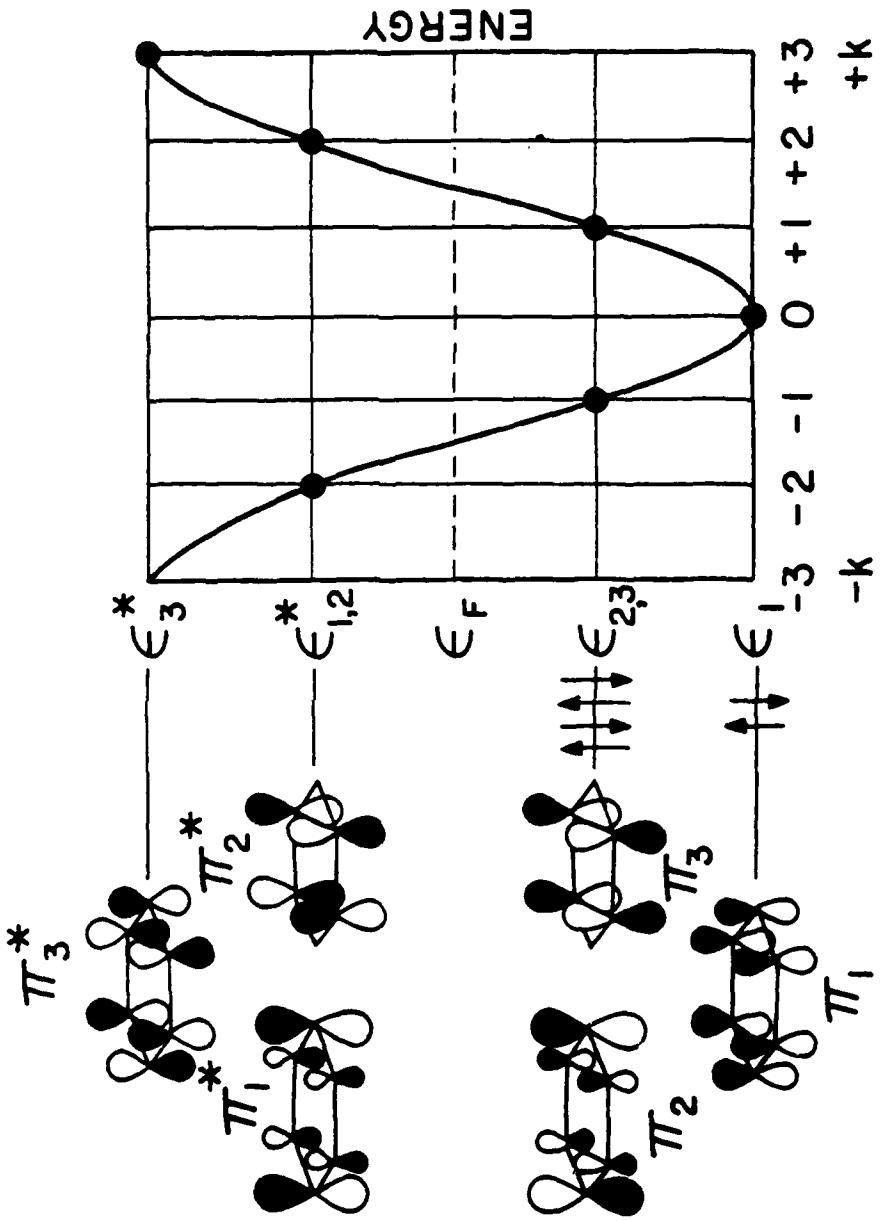
ENERGY
+k
+3
+2
+1
0
-1
-2
-3
-k
ϵ^*_3
$\epsilon^*_{1,2}$
ϵ_F
$\epsilon_{2,3}$
ϵ_1
π^*_3
π^*_2
π^*_1
π_3
π_2
π_1

FIGURE 1

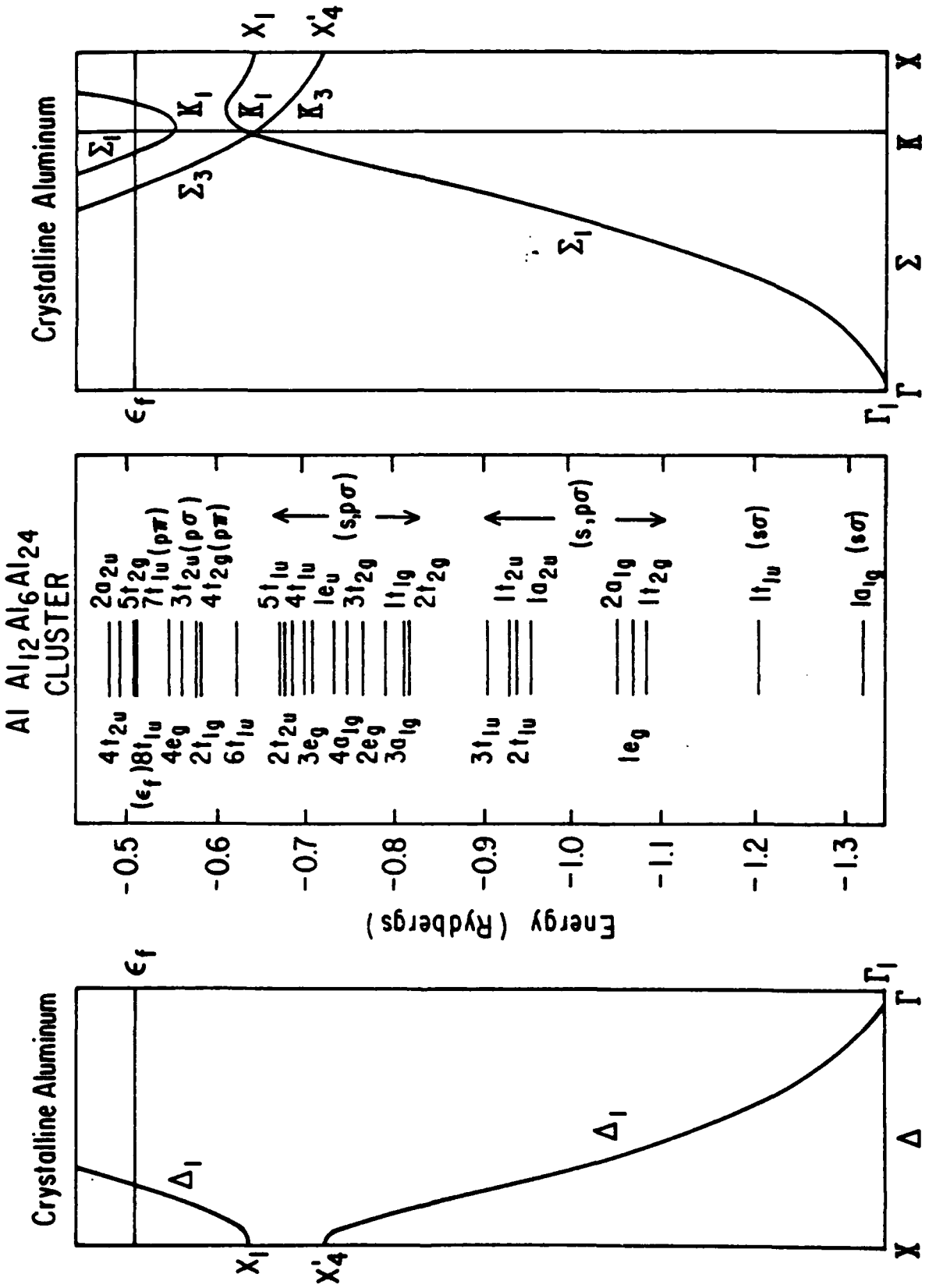
Crystalline Aluminum
X_1
X'_4
K_1
K_1
K_3
Σ_1
Σ_3
Σ_1
X
K
Σ
Γ
ϵ_f
Γ_1
Al $Al_{12}Al_6Al_{24}$
CLUSTER
$2a_{2u}$
$5t_{2g}$
$7t_{1u}(p\pi)$
$3t_{2u}(p\sigma)$
$4t_{2g}(p\pi)$
$5t_{1u}$
$4t_{1u}$
$1e_u$
$3t_{2g}$
$1t_{1g}$
$2t_{2g}$
(s,pσ)
$1t_{2u}$
$1a_{2u}$
(s,pσ)
$2a_{1g}$
$1t_{2g}$
$1t_{1u}$ (sσ)
$1a_{1g}$ (sσ)
$4t_{2u}$
$(\epsilon_f)8t_{1u}$
$4e_g$
$2t_{1g}$
$6t_{1u}$
$2t_{2u}$
$3e_g$
$4a_{1g}$
$2e_g$
$3a_{1g}$
$3t_{1u}$
$2t_{1u}$
$1e_g$
-0.5
-0.6
-0.7
-0.8
-0.9
-1.0
-1.1
-1.2
-1.3
Energy (Rydbergs)
Crystalline Aluminum
ϵ_f
Γ_1
Δ_1
Δ_1
X_1
X'_4
X
Δ
Γ

FIGURE 2

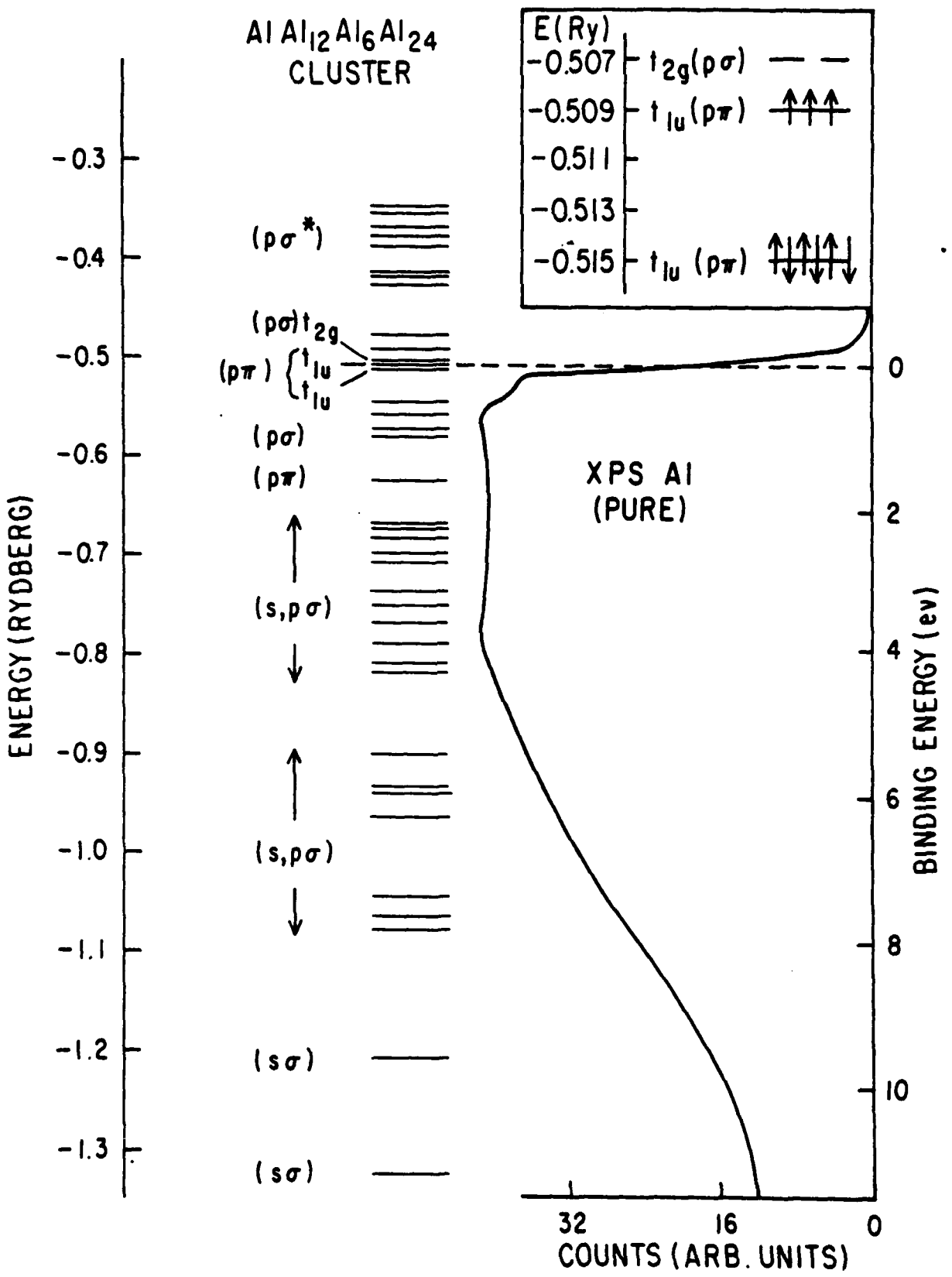
Al Al12 Al6 Al24
CLUSTER
E(Ry)
-0.507
-0.509
-0.511
-0.513
-0.515
t2g(pσ)
t1u(pπ)
t1u (pπ)
(pσ*)
(pσ)t2g
(pπ) t1u t1u
(pσ)
(pπ)
(s,pσ)
(s,pσ)
(sσ)
(sσ)
ENERGY (RYDBERG)
-0.3
-0.4
-0.5
-0.6
-0.7
-0.8
-0.9
-1.0
-1.1
-1.2
-1.3
XPS Al
(PURE)
BINDING ENERGY (ev)
0
2
4
6
8
10
32
16
0
COUNTS (ARB. UNITS)

FIGURE 3

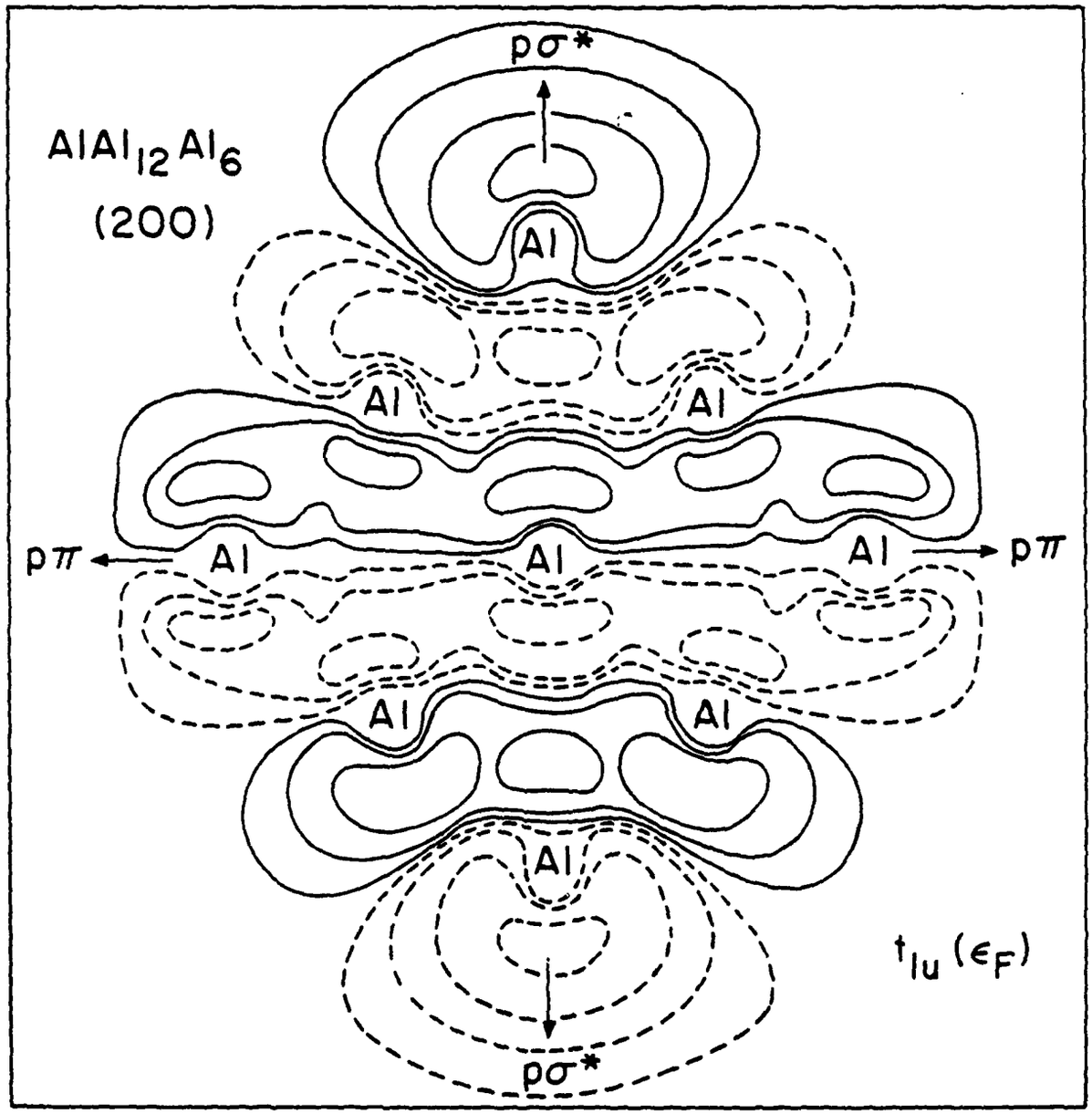

FIGURE 4

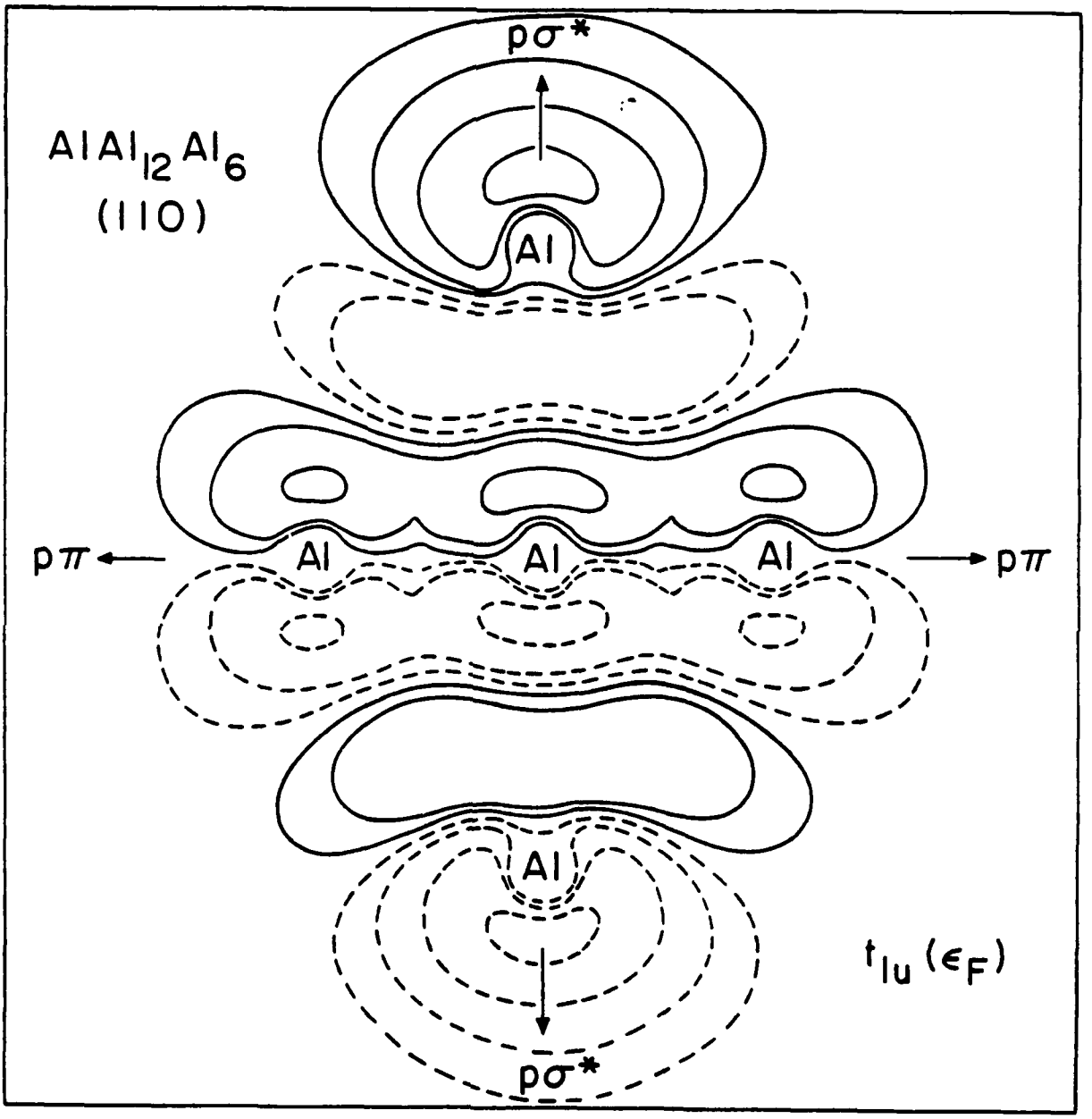

FIGURE 5

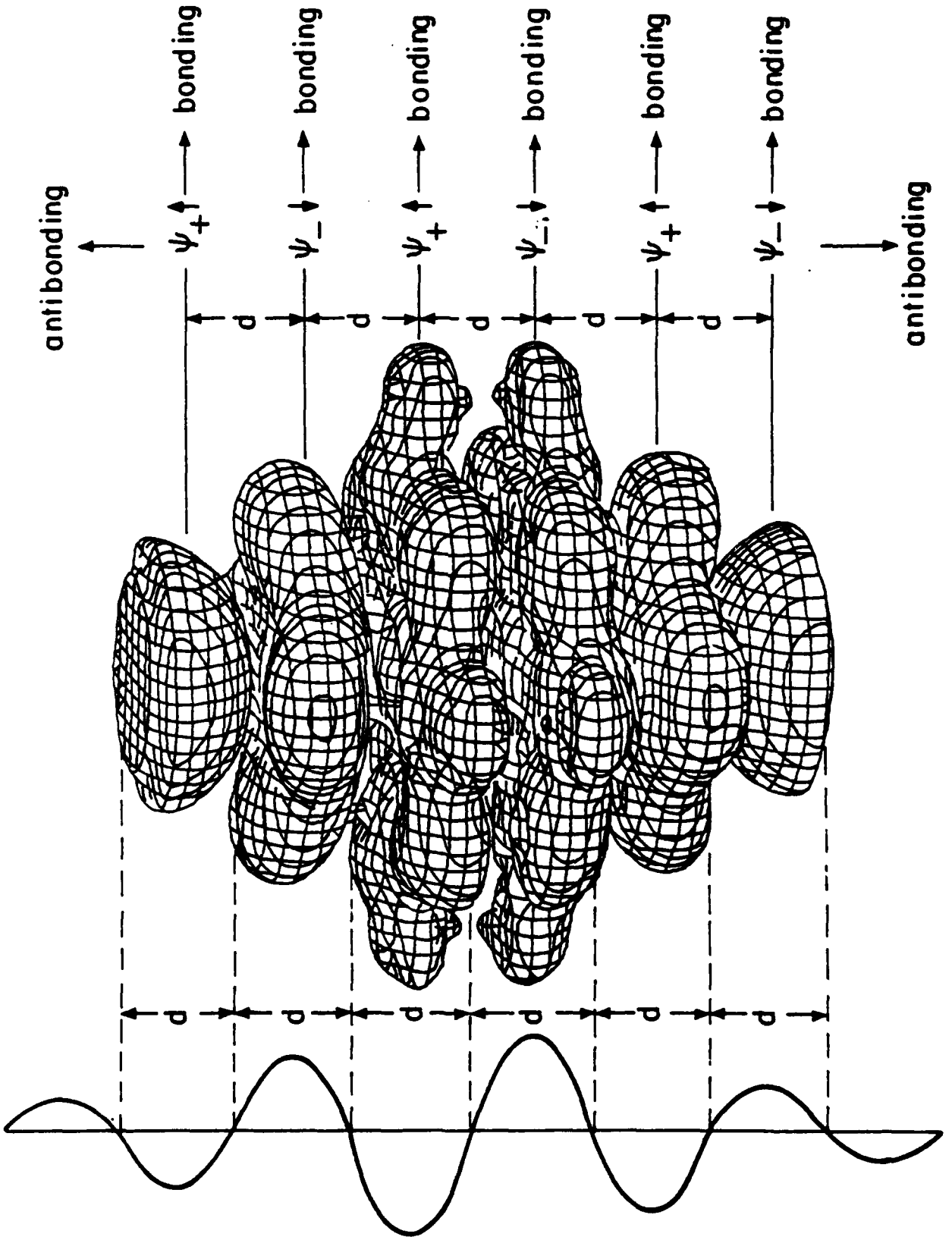
antibonding
bonding
bonding
bonding
bonding
bonding
antibonding
ψ_+
ψ_-
ψ_+
ψ_-
ψ_+
ψ_-
d
d
d
d
d
d
d
d
d
d
d
d

FIGURE 6

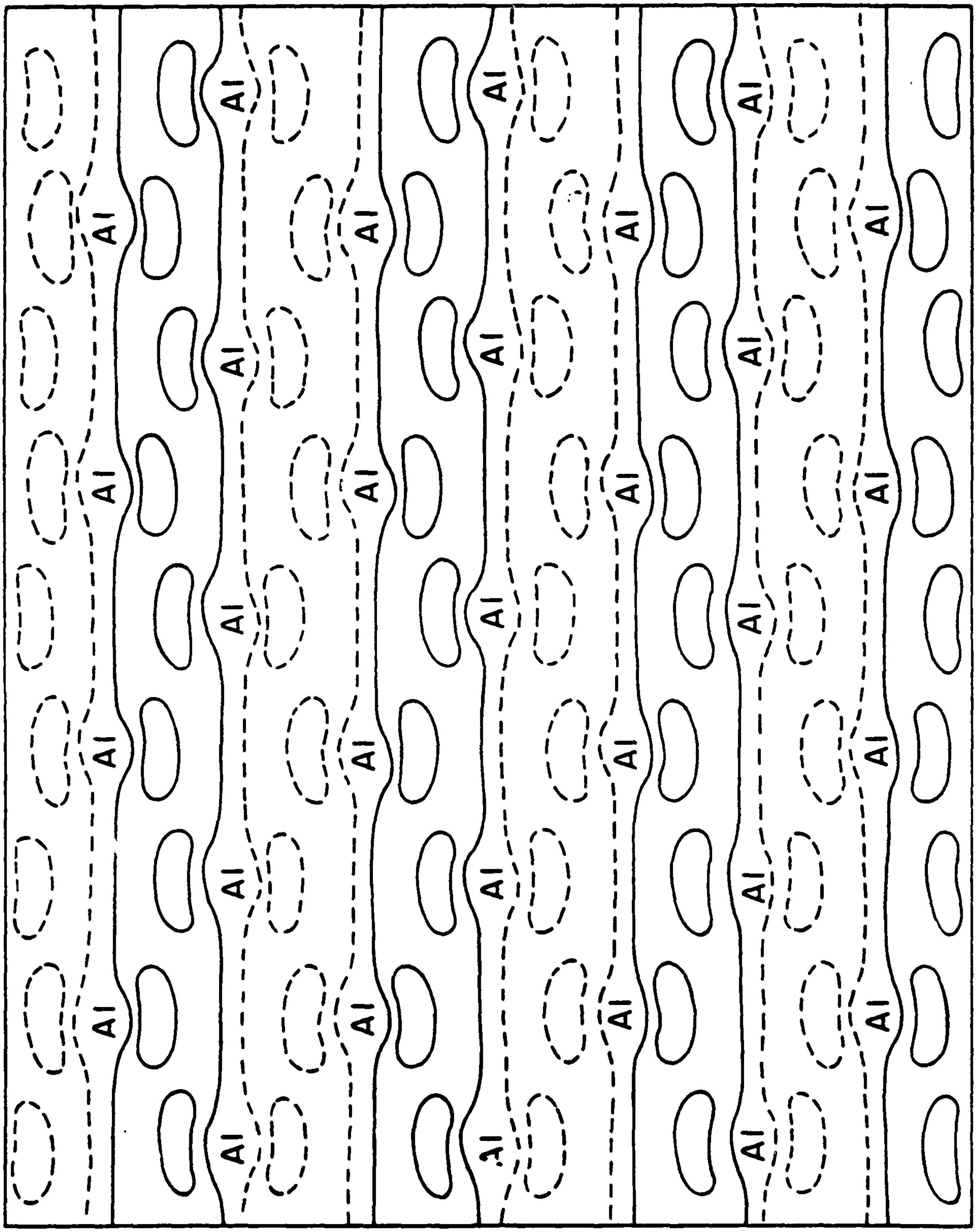

FIGURE 7

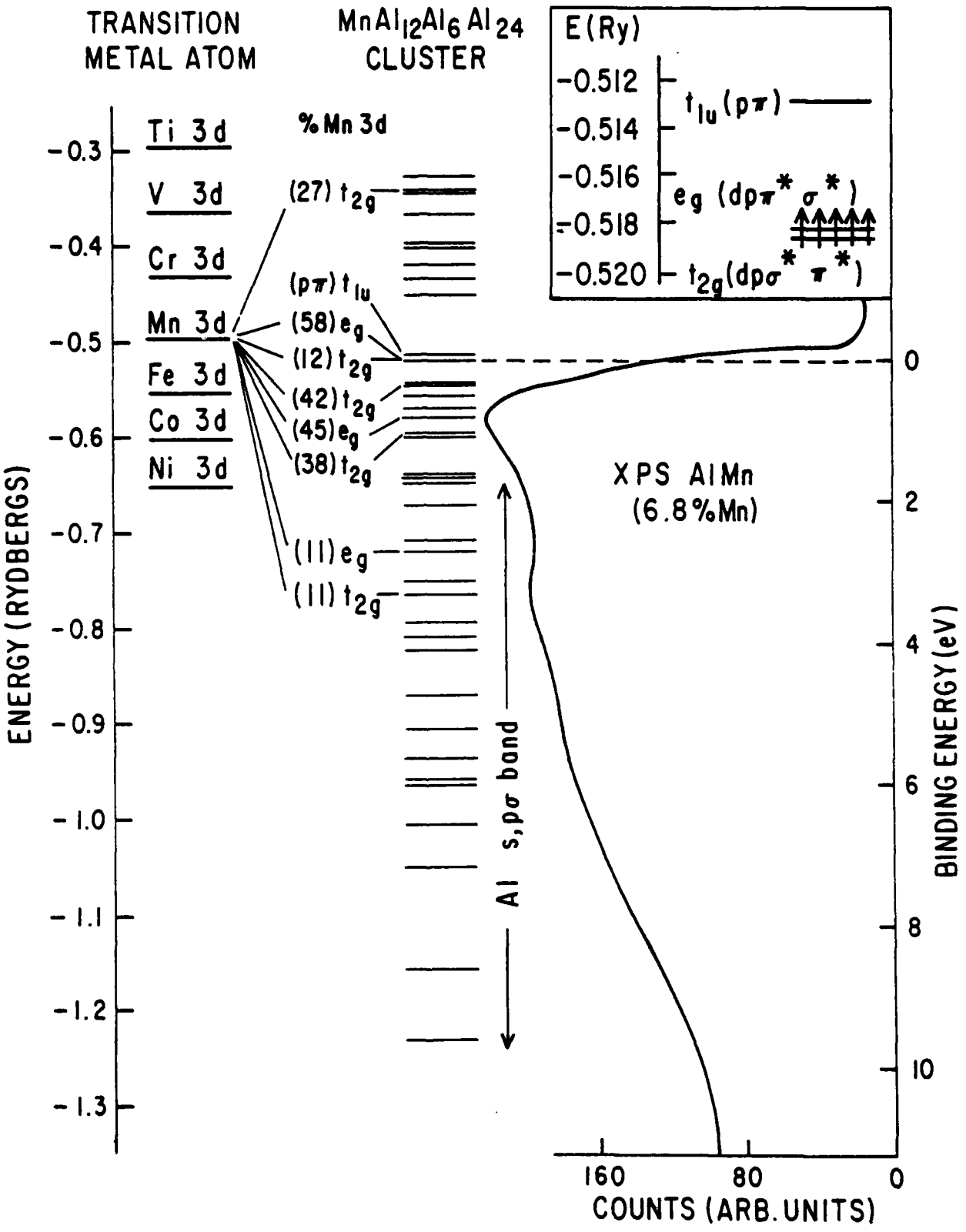
TRANSITION METAL ATOM
MnAl12Al6 Al24 CLUSTER
E(Ry)
-0.512
-0.514
-0.516
-0.518
-0.520
t1u (pπ)
eg (dpπ* σ*)
t2g (dpσ* π*)
% Mn 3d
Ti 3d
V 3d
Cr 3d
Mn 3d
Fe 3d
Co 3d
Ni 3d
(27) t2g
(pπ) t1u
(58) eg
(12) t2g
(42) t2g
(45) eg
(38) t2g
(11) eg
(11) t2g
Al s,pσ band
XPS AlMn
(6.8%Mn)
ENERGY (RYDBERGS)
-0.3
-0.4
-0.5
-0.6
-0.7
-0.8
-0.9
-1.0
-1.1
-1.2
-1.3
BINDING ENERGY (eV)
0
2
4
6
8
10
160
80
0
COUNTS (ARB. UNITS)

FIGURE 8

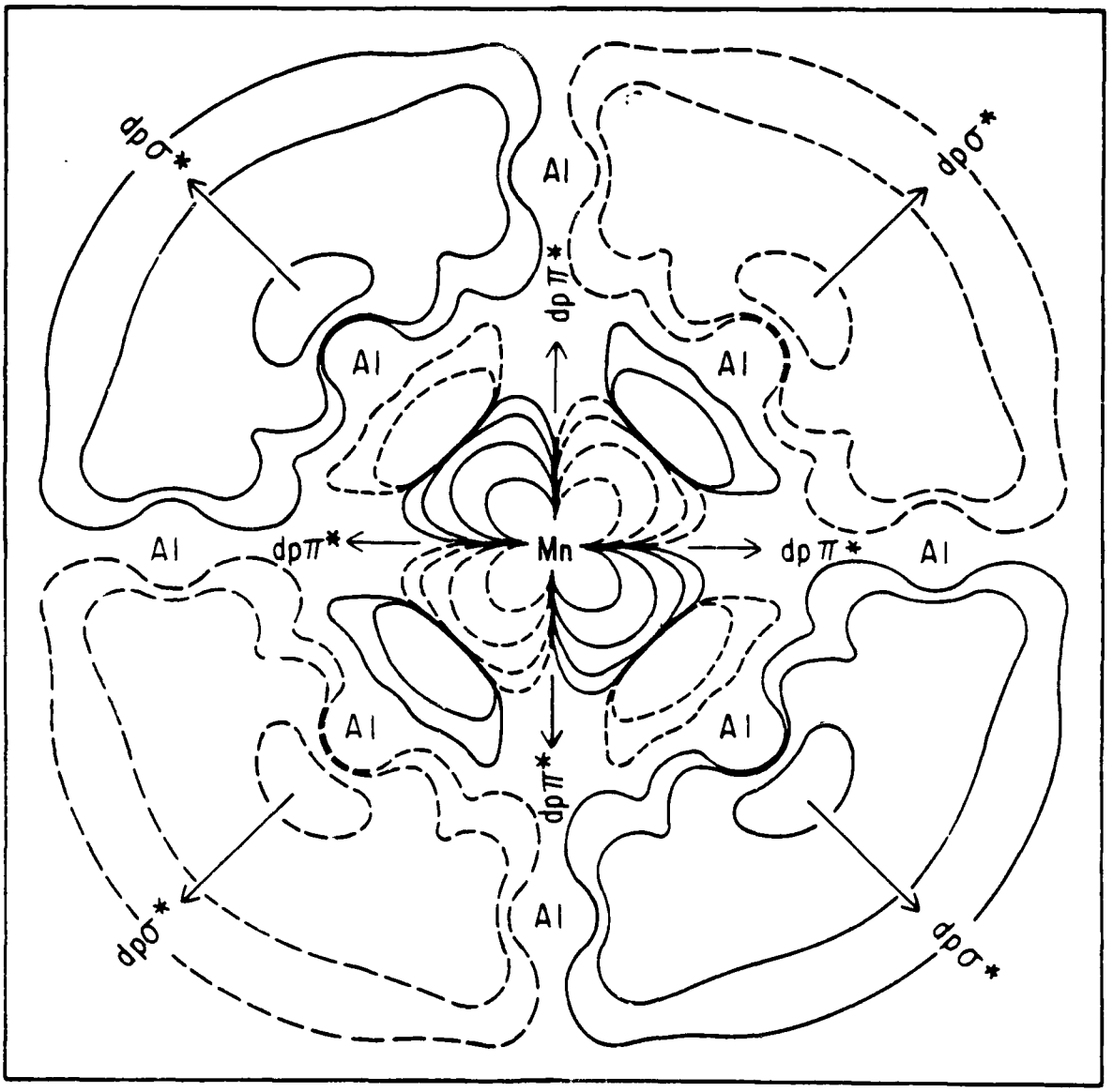

FIGURE 9

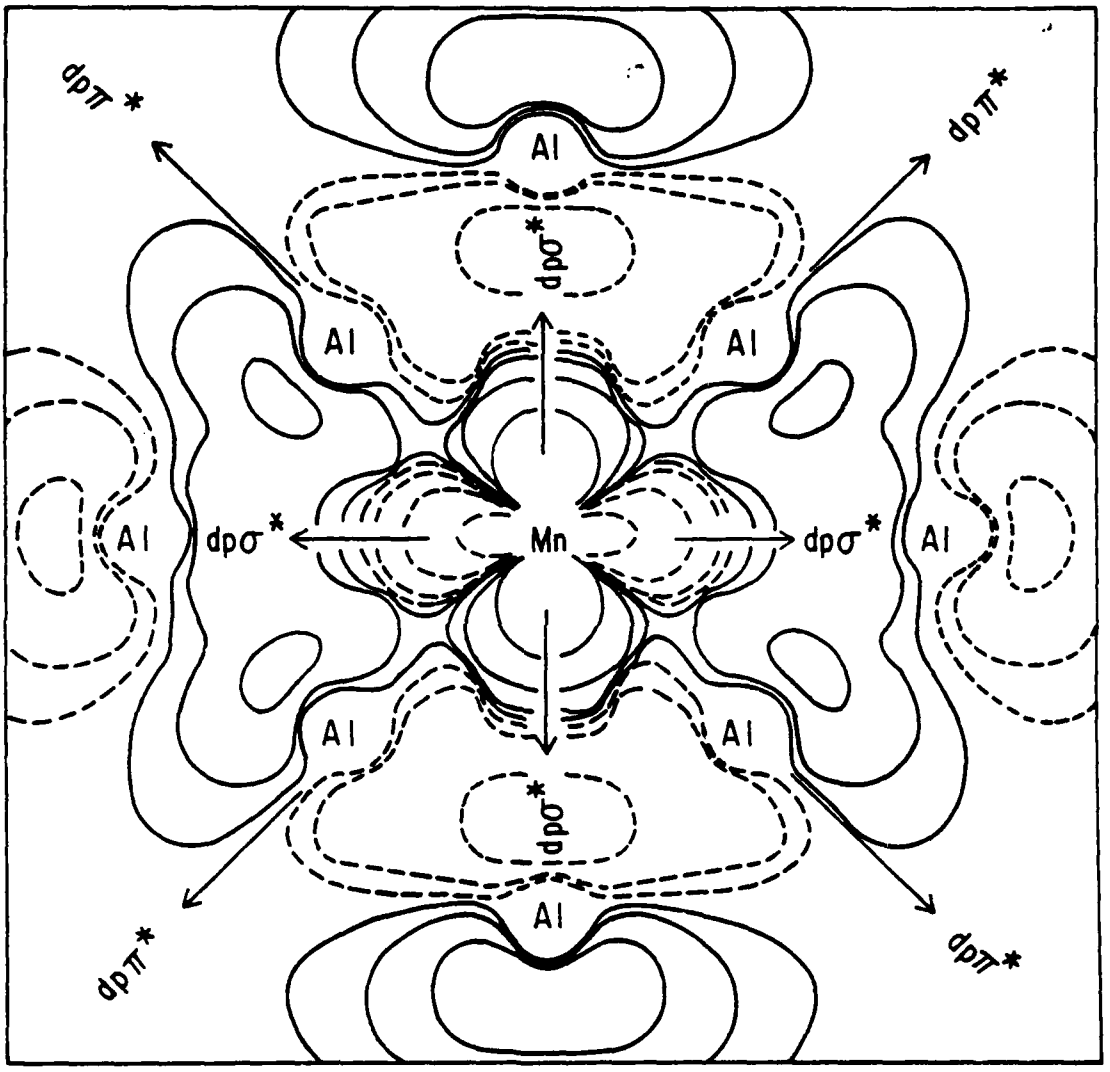

FIGURE 10

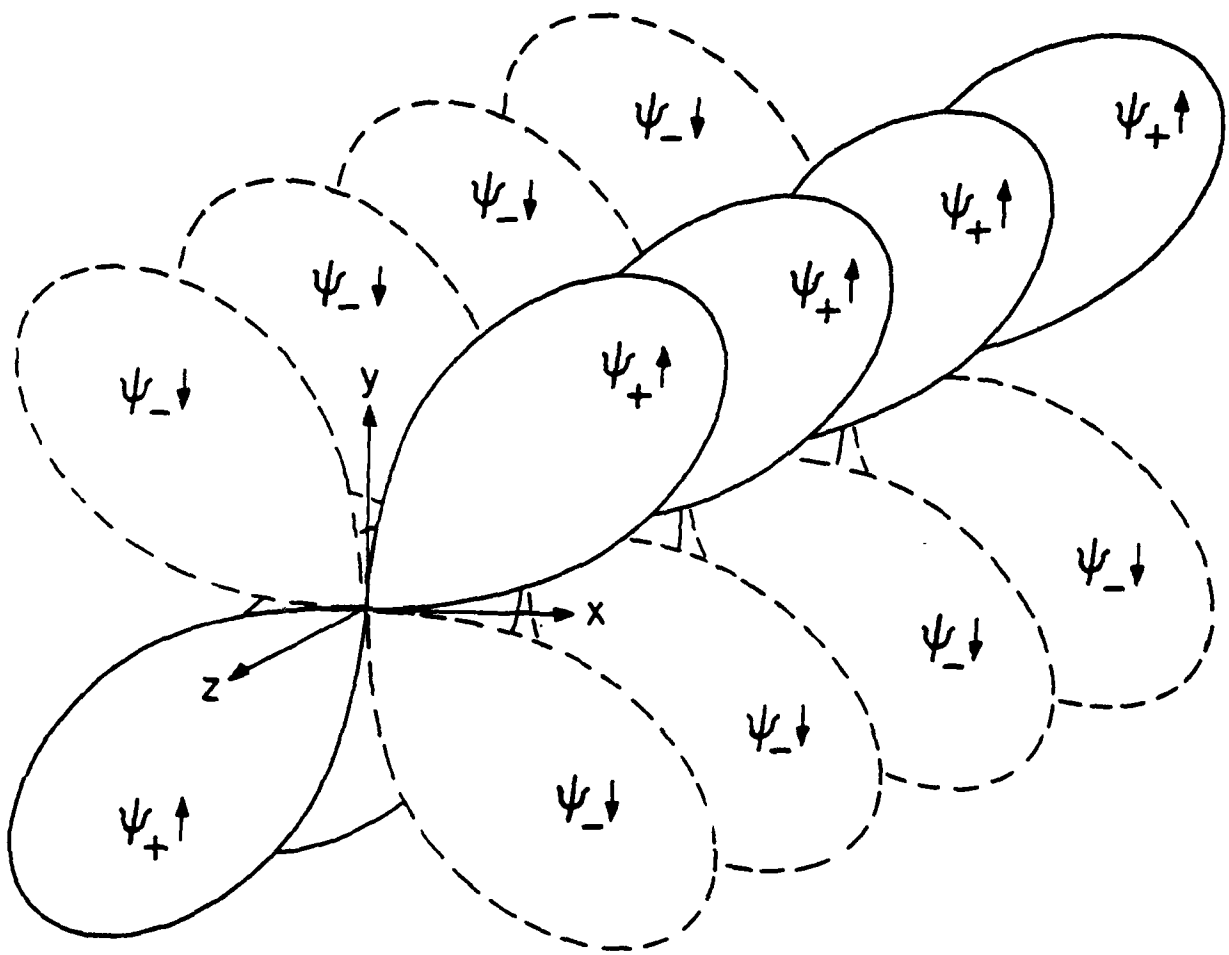

FIGURE 11

$d\ \delta(d_{x^2-y^2})$

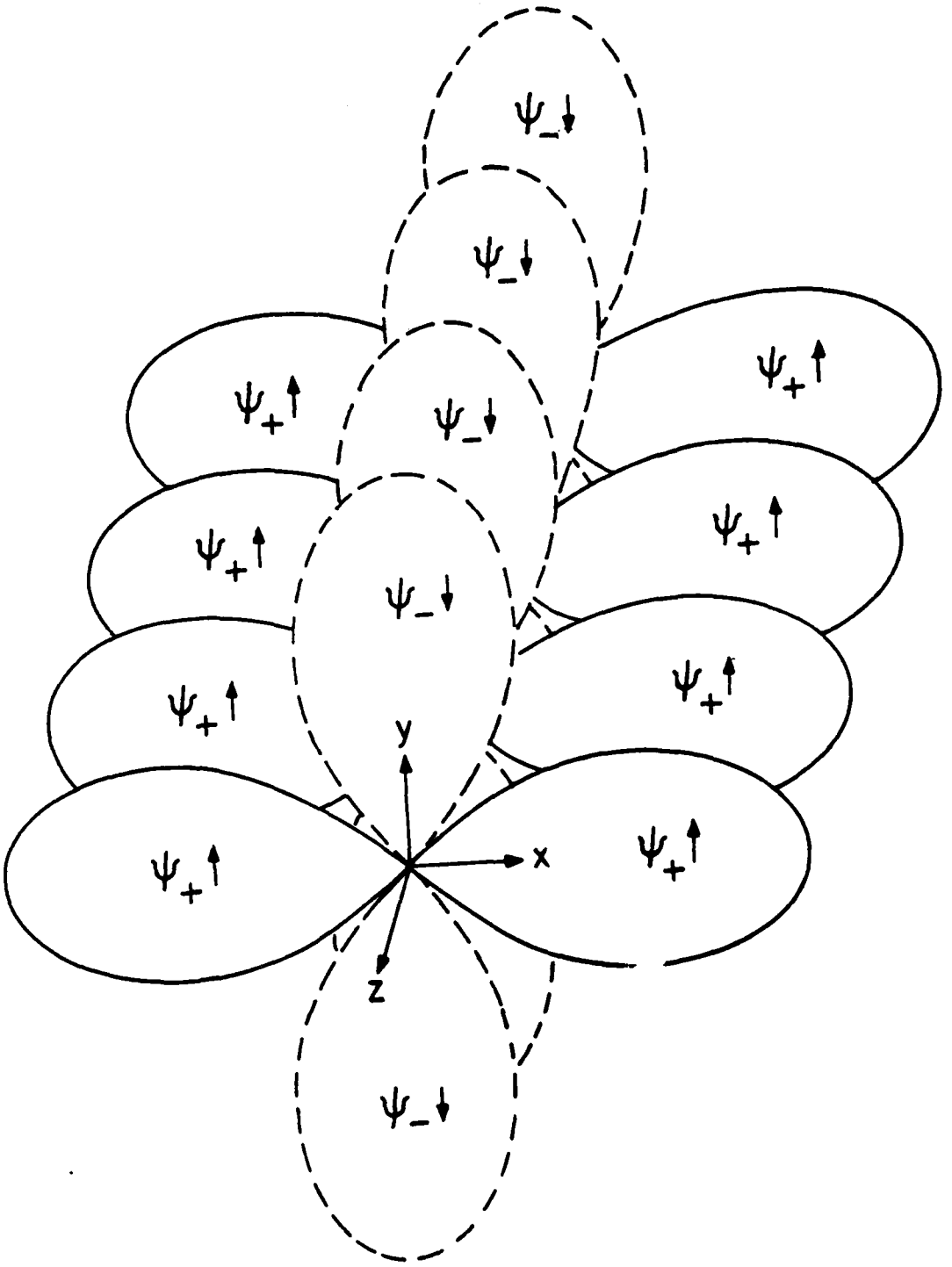

FIGURE 12

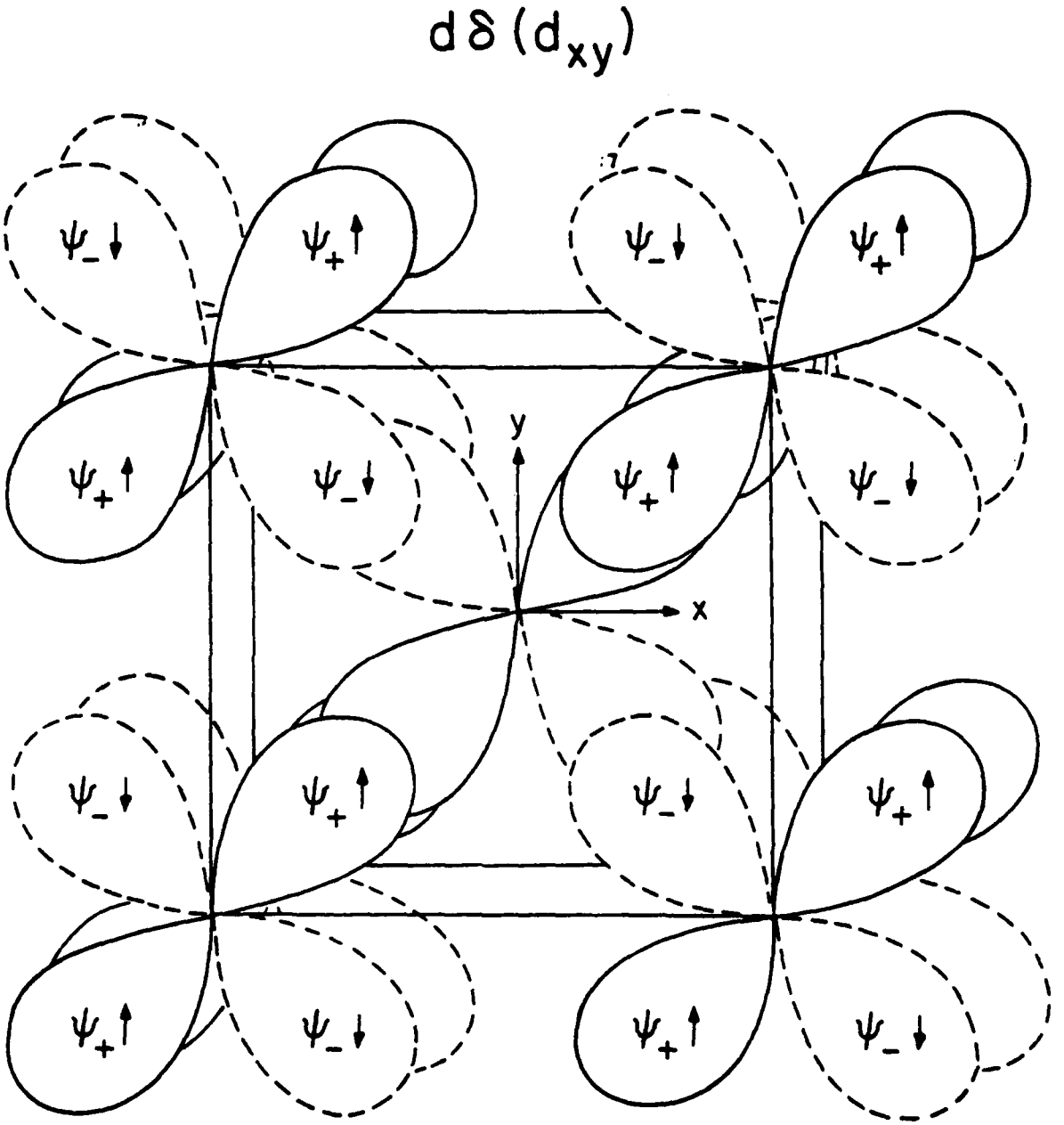

FIGURE 13

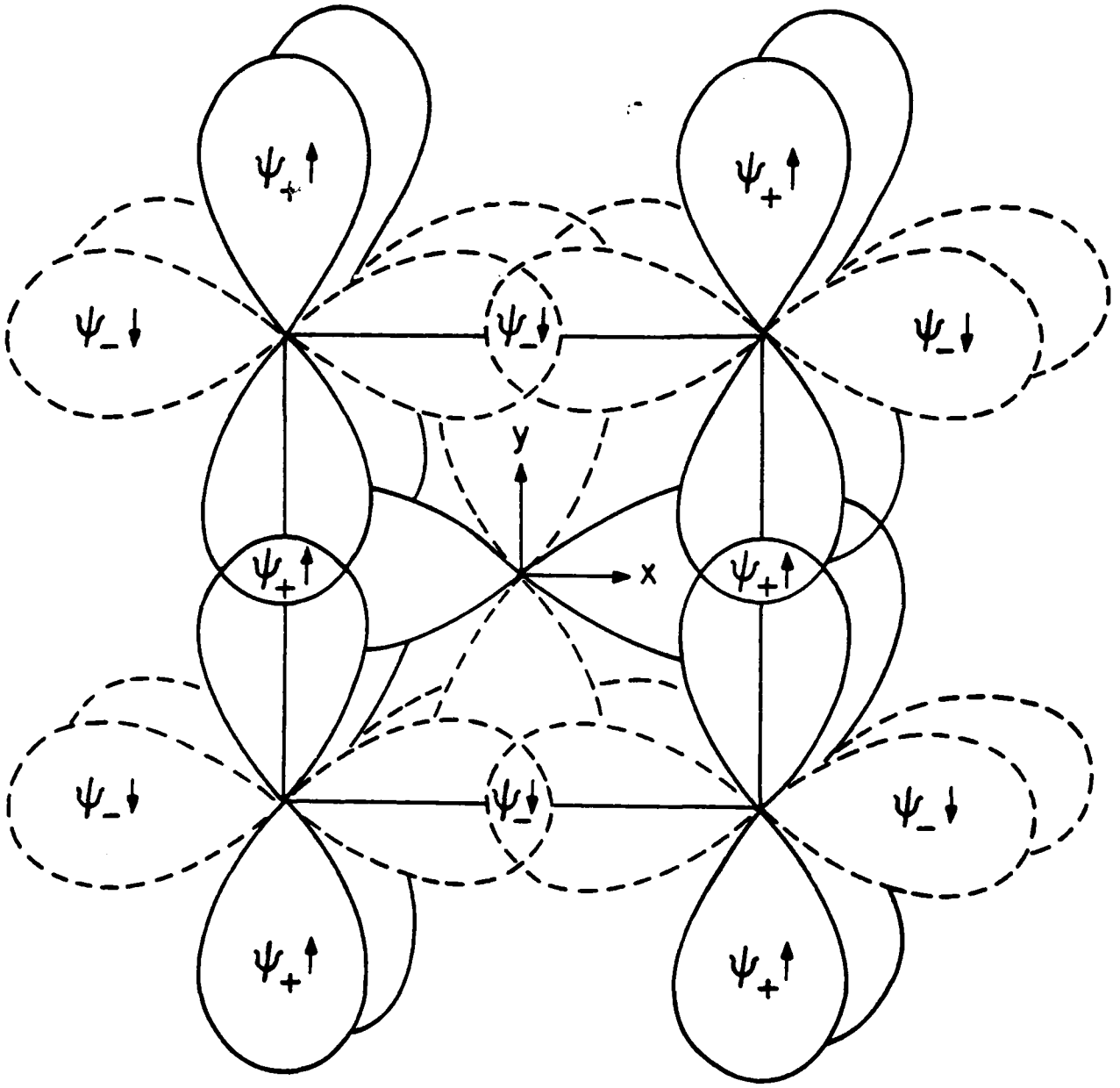

FIGURE 14

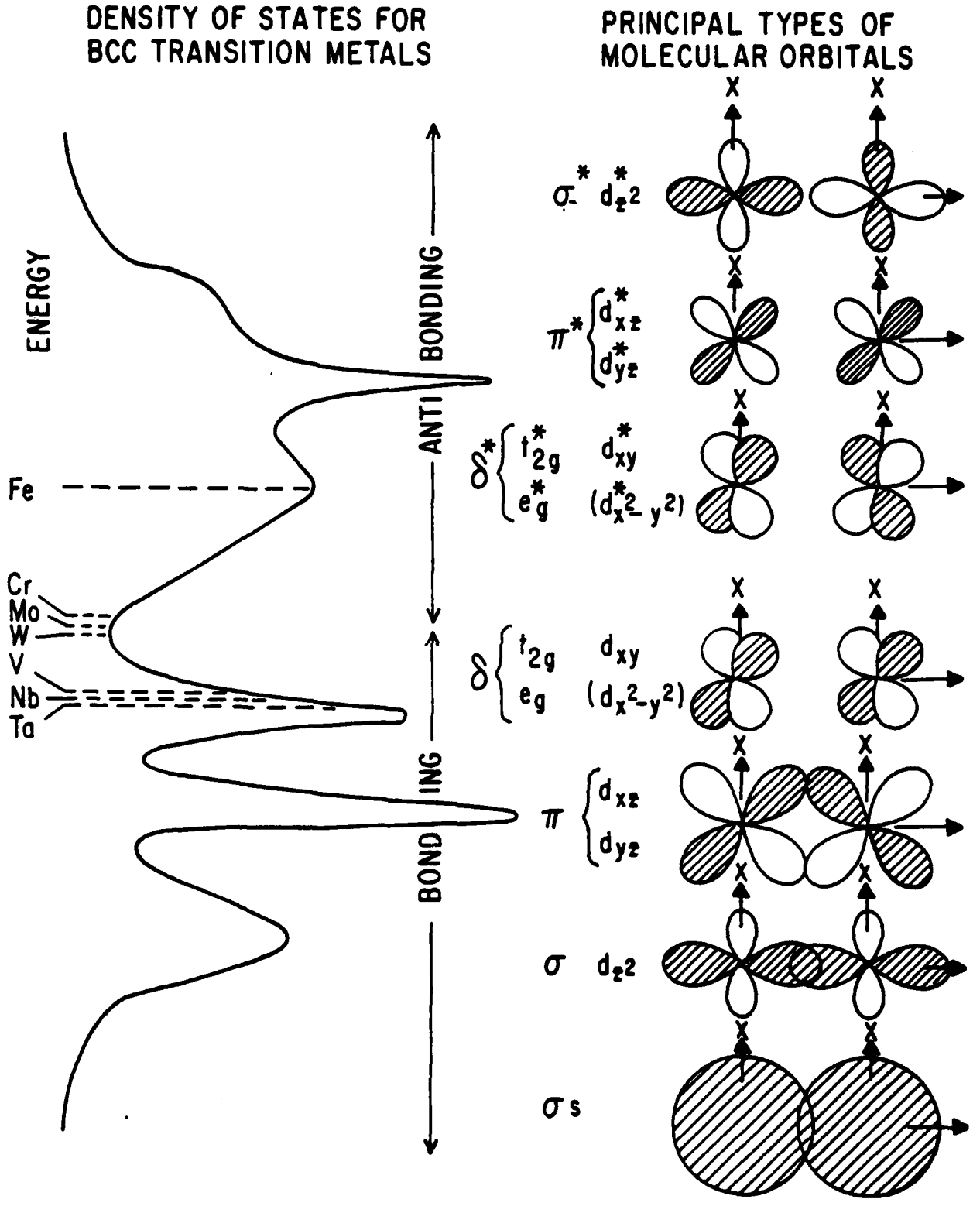
DENSITY OF STATES FOR
BCC TRANSITION METALS
ENERGY
BONDING
ANTI
ING
BOND
Fe
Cr
Mo
W
V
Nb
Ta
PRINCIPAL TYPES OF
MOLECULAR ORBITALS
X
σ* d*z2
π* d*xz
d*yz
δ* t*2g d*xy
e*g (d*x2-y2)
δ t2g dxy
eg (dx2-y2)
π dxz
dyz
σ dz2
σs

FIGURE 15

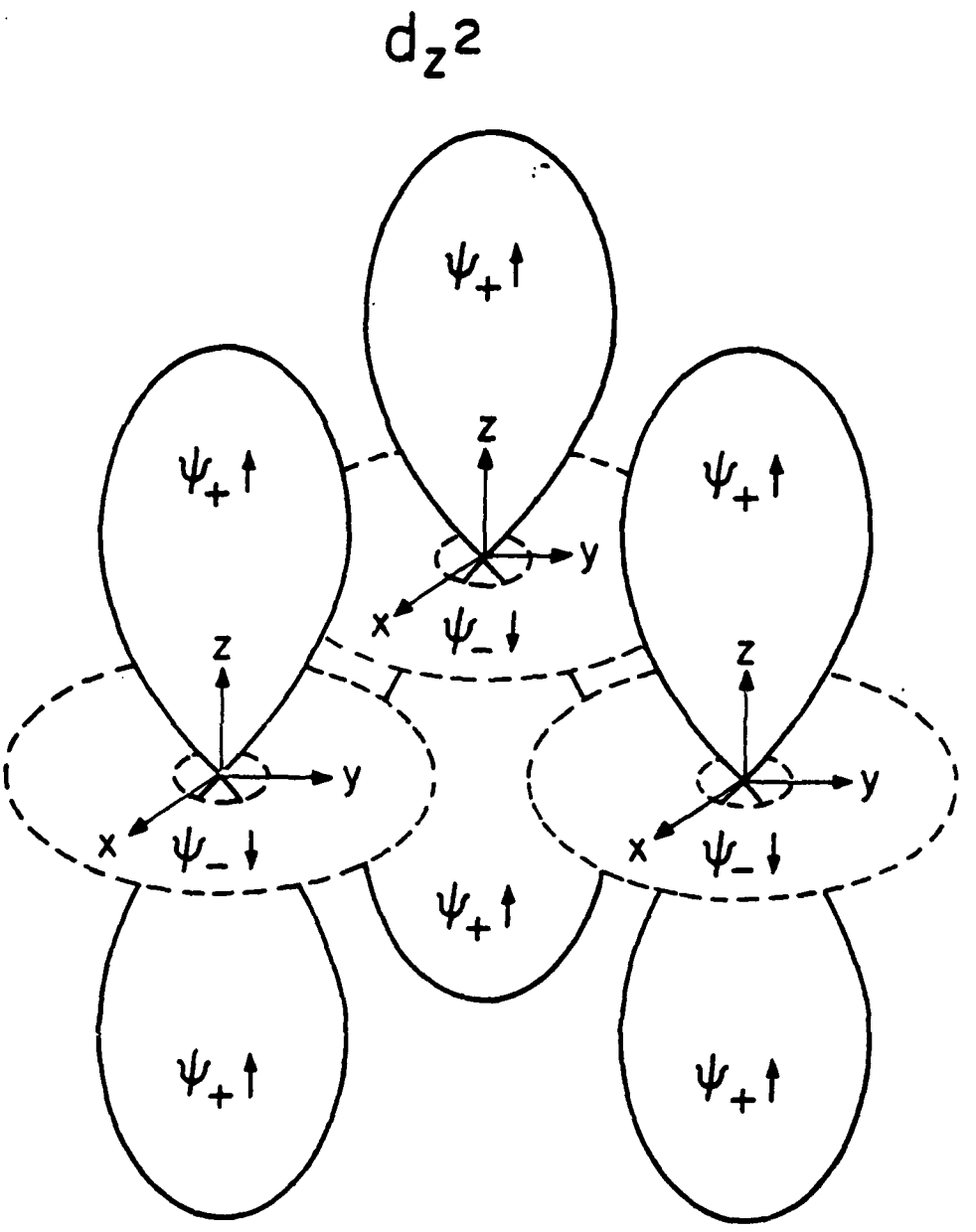
d_{z^2}
$\psi_+\uparrow$
$\psi_+\uparrow$
$\psi_+\uparrow$
z
y
x
$\psi_-\downarrow$
z
y
x
$\psi_-\downarrow$
z
y
x
$\psi_-\downarrow$
$\psi_+\uparrow$
$\psi_+\uparrow$
$\psi_+\uparrow$

FIGURE 16

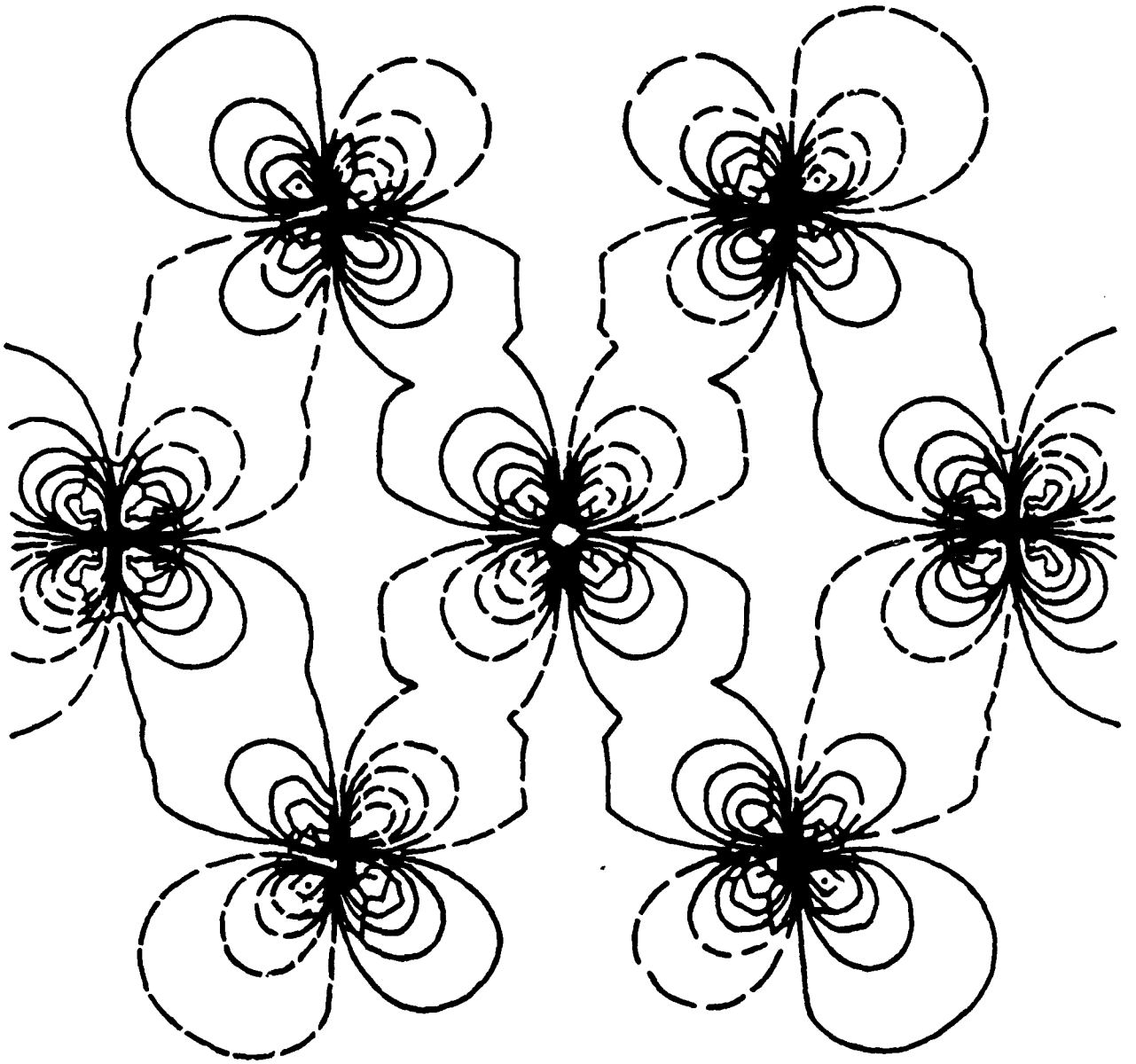

FIGURE 17

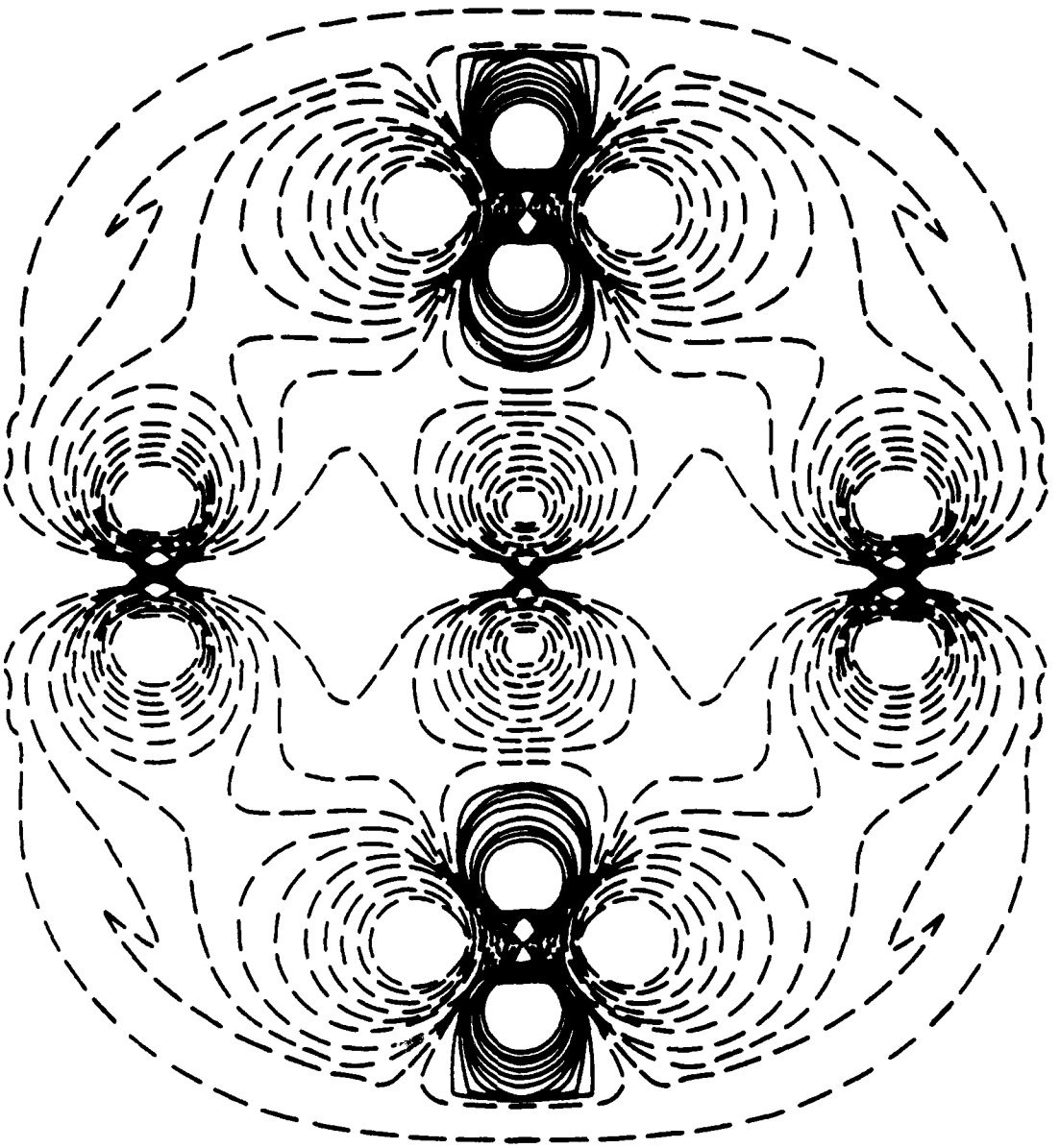

(a)

FIGURE 18(a)

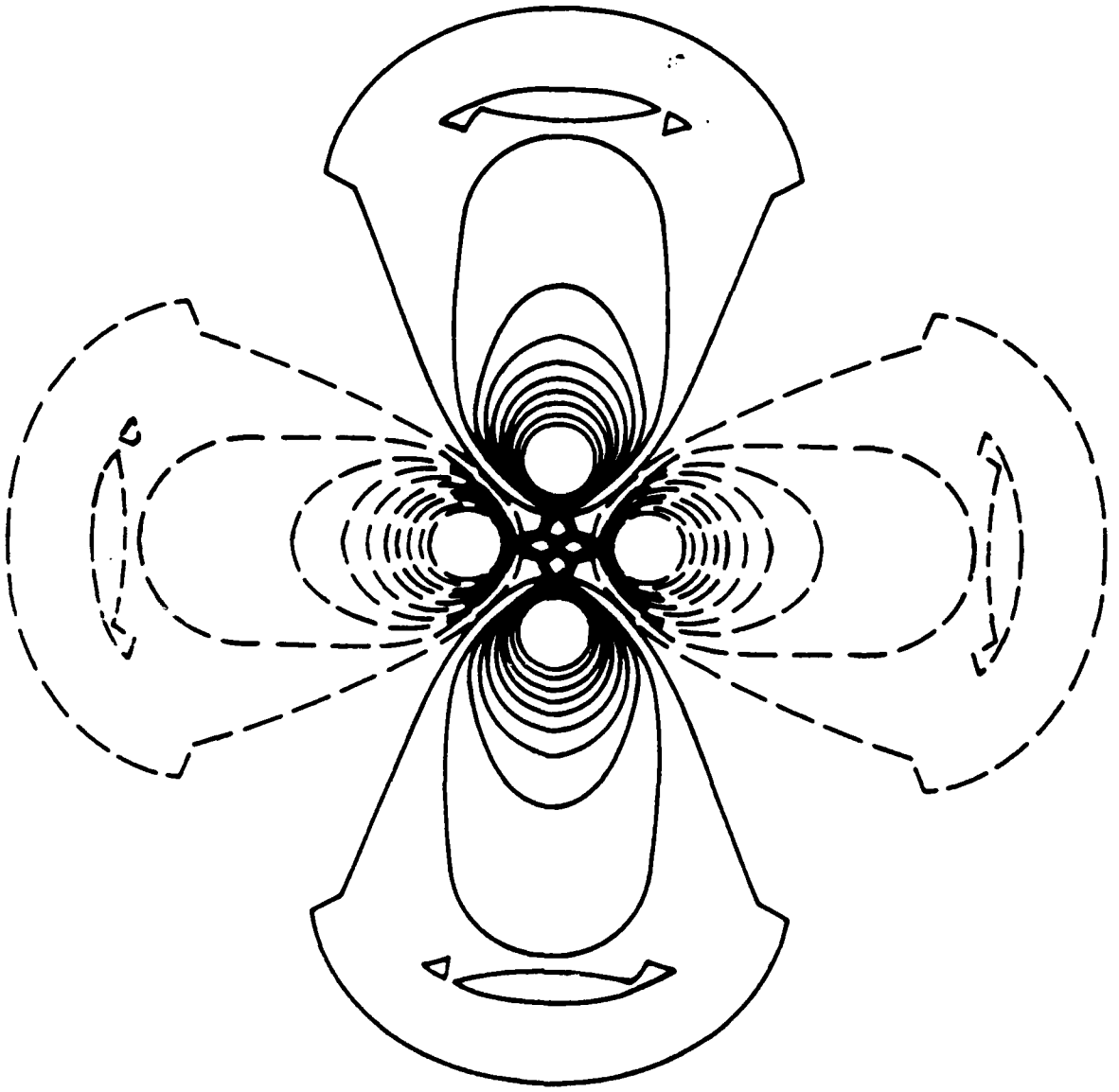

(b)

FIGURE 18(b)

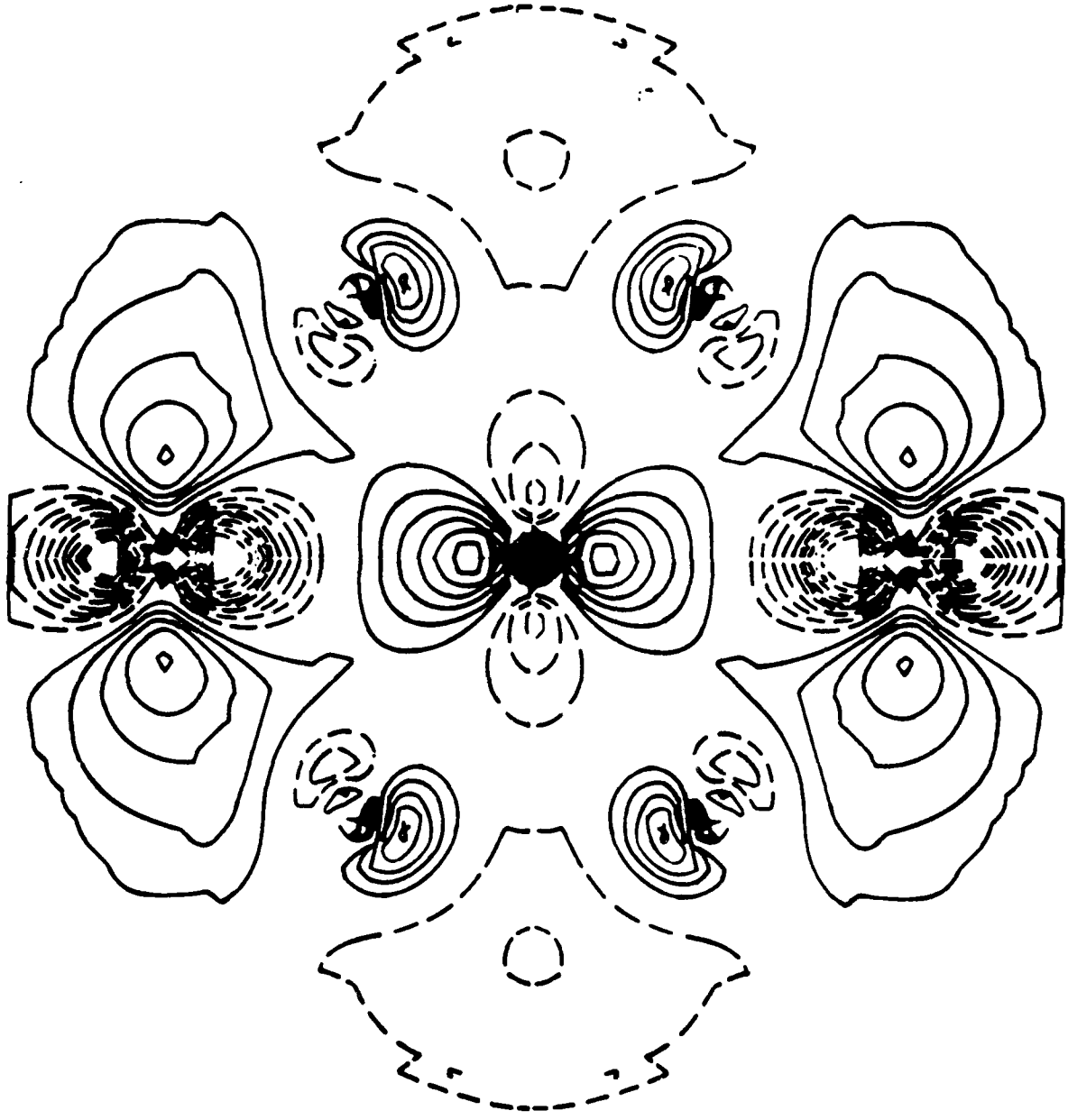

FIGURE 19

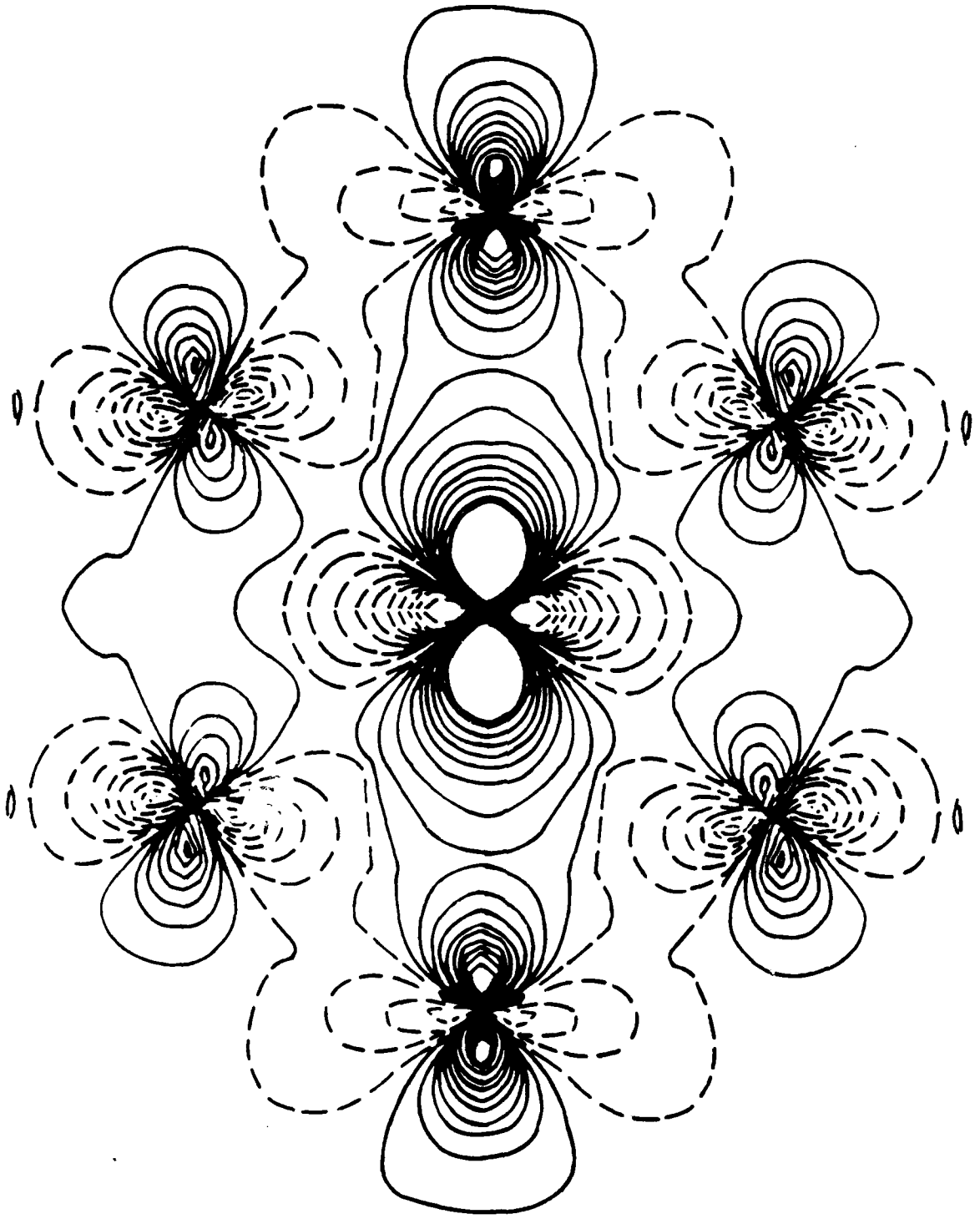

FIGURE 20

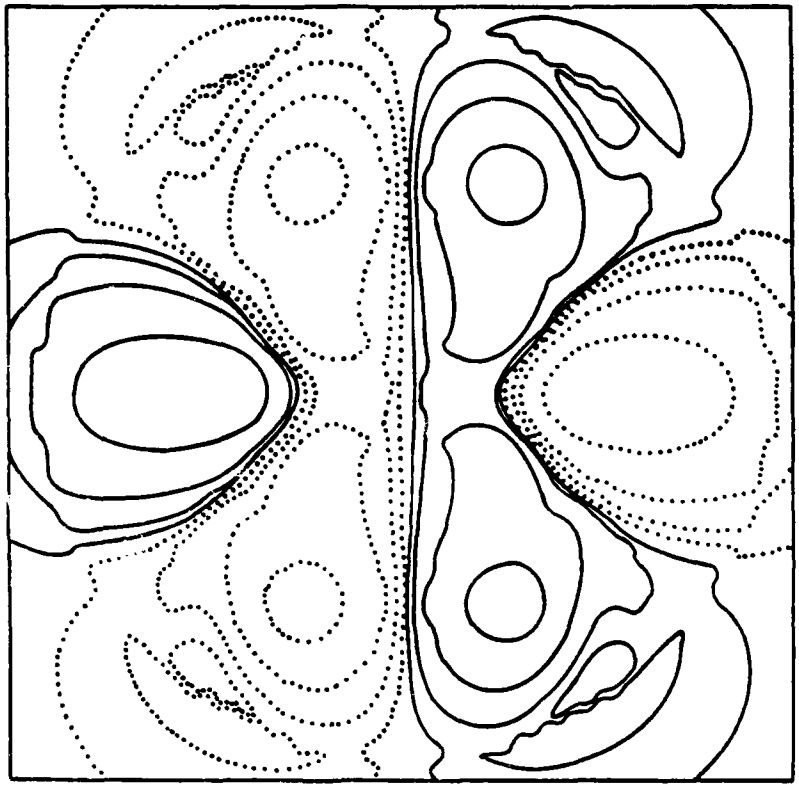

FIGURE 21

AD-A119 784 MASSACHUSETTS INST OF TECH CAMBRIDGE CENTER FOR MATE--ETC F/G 11/6
MOLECULAR-ORBITAL BASIS FOR SUPERCONDUCTIVITY IN HIGH- AND LOW----ETC(U)
SEP 82 K H JOHNSON, R P MESSMER N00014-81-K-0499
UNCLASSIFIED TR-4 NL

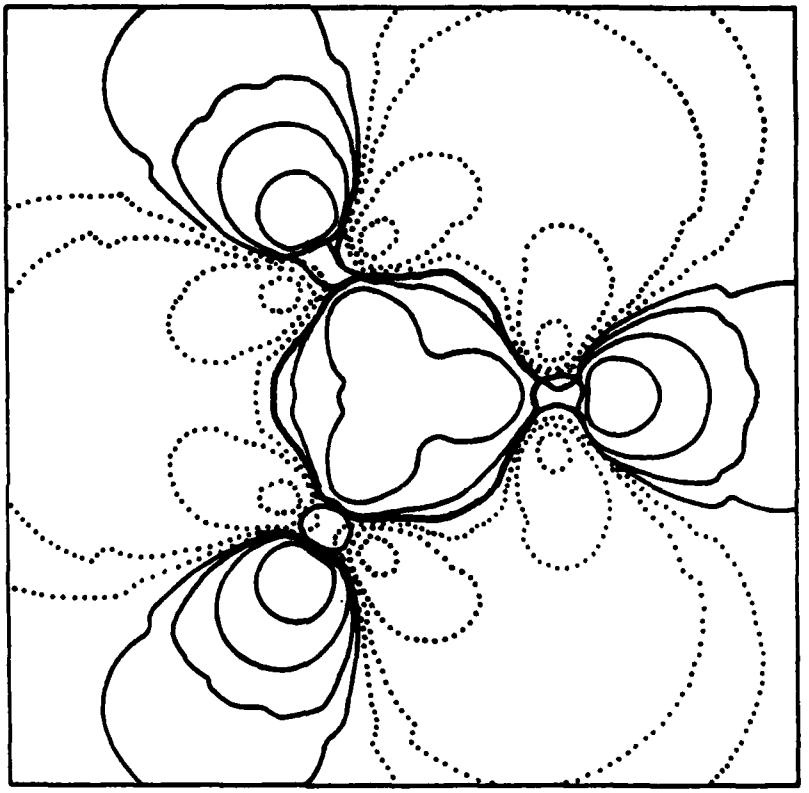

FIGURE 22

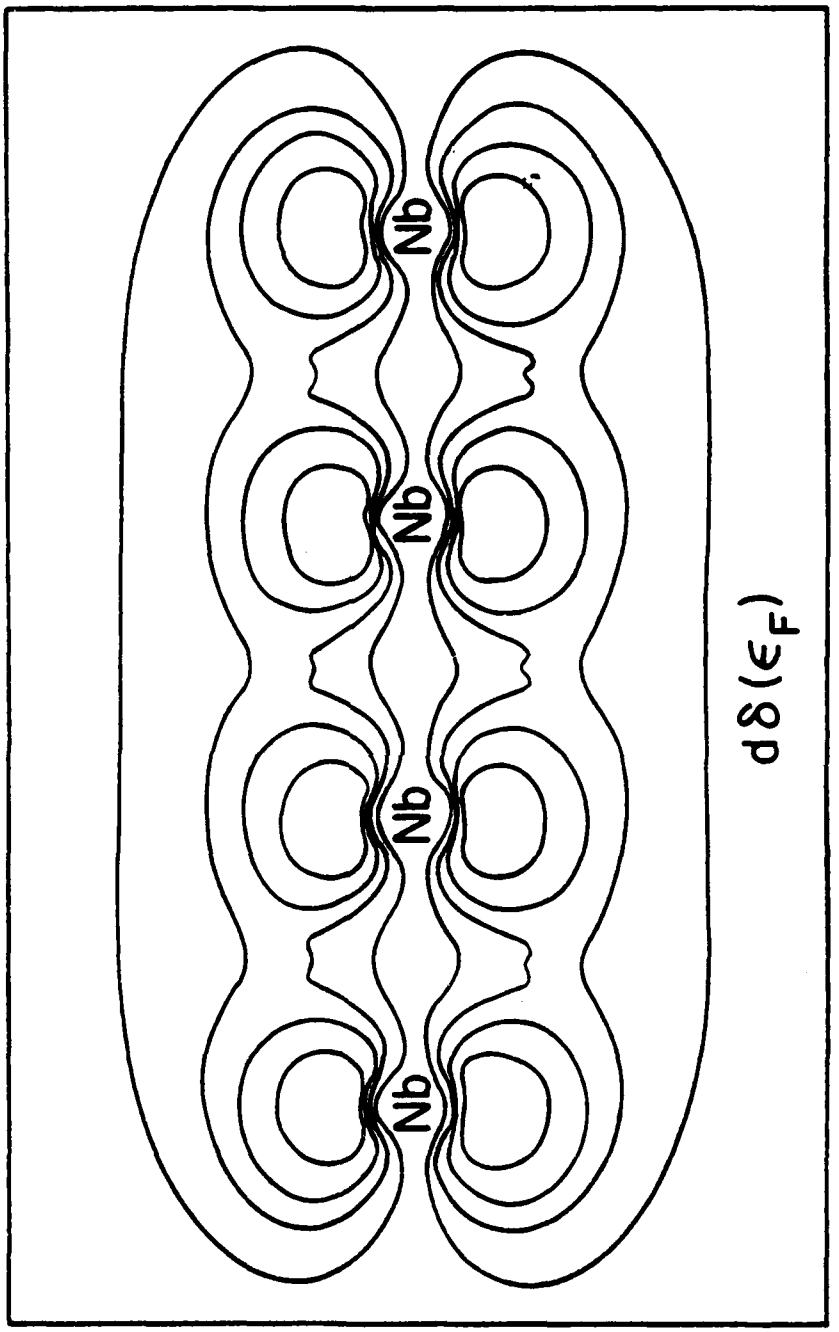

FIGURE 23

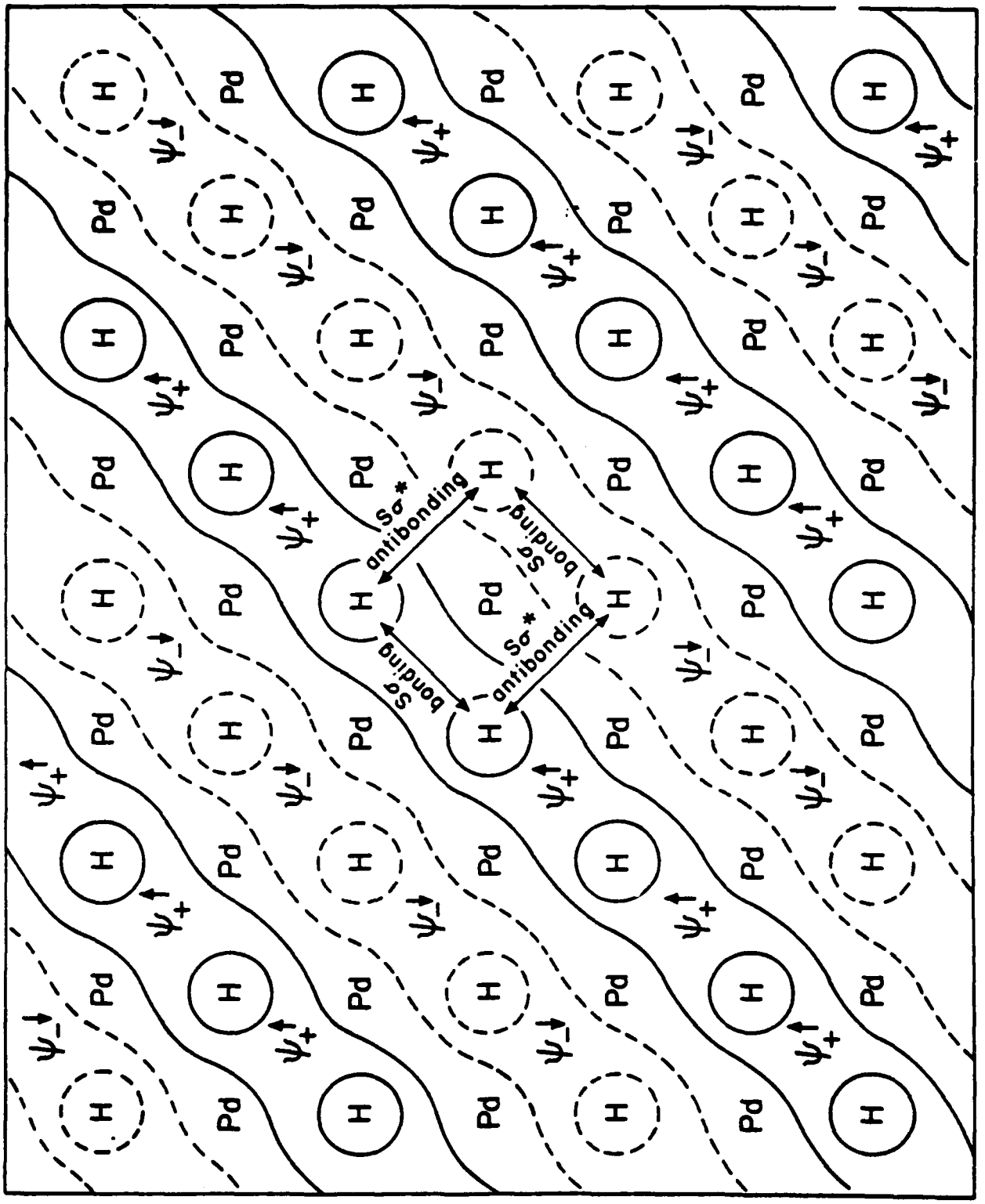
H
Pd
ψ_+
ψ_-
Sσ* antibonding
Sσ bonding
Sσ bonding
Sσ* antibonding

FIGURE 24

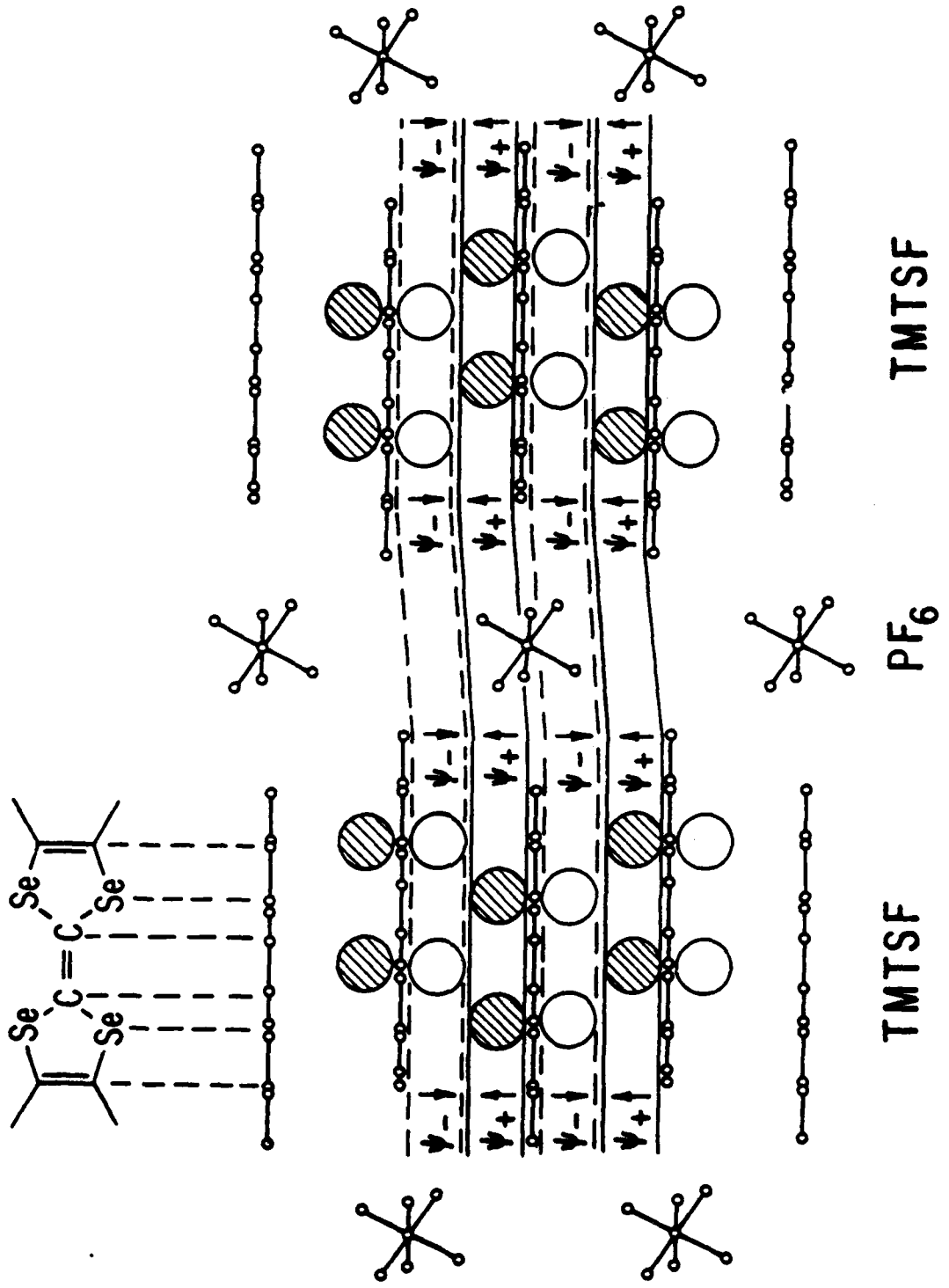

FIGURE 25

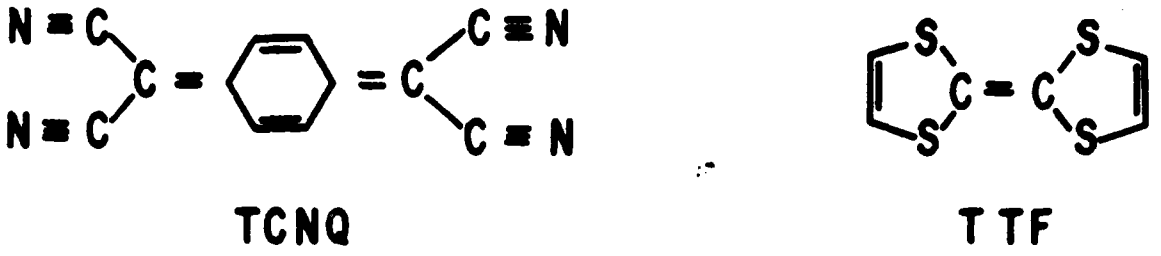

TCNQ TTF

(a)

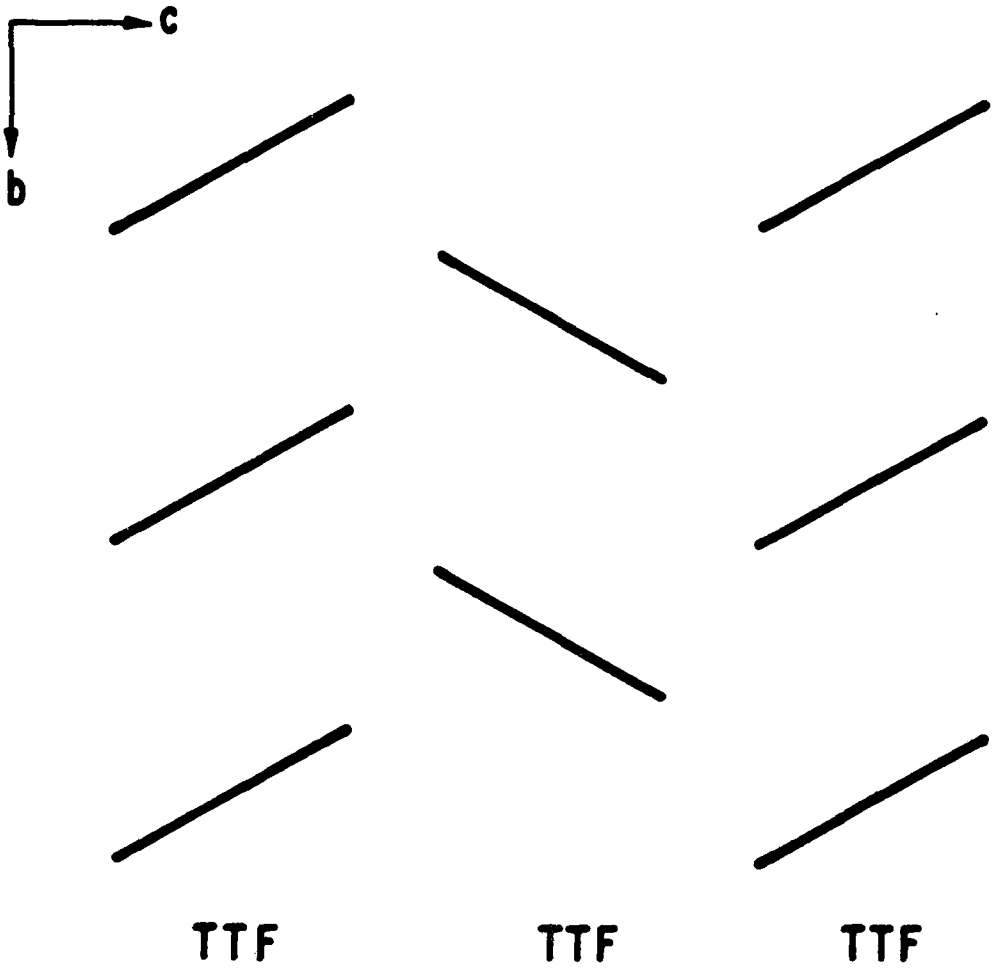

(b)

FIGURE 26

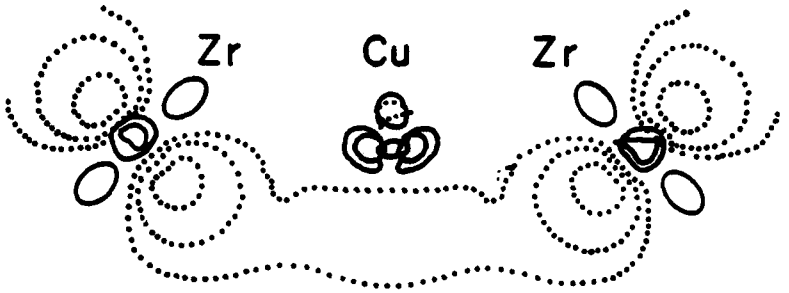

(a)

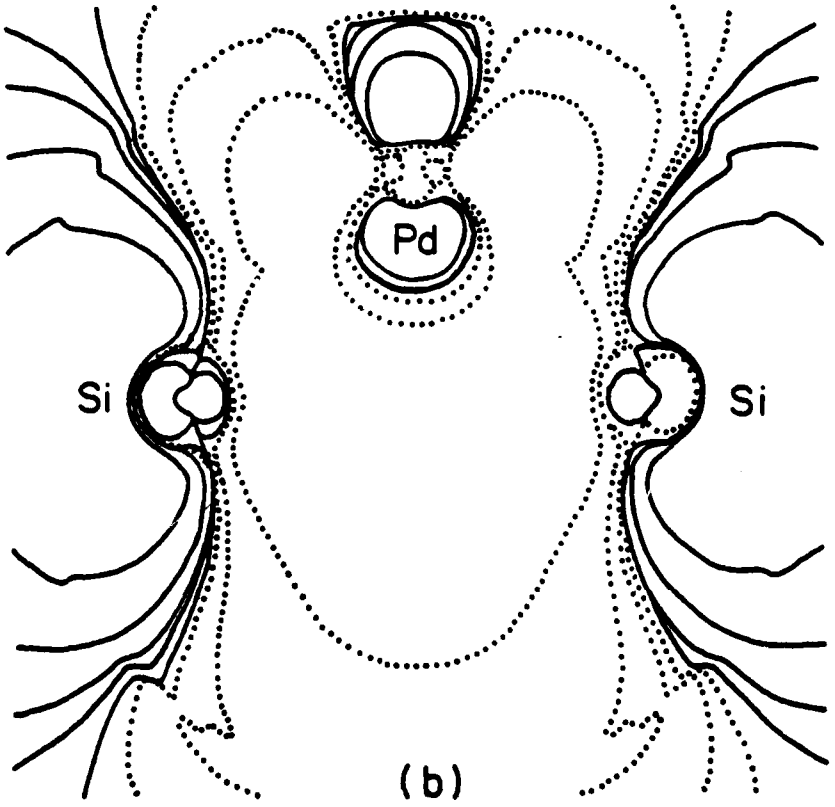

(b)

FIGURE 27

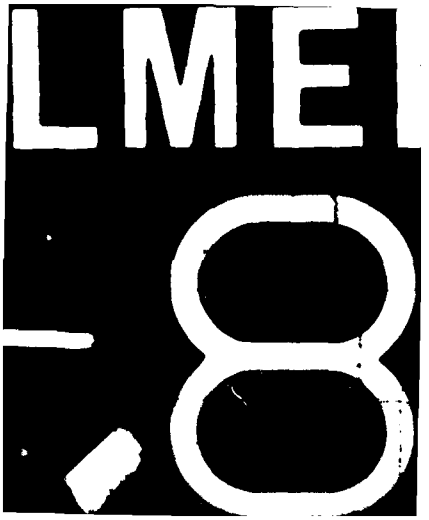
LME
8